RADC-TR-76-78
Final Technical Report
March 1976

ADAPTIVE SAME FREQUENCY REPEATER (SFR) STUDY

Magnavox/General Atronics Corporation

Sponsored by
Defense Advanced Research Projects Agency
ARPA Order 2750

Approved for public release;
distribution unlimited.

The views and conclusions contained in this document are those of the authors and should not be interpreted as necessarily representing the official policies, either expressed or implied, of the Defense Advanced Research Projects Agency or the U. S. Government.

Rome Air Development Center
Air Force Systems Command
Griffiss Air Force Base, New York 13441

This report has been reviewed by the RADC Information Office (OI) and is releasable to the National Technical Information Service (NTIS). At NTIS it will be releasable to the general public including foreign nations.

This report has been reviewed and is approved for publication.

APPROVED:

CARMEN J. LUVERA
Project Engineer

Do not return this copy. Retain or destroy.

ADAPTIVE SAME FREQUENCY REPEATER (SFR) STUDY

Burton S. Abrams
Michael R. Ducoff
Samuel J. Harris
Andrew E. Zeger

Contractor: Magnavox/General Atronics Corp.
Contract Number: F30602-74-C-0242
Effective Date of Contract: 16 April 1974
Contract Expiration Date: 1 August 1975
Amount of Contract: $79,973.00
Program Code Number: 5G10
Period of work covered: Apr 74 - Jul 75

Principal Investigator: Andrew E. Zeger
Phone: 215 248-3700

Project Engineer: Carmen J. Luvera
Phone: 315 330-3153

This research was supported by the Defense Advanced Research Projects Agency of the Department of Defense and was monitored by Carmen J. Luvera (DCCR), Griffiss AFB NY 13441.

UNCLASSIFIED

SECURITY CLASSIFICATION OF THIS PAGE (When Data Entered)

(19) REPORT DOCUMENTATION PAGE

READ INSTRUCTIONS BEFORE COMPLETING FORM

(18) 1. REPORT NUMBER: RADC-TR-76-78

2. GOVT ACCESSION NO.

(9) 3. RECIPIENT'S CATALOG NUMBER

(6) 4. TITLE (and Subtitle): ADAPTIVE SAME FREQUENCY RE ATER (SFR) STUDY,

5. TYPE OF REPORT & PERIOD COVERED: Final Technical Report. 16 Apr 74 - 15 Jul 75

(14) 6. PERFORMING ORG. REPORT NUMBER: GAC-2706-2876-22

(10) 7. AUTHOR(s): Burton S. Abrams, Michael R. Ducoff, Samuel J. Harris, Andrew E. Zeger

(15) 8. CONTRACT OR GRANT NUMBER(s): F30602-74-C-0242, ARPA Order-2750

9. PERFORMING ORGANIZATION NAME AND ADDRESS
Magnavox/General Atronics Corporation
1200 E. Mermaid Lane
Philadelphia PA 19118

10. PROGRAM ELEMENT, PROJECT, TASK AREA & WORK UNIT NUMBERS: J. O. 27500001

(12) 135p.

11. CONTROLLING OFFICE NAME AND ADDRESS
Defense Advanced Research Projects Agency
1400 Wilson Blvd
Arlington VA 22209

(11) 12. REPORT DATE: March 1976

13. NUMBER OF PAGES: 129

14. MONITORING AGENCY NAME & ADDRESS (if different from Controlling Office)
Rome Air Development Center (DCCR)
Griffiss AFB NY 13441

15. SECURITY CLASS. (of this report): UNCLASSIFIED

15a. DECLASSIFICATION/DOWNGRADING SCHEDULE: N/A

16. DISTRIBUTION STATEMENT (of this Report)

Approved for public release; distribution unlimited.

17. DISTRIBUTION STATEMENT (of the abstract entered in Block 20, if different from Report)

Same

18. SUPPLEMENTARY NOTES

Presented at the 1975 Adaptive Antenna Workshop, 29 October 1975

RADC Project Engineer: Carmen J. Luvera (DCCR) Copies available in DDC.

19. KEY WORDS (Continue on reverse side if necessary and identify by block number)

Interference Cancellation
Adaptive Antenna Array
VHF-UHF Communication
Same Frequency Radio Relays

20. ABSTRACT (Continue on reverse side if necessary and identify by block number)

This report documents the technical effort on Contract F30602-74-C-0242. It presents the results of an investigation of Real time, non-sampling, Same Frequency Repeater (SFR) concepts for various types of analog and digital signals using coherent interference cancellation techniques.

The report presents an analytical investigation of transmitter-to-receiver isolation achievable with a multi-channel interference cancellation system (ICS)
(Cont'd)

DD FORM 1 JAN 73 1473 EDITION OF 1 NOV 65 IS OBSOLETE

UNCLASSIFIED

SECURITY CLASSIFICATION OF THIS PAGE (When Data Entered)

391309

4B

when the repeater is used with a finite bandwidth antenna in an environment which includes random ground clutter and specular reflectors.

A design for a Same Frequency Repeater breadboard model is presented that incorporates the multi-channel interference cancellation system. The breadboard operates at 291 MHz with a bandwidth of 100 KHz and allows forward gain up to 120dB to be tested. The minimum input signal level is -90dBM, with a dynamic range of 60dB, for which the repeater will generate a 1 watt output using an AGC.

Experimental results are presented which verify the design concepts on which the SFR breadboard is predicated. They also show areas where further work is needed to utilize the Full forward gain potential of the breadboard.

In the present configuration, forward gains up to 67dB have been measured in the laboratory. With the incorporation of the suggested modifications, forward gain capability in excess of 102dB is anticipated. Further performance refinements may then be possible to push the forward gain capability to 120dB.

A Follow-on effort for the breadboard improvement is being conducted. Results of this improvement effort will also be documented in a final technical report.

TABLE OF CONTENTS

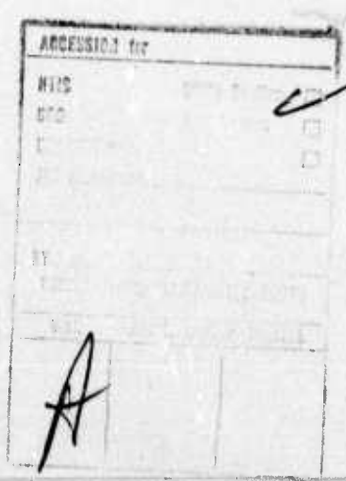

TABLE OF CONTENTS - continued

SUMMARY

This report documents the technical effort on Contract F30602-74-C-0242. It presents the results of an investigation of real time, nonsampling, Same-Frequency Repeater (SFR) concepts for various types of analog and digital signals using coherent interference cancellation techniques.

The report presents an analytical investigation of the transmitter-to-receiver isolation achievable with a multichannel interference cancellation system (ICS) when the repeater is used with a finite bandwidth antenna in an environment which includes random ground clutter and specular reflectors. Results of an investigation for obtaining high linearity in the interference canceller for low intermodulation generation in the SFR are also summarized.

A design for a Same-Frequency Repeater breadboard model is presented that incorporates the multichannel interference cancellation system. The breadboard operates at 291 MHz with a bandwidth of 100 kHz and allows forward gain up to 120 dB to be tested. The minimum input signal level is -90 dBm, with a dynamic range of 60 dB, for which the repeater will generate a 1 watt output using an AGC.

Experimental results are presented which verify the design concepts on which the SFR breadboard is predicated. They also show areas where further work is needed to utilize the full forward gain potential of the breadboard. These areas include elimination of stray coupling problems between the SFR transmitter and receiver, and modification to the multichannel ICS which will allow it to operate effectively with a 100 kHz wide signal. In the present configuration, forward gains up to 67 dB have been measured in the laboratory. With the incorporation of the suggested modifications, forward gain capability in excess of 102 dB is anticipated. Further performance refinements may then be possible to push the forward gain capability to 120 dB.

SECTION I

INTRODUCTION

This report documents the technical effort on Contract F30602-74-C-0242. It presents the results of an investigation of real time, nonsampling, Same-Frequency Repeater (SFR) concepts for various types of analog and digital signals using coherent interference cancellation techniques.

The analytical results presented here will develop the concept of a pilot-directed multichannel notch filter interference cancellation system (ICS) to provide isolation between the repeater transmitter and its receiver. The isolation capability of the ICS will be analyzed to determine the effects of signal returns from the SFR antenna, from specular reflectors, and from distributed ground clutter. The results will be given as functions of signal bandwidth and carrier frequency as well as other design parameters of the ICS.

Results of a hardware investigation of approaches for obtaining low signal distortion in the ICS complex weights will also be presented. Inband distortion products generated in the weights cannot be cancelled, and thus form a lower limit on the achievable ICS cancellation residue.

An SFR breadboard design will be presented which incorporates a pilot-directed three-channel notch filter ICS to provide the transmitter-to-receiver isolation. The breadboard is designed to operate at 291 MHz with a 100 kHz bandwidth, providing a 1 watt output with the capability for testing forward gain up to 120 dB.

Experimental results will be presented which verify the design concepts on which the SFR breadboard is predicated. They also show areas where further work is needed to utilize the full forward gain potential of the breadboard. The areas requiring further work will be discussed in some detail.

SECTION II

MULTICHANNEL NOTCH FILTER ICS

1. MULTICHANNEL ICS ANALYSIS

In this section the concept of a multichannel notch-filter ICS is developed in subsection a. In subsection b, a detailed analysis is performed to determine the performance of a one-channel and a two-channel ICS under general transmitter-to-receiver coupling conditions. These analytical results are applied to the case of reflecting terrain in subsection c and to the case of antenna reflections in subsection d. Subsection e presents numerical examples using the analytical results. Subsection f presents a discuss of the results -- their implications and their extensions.

The purpose of the ICS in the SFR design is to cancel signals at the receiver input that emanate from the SFR transmitter. The signals from the transmitter are coupled to the receiver through a number of different coupling paths, including leakage through the antenna coupler, reflection from the antenna, and reflection from the surrounding terrain. A single channel ICS, shown in Figure 1, uses a complex (amplitude and phase) weight to duplicate as well as possible the amplitude and phase of the composite coupling path.

Because the coupling paths have frequency-dependent transfer functions (e.g., the antenna, reflected returns with delay due to propagation distance), the amplitude and phase setting is precise at only one frequency. Thus, perfect cancellation is possible at only one frequency. Broadband signals are cancelled well at band center, and progressively worse toward the band edges. This effect places a bandwidth limitation on achievable cancellation which may be quite severe for a single-channel ICS. As an illustration, Figure 2 shows the achievable cancellation ratio with a single-channel ICS used in a two-element adaptive array [1], where the antenna spacing produces

[1] Abrams, B.S., *et al*, "Interference Cancellation," General Atronics Rpt 2324-2626-15, prepared for Rome Air Development Center under Contract F30602-72-C-0459, August 1973.
[2] Rosenberg, J.R., E.J. Thomas, "Performance of an Adaptive Echo Canceller Operating in a Noisy, Linear, Time-Invariant Environment," *BSTJ*, vol. 50,no. 3, March 1971, pp. 785-813.
[3] Sandhi, M.M., "An Adaptive Echo Canceller," *BSTJ*, vol. 46, no. 3, March 1967, pp. 497-511.
[4] Becker,F.K., H.R. Rudin, "Application of Automatic Transversal Filters to the Problem of Echo Suppression," *BSTJ*, vol. 45, no. 12, December 1966, pp. 1847-1850.
[5] Sandhi, M.M., A.J. Presti, "A Self-Adaptive Echo Canceller," *BSTJ*, vol. 45, no. 12, December 1966, pp. 1851-1854.

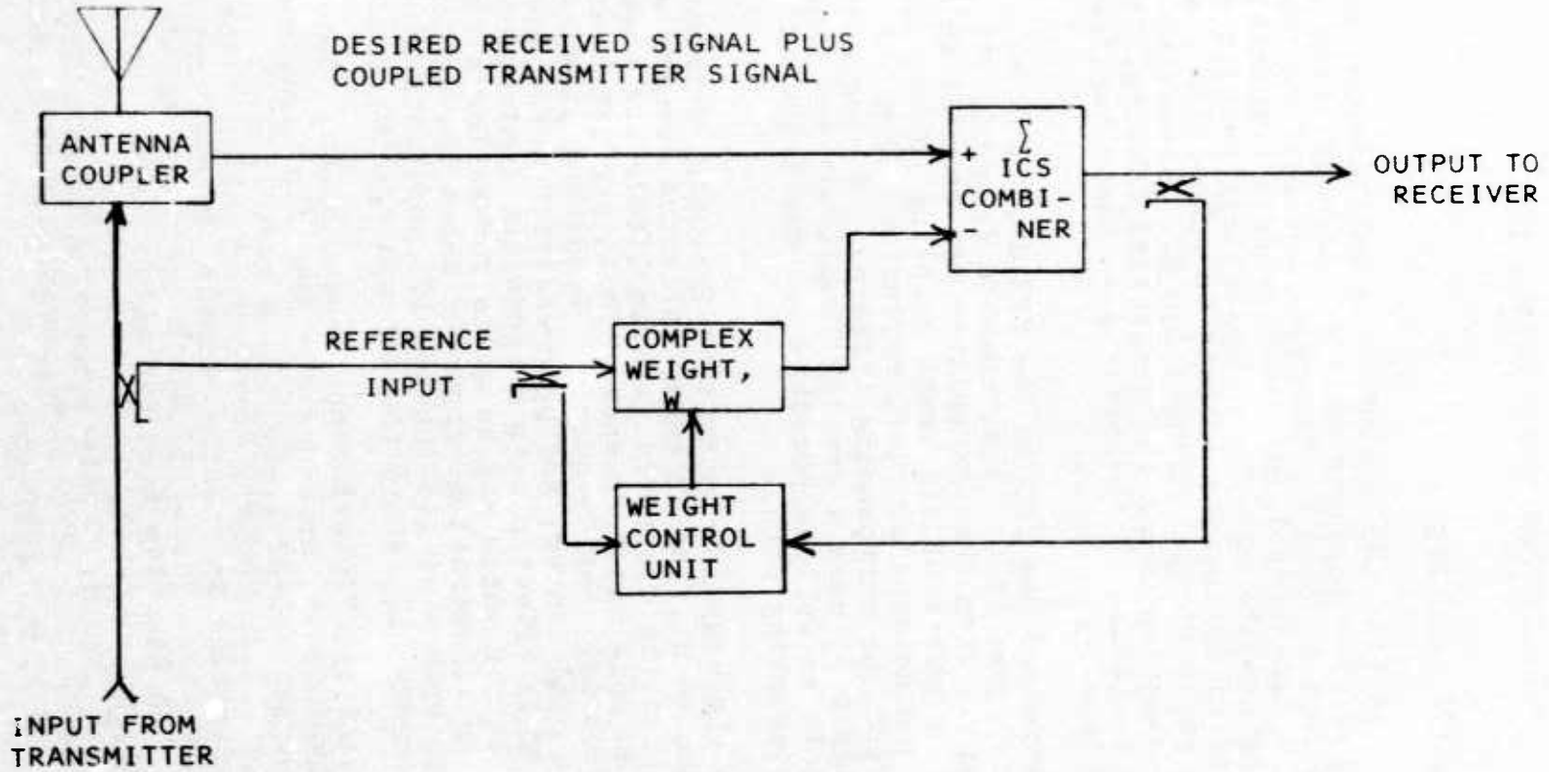

FIGURE 1

SINGLE-CHANNEL ICS

FIGURE 2

BEST POSSIBLE CANCELLATION RATIO VS
INTERFERENCE BANDWIDTH FOR VARIOUS
ANTENNA SPACINGS (RECTANGULAR SPECTRUM)

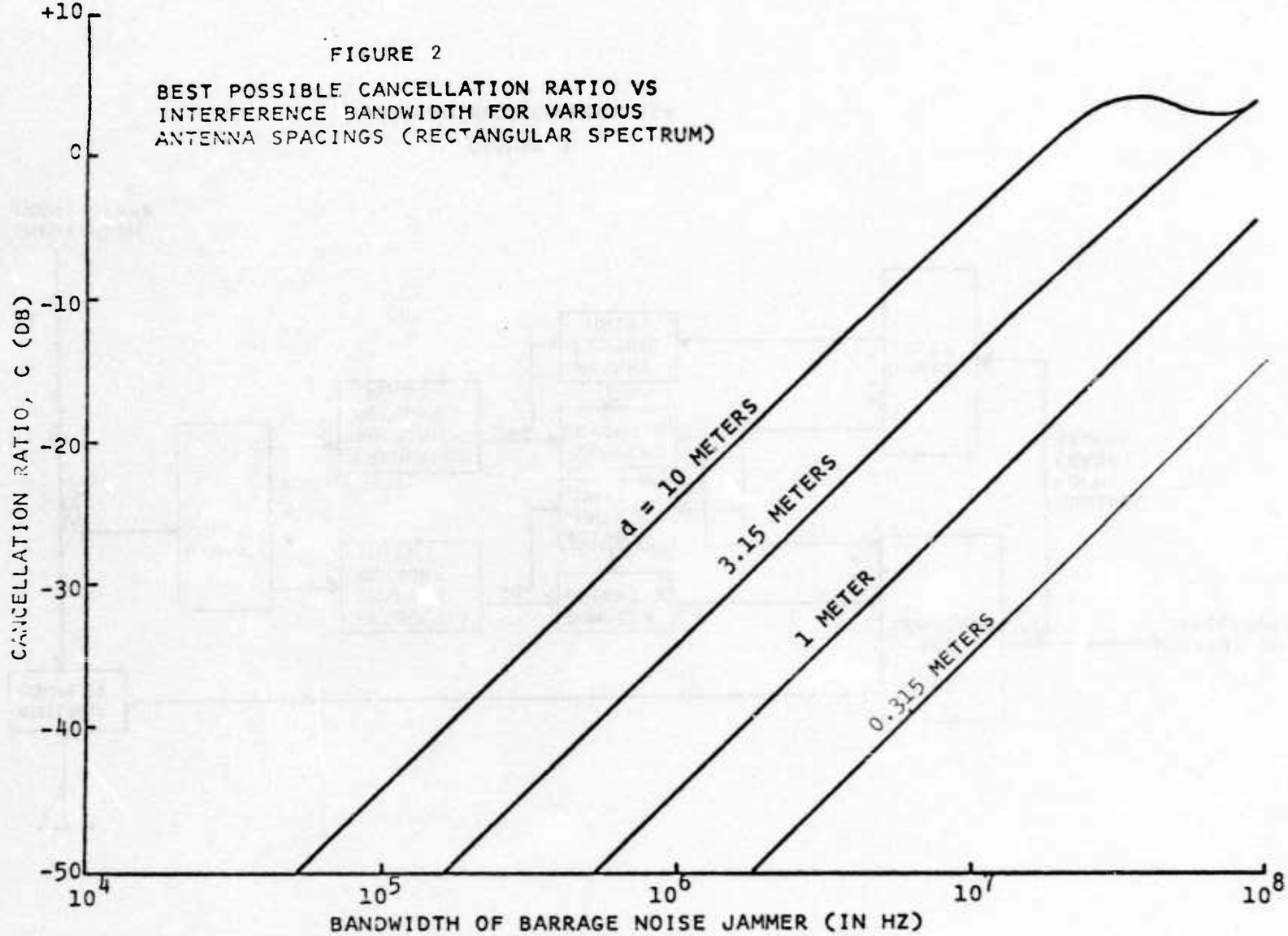

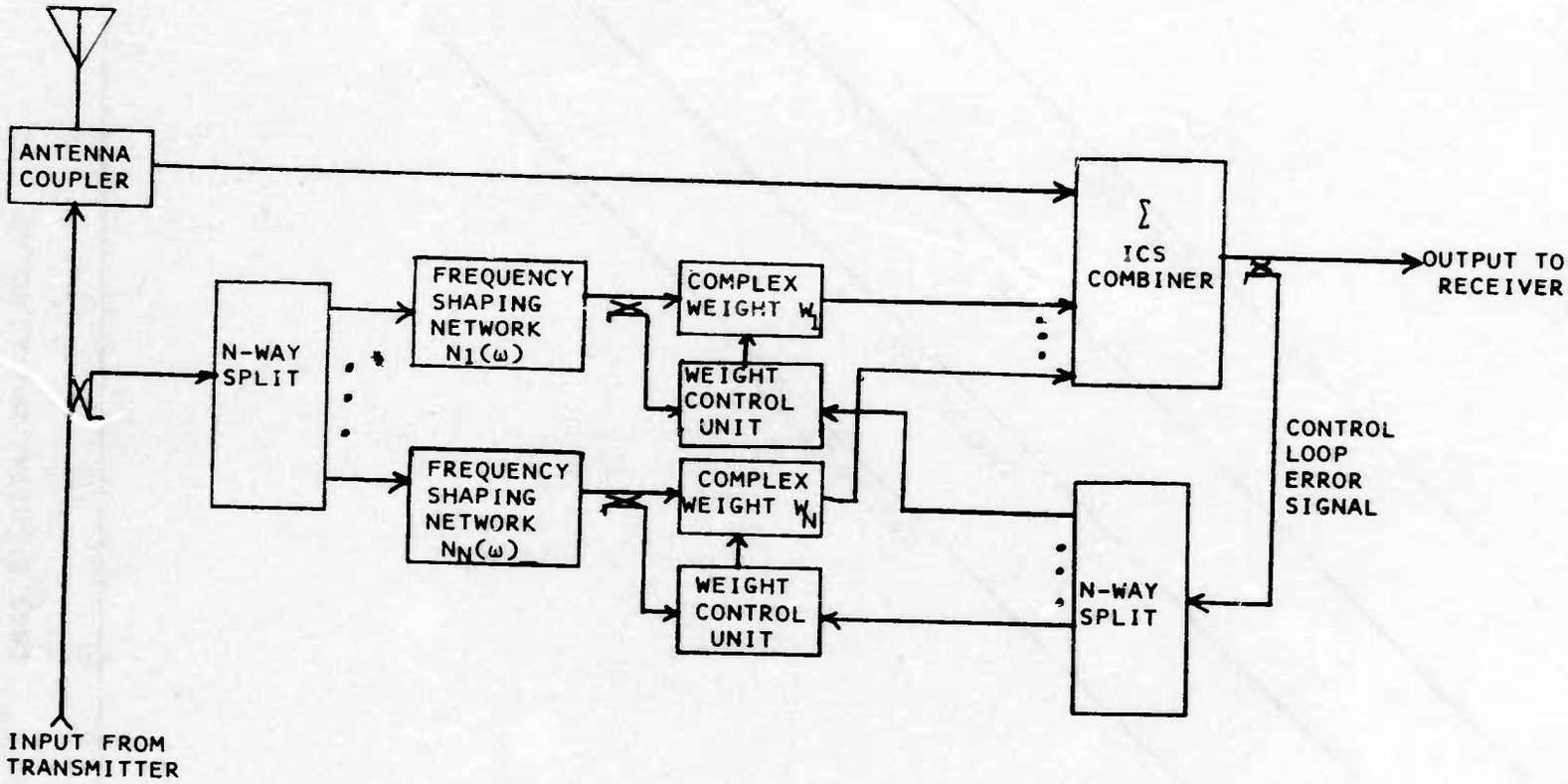

FIGURE 3

GENERAL MULTICHANNEL ICS

a delay (frequency-dependent phase shift) between the two ICS inputs.

Multichannel ICS configurations have been used to provide good broadband cancellation performance. The structure of the multichannel ICS used in the SFR is given in Figure 3. Each weight is preceded by a frequency shaping network, and generally each network is unique. This general structure has been used for wireline echo cancellers [2,3,4,5] where the frequency shaping networks were ones whose impulse responses are elements of an orthonormal set. Specific implementations used delay lines and Laguerre networks. Delay line implementations have also been studied for both electromagnetic [6] and acoustic [7] adaptive arrays.

For analysis purposes, the multichannel ICS in the SFR may be modelled in the following manner. Let us define a frequency-dependent transfer function $H_C(\omega)$ to represent the undesired coupling from transmitter output to receiver input. The N channels of the ICS provide a second transfer function between transmitter and receiver which, from Figure 3, may be written as

$$H_N(\omega) = \sum_{i=1}^{N} W_i N_i(\omega) \qquad (1)$$

The model is shown diagrammatically in Figure 4. The transmitter waveform is assumed to have a Fourier transform represented by $S_T(\omega)$, and $S_R(\omega)$ is used to represent the Fourier transform of the ICS output to the receiver.

As shown in the figure, we define the N-Channel ICS transmitter-to-receiver isolation ratio as the ratio of the energy going into the receiver to the energy coming from the transmitter.

$$(R/T)_N = \frac{\frac{1}{\pi}\int_0^\infty |S_R(\omega)|^2 d\omega}{\frac{1}{\pi}\int_0^\infty |S_T(\omega)|^2 d\omega}$$

$$= \frac{\int_0^\infty |S_T(\omega)|^2 |H_C(\omega)+H_N(\omega)|^2 d\omega}{\int_0^\infty |S_T(\omega)|^2 d\omega} \qquad (2)$$

The best ICS performance is obtained when $(R/T)_N$ is minimized, which is accomplished by allowing the weights W_i to be adjusted so that $H_N(\omega)$ matches $-H_C(\omega)$ as closely as possible. $H_C(\omega)$ may be slowly varying with respect to the transmitted waveform, but it

[6] Widrow, B., *et al*, "Adaptive Antenna Systems," *Proc* IEEE, vol. 55, no. 12, December 1967, pp. 2143-2159.
[7] Bryn, F., "Optimum Signal Processing of Three-Dimensional Arrays Operating on Gaussian Signals and Noise," *J Acous Soc Am*, vol. 34, March 1962, pp. 289-297.

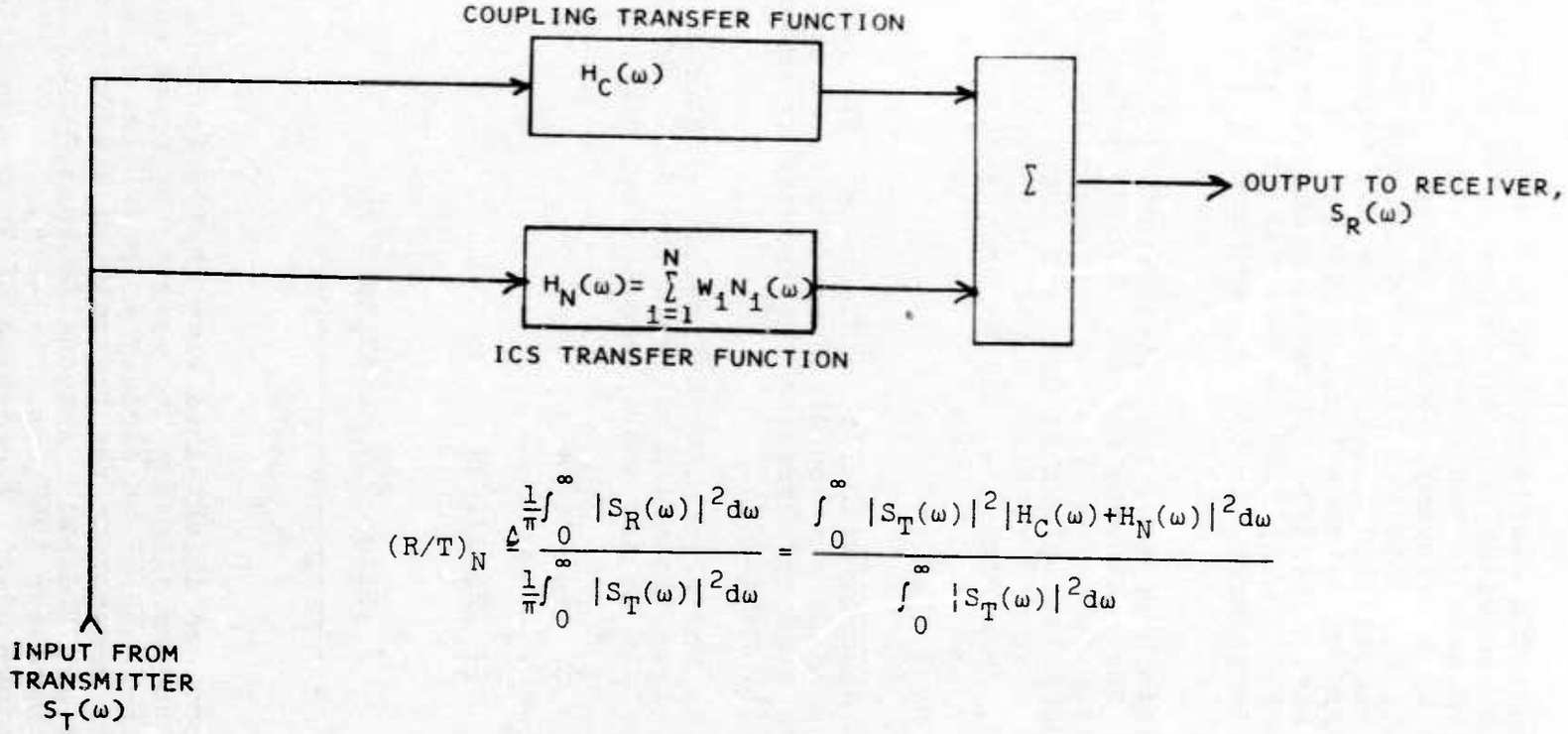

$$(R/T)_N \triangleq \frac{\frac{1}{\pi}\int_0^\infty |S_R(\omega)|^2 d\omega}{\frac{1}{\pi}\int_0^\infty |S_T(\omega)|^2 d\omega} = \frac{\int_0^\infty |S_T(\omega)|^2 |H_C(\omega)+H_N(\omega)|^2 d\omega}{\int_0^\infty |S_T(\omega)|^2 d\omega}$$

FIGURE 4
ANALYTICAL MODEL OF MULTICHANNEL ICS

will be presumed that $H_N(\omega)$ will have similar compensating variations by adaptively controlled the weight values W_i.

a. Choice of Frequency Shaping Networks

In order to determine the set of network functions $\{N_i(\omega)\}$ to be used in the multichannel ICS, let us first consider a single-channel ICS in which

$$N_1(\omega) = 1 \tag{3}$$

That is, the network $N_1(\omega)$ is not frequency-dependent. We will now examine the isolation ratio $(R/T)_1$ when $S_T(\omega)$ is a flat band-limited spectrum in an environment which consists of a single reflector removed from the repeater by a delay τ. Thus, we let

$$|S_T(\omega)|^2 = \begin{cases} P_0 \text{ for } |\omega \pm \omega_0| \leq \pi B \\ 0 \text{ elsewhere} \end{cases} \tag{4}$$

where $f_0 = \omega_0/2\pi$ is the carrier frequency of the transmitted signal and B is its bandwidth. The coupling function is

$$H_C(\omega) = ae^{j\phi}e^{-j\omega\tau} \tag{5}$$

where a represents the gain of the coupling path, ϕ its phase shift, and τ its delay. Using (1), (3), (4) and (5) in (2) gives

$$(R/T)_1 = \frac{1}{2\pi B}\int_{\omega_0-\pi B}^{\omega_0+\pi B} |ae^{j\phi}e^{-j\omega\tau}+W_1|^2 d\omega \tag{6}$$

When $\pi B\tau$ is small, the ICS ideally will cause W_1 to adapt to the solution

$$W_1 = -ae^{j\phi}e^{-j\omega_0\tau} \tag{7}$$

which, when applied to (6) results in

$$(R/T)_1 = \frac{a^2}{2\pi B}\int_{\omega_0-\pi B}^{\omega_0+\pi B} |1-e^{-j(\omega-\omega_0)\tau}|^2 d\omega \tag{8}$$

Integrating (8) gives

$$\begin{aligned}(R/T)_1 &= 2a^2\left[1 - \frac{\sin\pi B\tau}{\pi B\tau}\right] \\ &\simeq a^2(\pi B\tau)^2/3 \quad \text{for } |\pi B\tau| << 1\end{aligned} \tag{9}$$

It is clear from (9) that high isolation with a large requires that the product $\pi B\tau$ be small, so that we will concentrate our attention on that condition. It is important to note that the approximate result given in (9) for small $B\tau$ would have been achieved if the integrand in (8) had been approximated by the first term of its Taylor series expansion, i.e., approximating

$$1-e^{-j(\omega-\omega_0)\tau} \simeq j(\omega-\omega_0)\tau \tag{10}$$

Thus, the voltage spectrum of the single-channel ICS residue is dominated by a term linear in frequency, passing through zero at $\omega=\omega_0$.

We now consider the addition of a second channel to the ICS. If the first channel leaves a residue whose dominant spectral term is proportional to $(\omega-\omega_0)$, it is intuitively felt that making the frequency shaping network $N_2(\omega)$ for the second channel have the same characteristic will allow it to be most effective in improving the isolation. Thus, we make

$$N_2(\omega) = j\frac{(\omega-\omega_0)}{\omega_B} \tag{11}$$

which may be approximated by a single resonant stage notch filter centered at $f_0 = \omega_0/2\pi$ with 3 dB bandwidth $B_N = \omega_B/\pi$, for $B<<B_N$.

Using (1), (3), (4), (5) and (11) in (2) gives

$$(R/T)_2 = \frac{1}{2\pi B}\int_{\omega_0-\pi B}^{\omega_0+\pi B} \left| ae^{j\phi}e^{-j\omega\tau}+W_1+jW_2\frac{(\omega-\omega_0)}{\omega_B}\right|^2 d\omega$$

$$= \frac{1}{2\pi B}\int_{\omega_0-\pi B}^{\omega_0+\pi B} \left| ae^{j(\phi-\omega_0\tau)}e^{-j(\omega-\omega_0)\tau}+W_1+jW_2\frac{(\omega-\omega_0)}{\omega_B}\right|^2 d\omega \tag{12}$$

For $|\pi B\tau|<<1$, we can expand

$$e^{-j(\omega-\omega_0)\tau} \simeq 1-j(\omega-\omega_0)\tau-(\omega-\omega_0)^2\tau^2/2 \tag{13}$$

Then, if the ICS adapts its weights to

$$W_1 = -ae^{j(\phi-\omega_0\tau)}$$

$$W_2 = a\omega_B\tau e^{j(\phi-\omega_0\tau)} \tag{14}$$

we have a residue whose voltage spectrum is parabolic about ω_0. The isolation is given by

$$(R/T)_2 \simeq \frac{a^2}{2\pi B}\int_{\omega_0-\pi B}^{\omega_0+\pi B}\left[\frac{(\omega-\omega_0)^2\tau^2}{2}\right]^2 d\omega$$

$$= a^2(\pi B\tau)^4/20 \qquad \text{for } |\pi B\tau|<<1 \tag{15}$$

By comparing (9) with (15) we see that the isolation afforded by the two-channel ICS improves that available from the single-channel ICS by a factor of $3(\pi B\tau)^2/20$.

By extrapolating the above arguments for additional channels, it becomes evident that the i-th channel should have a frequency shaping network of the form

$$N_i(\omega) \simeq [j\frac{(\omega-\omega_0)}{\omega_B}]^{i-1} \tag{16}$$

which may be approximated by a cascade of i-1 identical notch filters with isolation between them. For $\pi B\tau<<1$, an N-channel notch-filter ICS will have an isolation ratio $(R/T)_N$ of the order of $(\ B\ )^{2N}$. A block diagram of an N-channel notch filter ICS is given in Figure 5.

b. Detailed Analysis of Two-Channel Notch Filter ICS

(1) Problem Formulation

The objective of this analysis is to determine the transmitter-to-receiver isolation that can be provided by a two-channel ICS using the notch filter technique heuristically described in Section II.1.a. The analytical model adopted for this performance evaluation is shown in Figure 6. All signals shown are complex envelope representations with respect to a selected center frequency f_0 of corresponding bandpass signals. Thus, $x(t)$ is the input from the transmitter, $x_1(t)$ and $x_2(t)$ are the ICS reference channel inputs, and $r(t)$ is the ICS output to the receiver. For this analysis the transmitter-to-receiver coupling channel is considered to be a linear time-invariant system with a lowpass equivalent transfer function $H_c(f)$. Finally, $N(f)$ and $H_L(f)$ are the lowpass equivalent transfer functions of the notch filter and the integrating filters utilized in the weight control units.

The initial step in the system analysis is to obtain the differential equations describing the operation of the control loops. From Figure 6, the time-varying complex weights $W_1(t)$ and $W_2(t)$ must satisfy the set of simultaneous differential equations

$$\begin{aligned} T\frac{dW_1}{dt} + W_1 &= -G_1 x_1^*(t) r(t) \\ T\frac{dW_2}{dt} + W_2 &= -G_2 x_2^*(t) r(t) \end{aligned} \tag{17}$$

where the receiver output is

$$r(t) = y(t) + W_1(t)x_1(t) + W_2(t)x_2(t) \tag{18}$$

G_1 and G_2 are the voltage gains of the control loop amplifiers, and T is the time constant of the loop filters, and $x_1(t)$ and $x_2(t)$ are linearly related to $x(t)$ as shown in Figure 6. After substituting (18) into (17), the system differential equations are found to be

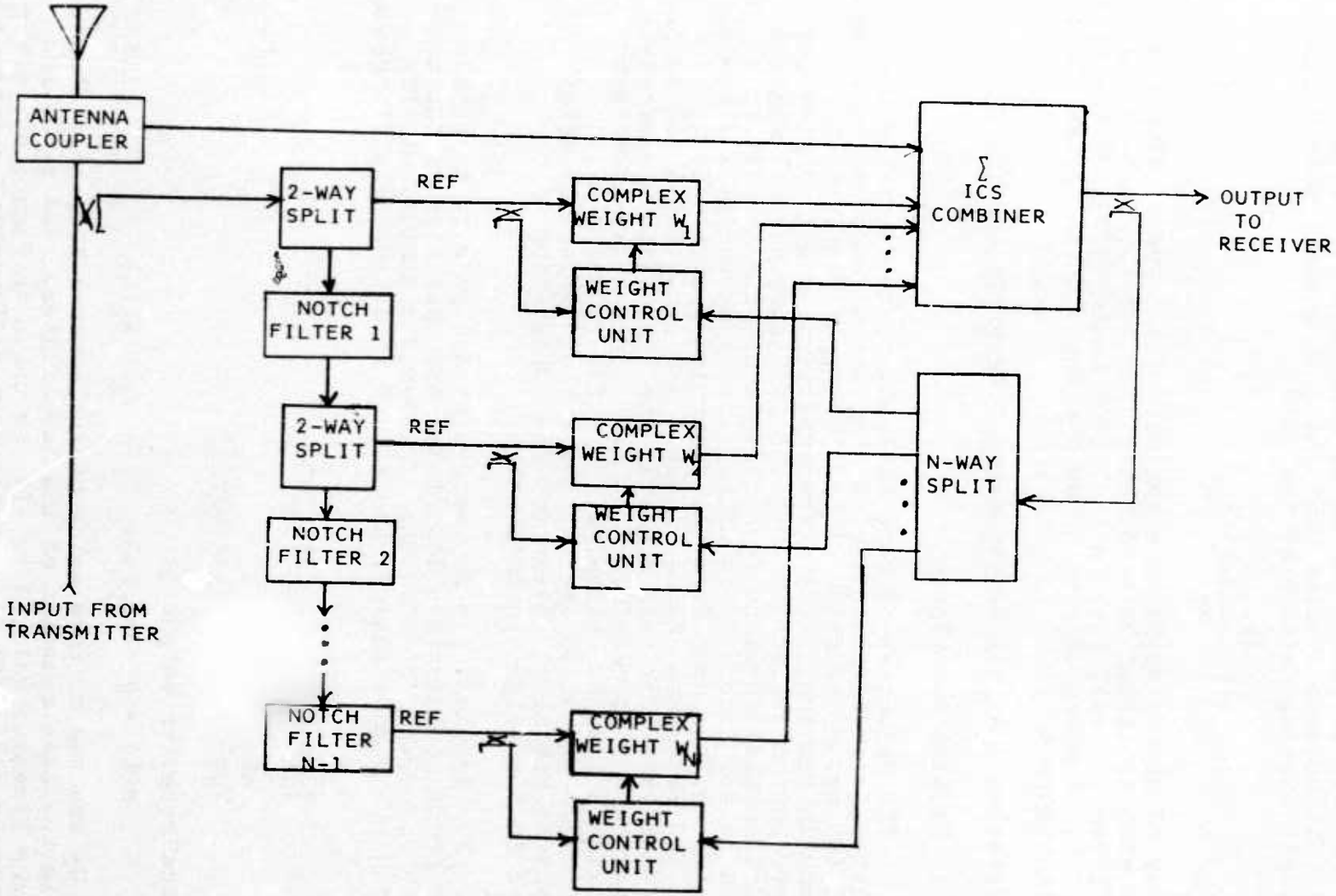

FIGURE 5

MULTICHANNEL NOTCH FILTER ICS

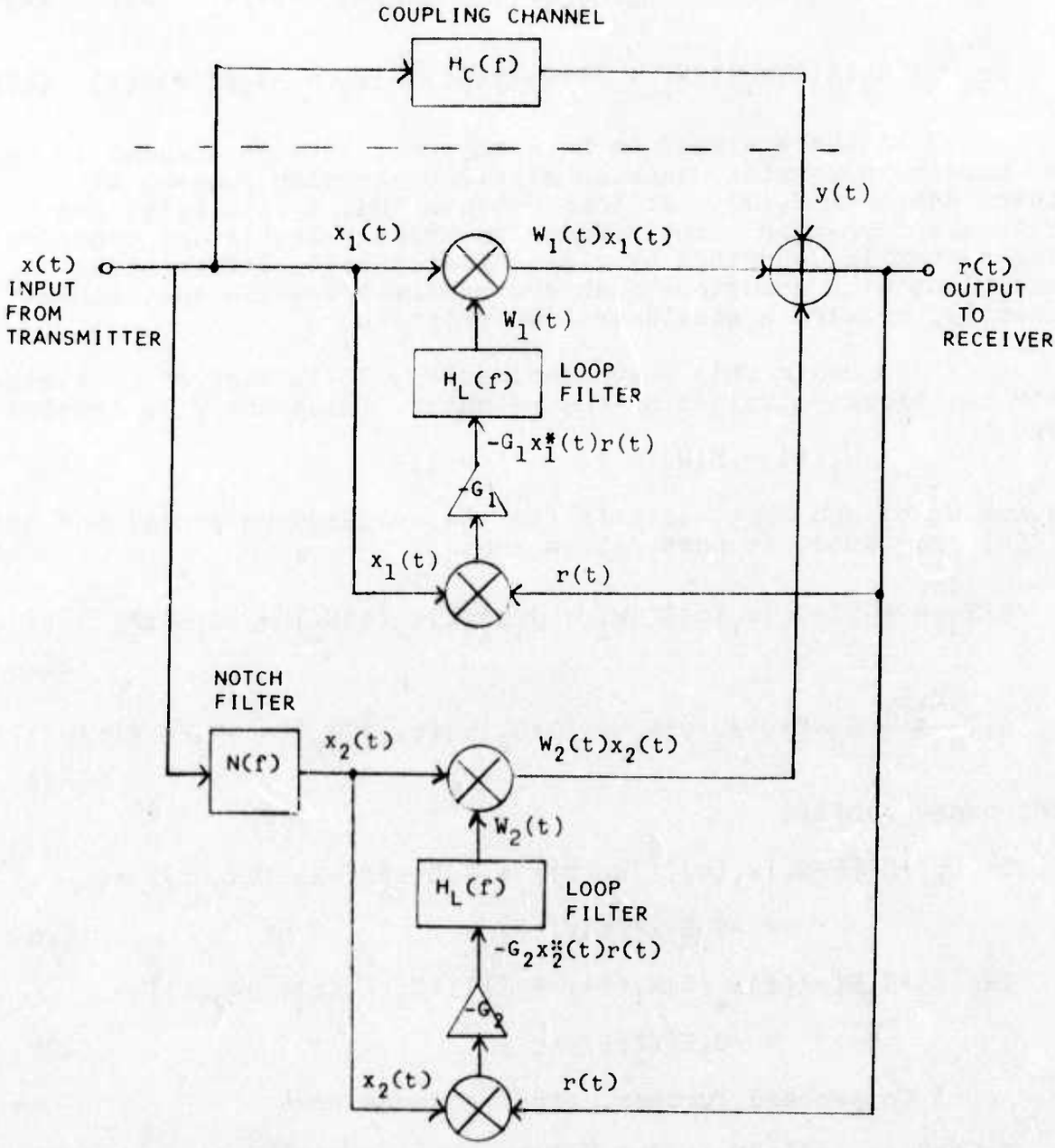

$$H_L(f) = \frac{1}{(1+j2\pi fT)}$$

$$r(t) = y(t)+W_1(t)x_1(t)+W_2(t)x_2(t)$$

FIGURE 6

MODEL FOR THE ANALYSIS OF THE TWO-CHANNEL NOTCH FILTER ICS

$$T\frac{dW_1}{dt} + [1+G_1|x_1(t)|^2]W_1 + G_1x_1^*(t)x_2(t)W_2 = -G_1x_1^*(t)y(t) \quad (19a)$$

$$T\frac{dW_2}{dt} + G_2x_2^*(t)x_1(t)W_1 + [1+G_2|x_2(t)|^2]W_2 = -G_2x_2^*(t)y(t) \quad (19b)$$

In the analysis to be performed, $x(t)$ is assumed to be a zero-mean complex Gaussian stationary random process with power spectrum $S_x(f)$. It then follows that $x_1(t)$, $x_2(t)$ and $y(t)$ are zero-mean complex Gaussian jointly stationary processes. The system is described by a set of stochastic differential equations with solutions that are random processes and, consequently, require a statistical description.

To begin this characterization, it is desired to evaluate the expected values of the weights; these shall be denoted as

$$\bar{W}_i(t) = E\{W_i(t)\} \qquad i = 1,2 \quad (20)$$

Since $W_1(t)$ and $W_2(t)$ satisfy (in the mean-square sense) the set (19a) and (19b), it must follow that

$$E\{T\frac{dW_1}{dt} + [1+G_1|x_1(t)|^2]W_1 + G_1x_1^*(t)x_2(t)W_2\} = -G_1E\{x_1^*(t)y(t)\} \quad (21a)$$

$$E\{T\frac{dW_2}{dt} + G_2x_2^*(t)x_1(t)W_1 + [1+G_2|x_2(t)|^2]W_2\} = -G_2E\{x_2^*(t)y(t)\} \quad (21b)$$

and consequently,

$$T\dot{\bar{W}}_1(t)+E\{[1+G_1|x_1(t)|^2]W_1(t)\} + G_1E\{x_1^*(t)x_2(t)W_2(t)\} = -G_1E\{x_1^*(t)y(t)\} \quad (22a)$$

$$T\dot{\bar{W}}_2(t)+G_2E\{x_2^*(t)x_1(t)W_1(t)\} + E\{[1+G_2|x_2(t)|^2]W_2(t)\} = -G_2E\{x_2^*(t)y(t)\} \quad (22b)$$

To proceed further, first observe that

$$E\{[1+G_1|x_1(t)|^2]W_1(t)\} = \bar{W}_1(t) + G_1E\{|x_1(t)|^2W_1(t)\} \quad (23)$$

Next, invoke the assumption that, for any value of t, $|x_1(t)|^2$ and $W_1(t)$ are uncorrelated random variables; that is,

$$E\{|x_1(t)|^2W_1(t)\} = E\{|x_1(t)|^2\}E\{W_1(t)\}$$

By this assumption, (23) becomes

$$E\{[1+G_1|x_1(t)|^2]W_1(t)\} = [1+G_1E\{|x_1(t)|^2\}]\bar{W}_1(t) \qquad (24)$$

If a similar procedure is carried out for the remaining terms in (22a) and (22b) it is found that $\bar{W}_1(t)$ and $\bar{W}_2(t)$ must satisfy the differential equations

$$T\dot{\bar{W}}_1(t)+[1+G_1E\{|x_1(t)|^2\}]\bar{W}_1(t) + G_1E\{x_1^*(t)x_2(t)\}\bar{W}_2(t) = \\ = -G_1E\{x_1^*(t)y(t)\} \qquad (25a)$$

$$T\dot{\bar{W}}_2(t)+G_2E\{x_2^*(t)x_1(t)\}\bar{W}_1(t) + [1+G_2E\{|x_2(t)|^2\}]\bar{W}_2(t) = \\ = -G_2E\{x_2^*(t)y(t)\} \qquad (25b)$$

Equations (25a) and (25b) can also be written in matrix form as

$$\dot{\bar{W}}(t) = A\bar{W}(t) + B\bar{V} \qquad (26)$$

where $\bar{W}(t)$ is the column vector.

$$\bar{W}(t) = \begin{bmatrix} \bar{W}_1(t) \\ \bar{W}_2(t) \end{bmatrix} \qquad (27a)$$

A and B are the matrices

$$A = -\frac{1}{T}\begin{bmatrix} (1+G_1E\{|x_1(t)|^2\}) & G_1E\{x_1^*(t)x_2(t)\} \\ G_2E\{x_2^*(t)x_1(t)\} & (1+G_2E\{|x_2(t)|^2\}) \end{bmatrix} \qquad (27b)$$

$$B = \frac{1}{T}\begin{bmatrix} -G_1 & 0 \\ X\ 0 & -G_2 \end{bmatrix} \qquad (27c)$$

and $\bar{V}$ is the column vector

$$\bar{V} = \begin{bmatrix} E\{x_1^*(t)y(t)\} \\ E\{x_2^*(t)y(t)\} \end{bmatrix} \qquad (27d)$$

Notice that A and $\bar{V}$ do not vary with time since $x_1(t)$, $x_2(t)$ and $y(t)$ are jointly stationary processes.

The solution to (27) is given by [8]

$$\bar{W}(t) = e^{At}\bar{W}(0) + \int_0^t e^{A(t-\tau)}B\bar{V}\,d\tau \quad 0\le t<\infty \qquad (28)$$

where $\bar{W}(0)$ is the mean value of the weight vector at t=0. In addition, if all eigenvalues of A have negative real parts, the

---

[8] DeRusso, P.M., R.J. Roy, C.M. Close, *State Variables for Engineers*, John Wiley and Sons, 1967, pp. 358-360.

expected value of the weight vector approaches a finite limit

$$\bar{W} = \lim_{t\to\infty} \bar{W}(t) = -A^{-1}B\bar{V} \tag{29}$$

Using (27) and (29) it is found that the steady state value of the mean weight vector is

$$\bar{W} = \begin{bmatrix} (1+G_1K_{11}) & G_1K_{12} \\ G_2K_{21} & (1+G_2K_{22}) \end{bmatrix}^{-1} \begin{bmatrix} -G_1L_1 \\ -G_2L_2 \end{bmatrix}$$

$$= \frac{1}{(1+G_1K_{11})(1+G_2K_{22})-G_1G_2K_{12}K_{21}} \begin{bmatrix} 1+G_2K_{22} & -G_1K_{12} \\ -G_2K_{21} & 1+G_1K_{11} \end{bmatrix} \begin{bmatrix} -G_1L_1 \\ -G_2L_2 \end{bmatrix} \tag{30}$$

where

$$\begin{aligned} K_{11} &= E\{|x_1(t)|^2\} \\ K_{12} &= E\{x_1^*(t)x_2(t)\} \\ K_{21} &= E\{x_2^*(t)x_1(t)\} \\ K_{22} &= E\{|x_2(t)|^2\} \end{aligned} \tag{31}$$

and

$$\begin{aligned} L_1 &= E\{x_1^*(t)y(t)\} \\ L_2 &= E\{x_2^*(t)y(t)\} \end{aligned} \tag{32}$$

Notice that K_{mn} is the covariance of $x_m(t)$ and $x_n(t)$, the m-th and n-th reference inputs, while L_i is the covariance of the i-th reference $x_i(t)$ and the interference $y(t)$ present at the ICS input from the antenna. In addition, K_{mn} is the (m,n)-th element of the covariance matrix

$$K = E\{X^*X^T\} \tag{33}$$

where X is the column vector of reference inputs $x^T = [x_1(t)x_2(t)]$.

The covariances required to evaluate (30) can be found by first observing that $x_1(t)$, $x_2(t)$ and $y(t)$ are the outputs of the system shown in Figure 7. Application of the results developed in [9] for the system shown in Figure 8 then yields

$$K_{11} = E\{|x_1(t)|^2\} = \int_{-\infty}^{\infty} S_x(f)\, df \tag{34a}$$

$$K_{12} = E\{x_2(t)x_1^*(t)\} = \int_{-\infty}^{\infty} N(f)S_x(f)\, df \tag{34b}$$

---

[9] Papoulis, A., *Probability, Random Variables, and Stochastic Processes*, McGraw-Hill Book Co., 1965, pp. 352-353.

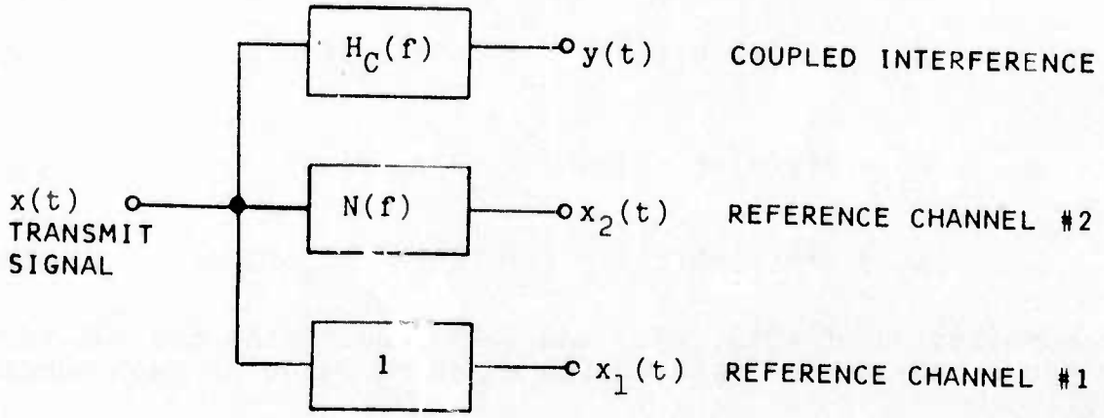

FIGURE 7

SYSTEM REPRESENTATION FOR THE COUPLED INTERFERENCE AND REFERENCE CHANNEL INPUTS

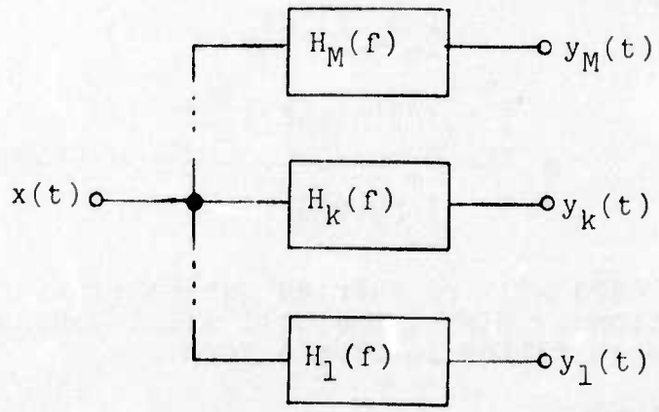

FIGURE 8

A GENERAL SINGLE INPUT M-OUTPUT LINEAR SYSTEM

$$K_{21} = E\{x_1(t)x_2^*(t)\} = K_{12}^* \tag{34c}$$

$$K_{22} = E\{|x_2(t)|^2\} = \int_{-\infty}^{\infty} |N(f)|^2 S_x(f)\, df \tag{34d}$$

and

$$L_1 = E\{y(t)x_1^*(t)\} = \int_{-\infty}^{\infty} H_c(f) S_x(f)\, df \tag{35a}$$

$$L_2 = E\{y(t)x_2^*(t)\} = \int_{-\infty}^{\infty} H_c(f) N^*(f) S_x(f)\, df \tag{35b}$$

The combination of (34), (35) and (30) then yields the solution for the steady state limit of the expected value of each complex weight.

With a long integration time in the loop filters of Figure 6, the weight values are well approximated by their mean values [10]. Then, from Equation (1), the mean weight values determine an ICS transfer function, which, for the two-channel ICS, is given by

$$H_2(f) = \bar{W}_1 + \bar{W}_2 N(f) \tag{36}$$

The composite transmitter-to-receiver transfer function is then $H_{02}(f) = H_c(f)+H_2(f)$, allowing the transmitter-to-receiver isolation to be written as

$$(R/T)_2 = \frac{E\{|r(t)|^2\}}{E\{|x(t)|^2\}} = \frac{\int_{-\infty}^{\infty} S_x(f)|H_c(f)+H_2(f)|^2\, df}{\int_{-\infty}^{\infty} S_x(f)\, df}$$

$$= \frac{\int_{-\infty}^{\infty} S_x(f)|H_{02}(f)|^2 df}{\int_{-\infty}^{\infty} S_x(f) df} \tag{37}$$

The evaluation of (37) will be carried out based upon the following three assumptions. First, the equivalent lowpass transfer function of the notch filter is of the form

$$N(f) = 1 - \frac{(1-\alpha)}{[1+j(f/f_c)]} \qquad 0 \le \alpha \le 1 \tag{38}$$

$$f_c = B_N/2$$

---

[10] Brennan, L.E., *et al*, "Control-Loop Noise in Adaptive Array Antennas," IEEE *Trans AES*, vol. AES-7, no. 2, March 1971, pp. 254-262.

In (38), the parameter $\alpha = N(0)$ is a measure of the center frequency transmission of the notch filter ($-20 \log\alpha$ is the "notch depth" in dB), and $f_c = B_N/2$, where B_N is the 3 dB width of the notch filter stopband with $\alpha=0$. The second assumption made is that the channel transfer function $H_c(f)$ can be represented as an M-th degree polynomial in f over a specified interval $(-B/2, B/2)$.

$$H_c(f) = \sum_{m=0}^{M} C_m f^m = C_0+C_1 f+\ldots+C_M f^M \quad |f| \leq B/2 \qquad (39)$$

The final assumption invoked is that the power spectrum of x(t) is bandlimited, with bandwidth B, and constant over the interal $|f| \leq B/2$ defined in (39); consequently, $S_x(f)$ can be written as

$$S_x(f) = \begin{cases} \frac{P_0}{B} & |f| \leq B/2 \\ 0 & \text{elsewhere} \end{cases} \qquad (40)$$

From (37) and (40),

$$(R/T)_2 = \frac{1}{B} \int_{-B/2}^{B/2} |H_{02}(f)|^2 df \qquad (41)$$

To complete the evaluation of $(R/T)_2$ it is necessary to evaluate $\bar{W}_1$ and $\bar{W}_2$ using (30), (34), (35) and the notch filter and channel transfer functions (38) and (39). The composite transfer function $H_c(f)H_2(f)$ is then found and substituted into (41).

(2) Evaluation of the Steady State Weights

The covariance matrix entries of (34) are found as follows. First observe that

$$N(f) = 1 - \frac{(1-\alpha)}{[1+j(f/f_c)]} = 1 - \frac{(1-\alpha)(1-jf/f_c)}{1+(f/f_c)^2}$$

$$= 1 - \frac{(1-\alpha)}{1+(f/f_c)^2} + j(1-\alpha)\frac{f/f_c}{1+(f/f_c)^2} \qquad (42)$$

and

$$|N(f)|^2 = \frac{|(1+jf/f_c)-(1-\alpha)|^2}{|1+jf/f_c|^2} = \frac{\alpha^2+(f/f_c)^2}{1+(f/f_c)^2}$$

$$= 1 - \frac{(1-\alpha^2)}{[1+(f/f_c)^2]} \qquad (43)$$

Using (34), (40), (42) and (43), the K_{mn} are found to be

$$K_{11} = \int_{-B/2}^{B/2} \frac{P_0}{B}\, df = P_0 \tag{44}$$

$$K_{12} = \frac{P_0}{B} \int_{-B/2}^{B/2} \left\{1 - \frac{(1-\alpha)}{1+(f/f_c)^2}\right\} df$$

$$= \frac{2P_0}{B}\left[\frac{B}{2} - (1-\alpha) f_c \tan^{-1}\left(\frac{B}{2f_c}\right)\right]$$

$$= P_0\left[1-(1-\alpha)\,\frac{B_N}{B}\tan^{-1}\left(\frac{B}{B_N}\right)\right] \tag{45}$$

$$K_{21} = K_{12}^{*} = P_0\left[1-(1-\alpha)\,\frac{B_N}{B}\tan^{-1}\left(\frac{B}{B_N}\right)\right] \tag{46}$$

$$K_{22} = \frac{P_0}{B} \int_{-B/2}^{B/2} \left\{1 - \frac{(1-\alpha^2)}{1+(f/f_c)^2}\right\} df$$

$$= P_0\left[1-(1-\alpha^2)\frac{B_N}{B}\tan^{-1}\left(\frac{B}{B_N}\right)\right] \tag{47}$$

Define the variables

$$\gamma = B/B_N$$
$$\Delta = \frac{\tan^{-1}(\gamma)}{\gamma} \tag{48}$$

so that the K_{mn} can be written as

$$K_{11} = P_0 \tag{49a}$$

$$K_{12} = P_0[1-(1-\alpha)\Delta] \tag{49b}$$

$$K_{21} = P_0[1-(1-\alpha)\Delta] \tag{49c}$$

$$K_{22} = P_0[1-(1-\alpha^2)\Delta] \tag{49d}$$

Using (49) in (30) gives

$$\begin{bmatrix} \bar{W}_1 \\ \bar{W}_2 \end{bmatrix} = -\frac{1}{(1+G_1K_{11})(1+G_2K_{22})-G_1G_2K_{12}K_{21}} \cdot \begin{bmatrix} 1+G_2P_0[1-(1-\alpha^2)\Delta] & -G_1P_0[1-(1-\alpha)\Delta] \\ -G_2P_0[1-(1-\alpha)\Delta] & 1+G_1P_0 \end{bmatrix} \begin{bmatrix} G_1L_1 \\ G_2L_2 \end{bmatrix} \tag{50}$$

or

$$\bar{W}_1 = \frac{-G_1L_1\{1+G_2P_0[1-(1-\alpha^2)\Delta]\} + G_1G_2P_0L_2[1-(1-\alpha)\Delta]}{1+G_1P_0+G_2P_0[1-(1-\alpha^2)\Delta] + G_1G_2P_0^2(1-\alpha)^2\Delta(1-\Delta)} \tag{51a}$$

$$\bar{W}_2 = \frac{G_1G_2P_0L_1[1-(1-\alpha)\Delta] - G_2L_2(1+G_1P_0)}{1+G_1P_0+G_2P_0[1-(1-\alpha^2)\Delta] + G_1G_2P_0^2(1-\alpha)^2\Delta(1-\Delta)} \tag{51b}$$

From (35), (39), (40) and (42), we obtain

$$L_1 = \frac{P_0}{B}\int_{-B/2}^{B/2}\sum_{m=0}^{M} C_m f^m df$$

$$= \frac{P_0}{B}\sum_{m=0}^{M} C_m \int_{-B/2}^{B/2} f^m df \tag{52a}$$

and

$$L_2 = \frac{P_0}{B}\int_{-B/2}^{B/2} N^*(f)\sum_{m=0}^{M} C_m f^m df$$

$$= \frac{P_0}{B}\sum_{m=0}^{M} C_m \int_{-B/2}^{B/2} f^m N^*(f) df \tag{52b}$$

Since two-channel ICS is expected to cancel first and second order terms (m=0 and m=1), the principal remaining term is m=2. Thus, the summation will be taken up to M=2.

$$L_1 = C_0P_0 + C_2P_0(B^2/12) \tag{53a}$$

$$L_2 = C_0P_0[1-(1-\alpha)\Delta] - jC_1P_0(1-\alpha)(1-\Delta)B_N/2$$

$$+ C_2P_0\left[1 - \frac{3(1-\alpha)(1-\Delta)}{\gamma^2}\right] B^2/12 \tag{53b}$$

Inserting (53) into (51) then results in

$$\bar{W}_1 = -C_0\frac{G_1G_2P_0^2(1-\alpha)^2\Delta(1-\Delta)+G_1P_0}{D}$$

$$-jC_1\frac{B_N}{2}\frac{G_1G_2P_0^2(1-\alpha)(1-\Delta)[1-(1-\alpha)\Delta]}{D}$$

$$+C_2\frac{B^2}{12}\frac{G_1G_2P_0^2\{[1-(1-\alpha)\Delta][1-\frac{3(1-\alpha)(1-\Delta)}{\gamma^2}]-[1-(1-\alpha^2)\Delta]\}-G_1P_0}{D} \tag{54a}$$

$$\bar{W}_2 = -C_0 \frac{G_2P_0[1-(1-\alpha)\Delta]}{D} + j\,C_1 \frac{B_N}{2} \frac{(1+G_1P_0)G_2P_0(1-\alpha)(1-\Delta)}{D}$$

$$+C_2 \frac{B^2}{12} \frac{G_1G_2P_0^2[1-(1-\alpha)\Delta]-G_2P_0(1+G_1P_0)[1-\frac{3(1-\alpha)(1-\Delta)}{\gamma^2}]}{D} \quad (54b)$$

where

$$D \triangleq 1+G_1P_0+G_2P_0[1-(1-\alpha^2)\Delta]+G_1G_2P_0^2(1-\alpha)^2\Delta(1-\Delta) \quad (54c)$$

(3) Evaluation of the Composite Transfer Function

Now that the values for the weights have been determined using the notch filter transfer function N(f) of (38), the composite transfer function will be determined. This determination will be made using the power series expansion of $H_c(f)$ in (39), along with the weight values in (54) and a similar power series expansion of N(f). We can expand (38) as

$$N(f) = 1 - \frac{(1-\alpha)}{1+j(f/f_c)}$$

$$= \alpha+j(1-\alpha)(f/f_c)+(1-\alpha)(f/f_c)^2-j(1-\alpha)(f/f_c)^3+\ldots$$

$$\text{for } |f/f_c|<1 \quad (55)$$

Since we confine our attention to the frequency range $|f| \leq B/2$, the convergence condition in (55) is satisfied when

$$\gamma = B/B_N<1 \quad (56)$$

where $B_N = 2f_c$ is the two-sided 3 dB bandwidth of the notch filter.

The composite transfer function is then determined from (36), (39) and (55) to be

$$H_{02}(f) = H_c(f)+H_2(f) = H_c(f)+\bar{W}_1+\bar{W}_2N(f)$$

$$\approx h_{02}+h_{12}(f/f_c)+h_{22}(f/f_c)^2 \quad (57)$$

where the coefficients h_{12} are given by

$$h_{02} = C_0 + \bar{W}_1 + \alpha\bar{W}_2$$

$$h_{12} = (C_1B_N)/2 + j(1-\alpha)\bar{W}_2$$

$$h_{22} = (C_2B_N^2)/4 + (1-\alpha)\bar{W}_2 \quad (58)$$

Because it is the design objective of the two-channel ICS to cancel the zero-th order and first-order terms (i.e., $h_{02}, h_{12} \rightarrow 0$),

$H_{02}(f)$ is approximated by the power series expansion truncated after the square term.

The final results for h_{02}, h_{12}, h_{22} are found by substitution of (54) in (58) and are given below:

$$D = G_1G_2P_0^2(1-\alpha)^2\Delta(1-\Delta) + G_1P_0+G_2P_0[1-(1-\alpha^2)\Delta] + 1 \qquad (59)$$

$$h_{02} = C_0 \frac{G_2P_0(1-\alpha)(1-\Delta)+1}{D}$$

$$-j \frac{C_1B_N}{2} \frac{(1-\alpha)(1-\Delta)G_2P_0[G_1P_0(1-\alpha)(1-\Delta)-\alpha]}{D}$$

$$-C_2 \frac{B^2}{12} \frac{\frac{3}{\gamma^2}G_1G_2P_0^2(1-\alpha)^2(1-\Delta)^2+G_1P_0+\alpha G_2P_0[1-\frac{3(1-\alpha)(1-\Delta)}{\gamma^2}]}{D} \qquad (60)$$

$$h_{12} = -jC_0 \frac{(1-\alpha)G_2P_0[1-(1-\alpha)\Delta]}{D}$$

$$-C_1 \frac{B_N}{2} \frac{G_1G_2P_0^2(1-\alpha)^2(1-\Delta)^2-(1+G_1P_0)+\alpha G_2P_0[\alpha(1-2\Delta)-2(1-\Delta)]}{D}$$

$$+j(1-\alpha)C_2 \frac{B^2}{12} \frac{G_1G_2P_0^2[1-(1-\alpha)\Delta]-G_2P_0(1+G_1P_0)[1-\frac{3(1-\alpha)(1-\Delta)}{\gamma^2}]}{D} \qquad (61)$$

$$h_{22} = -C_0 \frac{(1-\alpha)G_2P_0[1-(1-\alpha)\Delta]}{D} + jC_1 \frac{B_N}{2} \frac{(1-\alpha)^2(1+G_1P_c)G_2P_0(1-\Delta)}{D}$$

$$+C_2 \frac{B_N^2}{4} \frac{G_1G_2P_0^2(1-\alpha)^2(1-\Delta^2)+1+G_1P_0+G_2P_0[2(1-\Delta)+\alpha(2\Delta-\alpha)]}{}$$

$$- \frac{\gamma^2}{} \frac{(1-\alpha)G_2P_0[1+(1-\alpha)G_1P_0\Delta]}{D} \qquad (62)$$

(4) Simplified Results for the Dual Channel ICS

The purpose of this section is to introduce design requirements that allow the two-channel ICS to approach optimum performance. It has been shown [11] that the optimum weight vector that minimizes the mean-square ICS output is given by

---

[11] Widrow, B., *et al*, "Adaptive Antenna Systems," *Proc* IEEE, vol. 55, no. 12, December 1967, pp. 2143-2159.

$$W^0 = \begin{bmatrix} K_{11} & K_{12} \\ K_{21} & K_{22} \end{bmatrix}^{-1} \begin{bmatrix} -L_1 \\ -L_2 \end{bmatrix} \tag{63}$$

which may be obtained from (30) by letting G_1 and G_2 approach ∞.

The coefficients of the optimum composite transfer function given in (60), (61) and (62) then become

$$h_{02}^0 = -j\,\frac{C_1 B_N}{2}\left(\frac{1-\Delta}{\Delta}\right) - \frac{C_2 B^2}{12}\left(\frac{3}{\gamma^2}\right)\left(\frac{1-\Delta}{\Delta}\right)$$

$$h_{12}^0 = -\frac{C_1 B_N}{2}\left(\frac{1-\Delta}{\Delta}\right) + jC_2\,\frac{B^2}{12}\,\frac{\frac{3}{\gamma^2}(1-\Delta)-\Delta}{\Delta(1-\Delta)}$$

$$h_{22}^0 = j\,\frac{C_1 B_N}{2}\left(\frac{1-\Delta}{\Delta}\right) + \frac{C_2 B_N^2}{4}\,\frac{[1-\Delta^2-\Delta\gamma^2/3]}{\Delta(1-\Delta)} \tag{64}$$

If we require that

$$1-\Delta \ll 1 \tag{65}$$

then

$$\frac{\gamma^2}{3} \simeq 1-\Delta \tag{66}$$

and

$$h_{02}^0 \simeq -(C_2+j2C_1/B_N)B^2/12$$

$$h_{12}^0 \simeq j(C_2+j2C_1/B_N)B^2/12 \tag{67}$$

$$h_{22}^0 \simeq (C_2+j2C_1/B_N)B_N^2/4$$

It is desirable to determine how large G_1 and G_2 must be for the approximations in (67) to be valid. It may be seen that if, in addition to (65), the following requirements are imposed:

$$\begin{aligned} &0<\alpha\ll 1 \\ &G_1P_0 \gg 1 \\ &(1-\Delta)G_2P_0 \gg 1 \\ &G_1P_0(1-\Delta) \gg \alpha \\ &G_2P_0(1-\Delta)^2 \gg \alpha^2 \end{aligned} \tag{68}$$

we then obtain from (60), (61) and (62)

$$h_{02} \simeq \frac{C_0}{G_1 P_0} + h_{02}^0$$

$$h_{12} \simeq -j \frac{C_0}{G_1 P_0} + h_{12}^0 \qquad (69)$$

$$h_{22} \simeq -\frac{C_0}{G_1 P_0} + h_{22}^0$$

If we assume that the gain in channel #1, G_1, is large enough so that

$$\left|\frac{C_0}{G_1 P_0}\right| << \left|C_2 + j \frac{2C_1}{B_N}\right| \frac{B^2}{12} \qquad (70)$$

then

$$h_{02} \simeq -(C_2 + j2C_1/B_N)B^2/12$$

$$h_{12} \simeq j(C_2 + j2C_1/B_N)B^2/12 \qquad (71)$$

$$h_{22} \simeq (C_2 + j2C_1/B_N)B_N^2/4$$

The isolation obtainable by a two-channel ICS is then determined from (41) and (57) to be

$$(R/T)_2 \simeq \frac{1}{B} \int_{-B/2}^{B/2} |h_{02} + h_{12}(f/f_c) + h_{22}(f/f_c)^2|^2 \, df \qquad (72)$$

Using (71) in (72) results in

$$(R/T)_2 \simeq \left|C_2 + j \frac{2C_1}{B_N}\right|^2 B^4/180 \qquad (73)$$

where the coefficients C_i were introduced in the power series expansion of the channel transfer function $H_C(f)$ given in Eq. (39).

(5) Single-Channel ICS Results - A Special Case of the Two-Channel ICS Results

Corresponding results for the single-channel canceller, in which the notch filter channel is omitted, are obtained by setting $G_2=0$ in the formulas (54), (60), (61) and (62) derived for the dual-channel canceller.

For the transmit power spectrum and channel model considered, these weight values are

$$\bar{W}_1 = -\frac{G_1P_0}{1+G_1P_0}\left(C_0+C_2\frac{B^2}{12}\right) \tag{74}$$

$$\bar{W}_2 = 0$$

The coefficients of the power series expansion of the composite transfer function become

$$h_{01} = \frac{C_0}{1+G_1P_0} - \frac{C_2B^2}{12}\frac{G_1P_0}{1+G_1P_0}$$

$$h_{11} = C_1\frac{B_N}{2} \tag{75}$$

$$h_{21} = C_2\frac{B_N^2}{4}$$

The coefficients h_{01}, h_{11}, h_{21} used here for the single-channel ICS correspond to h_{02}, h_{12}, h_{22} used previously for the two-channel ICS. The composite transfer function is

$$H_{01}(f) \simeq \left[\frac{C_0}{1+G_1P_0} - C_2\frac{B^2}{12}\frac{G_1P_0}{1+G_1P_0}\right] + C_1f + C_2f^2 \quad |f| \le \frac{B}{2} \tag{76}$$

where $H_{01}(f)$ is used for the single-channel ICS inplace of $H_{02}(f)$ used for the two-channel ICS.

If we require that

$$G_1P_0 >> 1$$

and

$$\frac{C_0}{1+G_1P_0} << \frac{C_2B^2}{12} \tag{77}$$

we have

$$H_{01}(f) \simeq -\frac{C_2B^2}{12} + C_1f + C_2f^2 \quad |f| \le \frac{B}{2} \tag{78}$$

The isolation achievable from the single-channel ICS is then determined by inserting (78) into

$$(R/T)_1 = \frac{1}{B}\int_{-B/2}^{B/2} |H_{01}(f)|^2\,df \tag{79}$$

to obtain

$$(R/T)_1 \simeq |C_1|^2\frac{B^2}{12} + |C_2|^2\frac{B^4}{180} \tag{80}$$

c. Multichannel ICS Performance in Reflecting Terrain

We now consider the case of the SFR operating in an environment with multiple reflectors, and we will determine the achievable transit-to-receive isolation. The coupling transfer function is given by

$$H_c(f) = \sum_i a_i e^{j\phi_i} e^{-j2\pi f\tau_i} \tag{81}$$

where a_i, ϕ_i and τ_i are the gain, phase shift and delay of the i-th reflection path. Expanding (81) in a Taylor Series expansion gives

$$H_c(f) = \sum_i a_i[1-j2\pi\tau_i f - 2\pi^2\tau_i f^2+\ldots] \tag{82}$$

consequently,

$$C_1 = -j2\pi\sum_i a_i\tau_i e^{j\phi_i}$$

$$C_2 = -2\pi^2\sum_i a_i\tau_i^2 e^{j\phi_i} \tag{83}$$

Using (83) in (80) gives, for the single-channel ICS,

$$(R/T)_1 \simeq \frac{\pi^2B^2}{3}\left|\sum_i a_i\tau_i e^{j\phi_i}\right|^2 + \frac{\pi^4B^4}{45}\left|\sum_i a_i\tau_i^2 e^{j\phi_i}\right|^2, \quad \text{for } \pi B\tau_{max}<<1$$

$$\simeq \frac{\pi^2B^2}{3}\left|\sum_i a_i\tau_i e^{j\phi_i}\right|^2, \quad \text{for } \pi B\tau_{max}<<1 \tag{84}$$

Using (83) in (73) gives, for the two-channel ICS,

$$(R/T)_2 \simeq \frac{\pi^4B^4}{45}\left|\sum_i a_i\tau_i(\tau_i - \frac{2}{\pi B_N})e^{j\phi_i}\right|^2, \quad \text{for } \pi B\tau_{max}<<1 \tag{85}$$

In (84) and (85) τ_{max} is equal to the largest of the τ_i. The transmit-to-receive isolation which would be present without the ICS is determined from (2) and (81) to be

$$(R/T)_0 = \frac{1}{B}\int_{-B/2}^{B/2}\left|\sum_i a_i e^{j\phi_i} e^{-j2\pi f\tau_i}\right|^2 df \tag{86}$$

which is valid for all values of $\pi B\tau_i$. When $\pi B\tau_i>1$, the ICS cannot provide significant cancellation because there is no longer appreciable correlation of the reference with the delayed return. Hence,

$$(R/T)_2 \simeq (R/T)_1 \simeq (R/T)_0 \quad \text{for } \pi B\tau_i>1 \tag{87}$$

when $\pi B\tau_i>1$ for all values of i.

(1) Single Dominant Specular Reflector

When the terrain is dominated by a single specular reflector, we have from (84), (85), (86) and (87)

$$(R/T)_0 = a^2 \tag{88}$$

$$(R/T)_1 = \begin{cases} \pi^2 a^2 B^2 \tau^2/3, & \text{for } \pi B\tau << 1 \\ a^2, & \text{for } \pi B\tau > 1 \end{cases} \tag{89}$$

$$(R/T)_2 = \begin{cases} \pi^4 a^2 B^4 \tau^2 (\tau - \frac{2}{\pi B_N})^2/45, & \text{for } \pi B\tau << 1 \\ a^2, & \text{for } \pi B\tau > 1 \end{cases} \tag{90}$$

The attenuation suffered by the signal returned from the specular reflector is determined from the radar equation [12]

$$a^2 = \frac{\lambda^2 G^2 \sigma}{(4\pi)^3 r^4} \tag{91}$$

where λ is the carrier wavelength in meters
G is the numerical value of the SFR antenna gain toward the reflector
σ is the radar cross-section of the reflector in meters^2
r is the one-way range to the reflector in meters

We can relate the range r in meters directly to the delay τ in seconds by

$$r = c\tau/2 \tag{92}$$

where $c = 3 \times 10^8$ meters/second.

Applying (91) and (92) to (88), (89), and (90) gives

$$(R/T)_0 = \frac{G^2 \sigma}{4\pi^3 c^2 f_0^2 \tau^4} \tag{93}$$

$$(R/T)_1 = \begin{cases} \frac{G^2 \sigma}{12\pi c^2 \tau^2} (B/f_0)^2, & \text{for } \pi B\tau << 1 \\ (R/T)_0, & \text{for } \pi B\tau > 1 \end{cases} \tag{94}$$

$$(R/T)_2 = \begin{cases} \frac{\pi G^2 \sigma}{180 c^2} B^2 (\frac{B}{f_0})^2 (1 - \frac{2}{\pi B_N \tau})^2, & \text{for } \pi B\tau << 1 \\ (R/T)_0, & \text{for } \pi B\tau > 1 \end{cases} \tag{95}$$

---

[12] Skolnik, M.I., *Introduction to Radar Systems*, McGraw-Hill Book Co., New York, 1962, Eq. 1.10b.

An asymptotic sketch of these three equations as functions of τ is shown in Figure 9, comparing the isolation with no ICS, a one-channel ICS, and a two-channel ICS. τ_{min} is used to represent a delay (range) closer than which no specular reflectors are present. These curves show the relative performance of a zero, one, and two-channel ICS for a specular reflector of fixed size σ as a function of its range (or delay).

The isolation achieved by a single-channel ICS in terrain with a single dominant specular reflector is plotted as a function of (B/f_0) with $G^2(\sigma/r^2)$ as a parameter in Figure 10 for $\pi B\tau<<1$. For $\tau<2/(\pi B_N)$, a two-channel ICS improves on the single-channel ICS by the ratio

$$\frac{(R/T)_2}{(R/T)_1} = \frac{4}{15}\left(\frac{B}{B_N}\right)^2 \tag{96}$$

For $2/\pi B_N<<\tau<1/\pi B$, the two-channel ICS performance is plotted in Figure 11.

(2) Continuous Clutter

For the continuous clutter environment with a single-channel ICS, we return to Equation (84), for which the summation is assumed to be operating over an extremely large number of scatterers, each of whose contributions are statistically independent with uniformly distributed phase. The squared magnitude of the sum in (84) then is a random variable with a probability distribution approaching an exponential and a mean value equal to the sum of the squared magnitudes of each contributor. Approximating the sum by its mean value, we have

$$(R/T)_1 \simeq \frac{\pi^2 B^2}{3} \sum_i a_i^2 \tau_i^2, \quad \text{for } \pi B\tau_{max}<<1 \tag{97}$$

Similarly,

$$(R/T)_1 \simeq \sum_i a_i^2, \quad \text{when } \pi B\tau_i>1 \text{ for all } i \tag{98}$$

Applying (91) and (92) to (97) and (98) gives

$$(R/T)_1 \simeq \frac{B^2G^2}{12\pi c^2 f_0^2} \sum_i \frac{\sigma_i}{\tau_i^2}, \quad \text{for } \pi B\tau_{max}<<1 \tag{99}$$

and

$$(R/T)_1 \simeq \frac{G^2}{4\pi^3 c^2 f_0^2} \sum_i \frac{\sigma_i}{\tau_i^4}, \quad \text{for all } i, \text{ where } \pi B\tau_i>1 \tag{100}$$

These results assume an azimuthally omnidirectional antenna for which the antenna gain is the same for each scatterer. The scatterer cross-section σ_i is now modelled as a constant area reflectivity σ_0 (dimensionless) times the differential area ΔA_i, so that

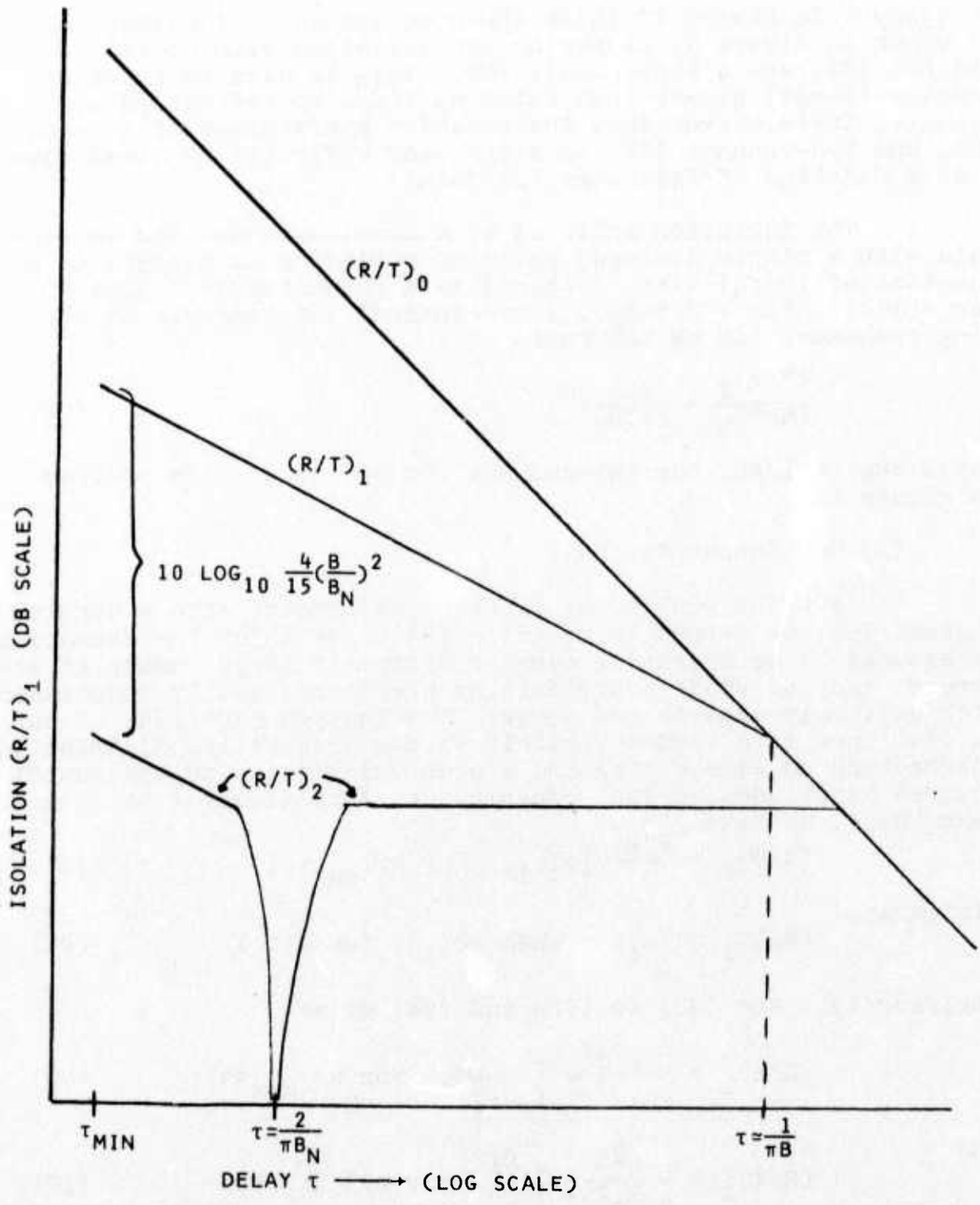

FIGURE 9

TRANSMIT-TO-RECEIVE ISOLATION WITH A SINGLE DOMINANT SPECULAR REFLECTOR VS ROUND-TRIP PROPAGATION DELAY

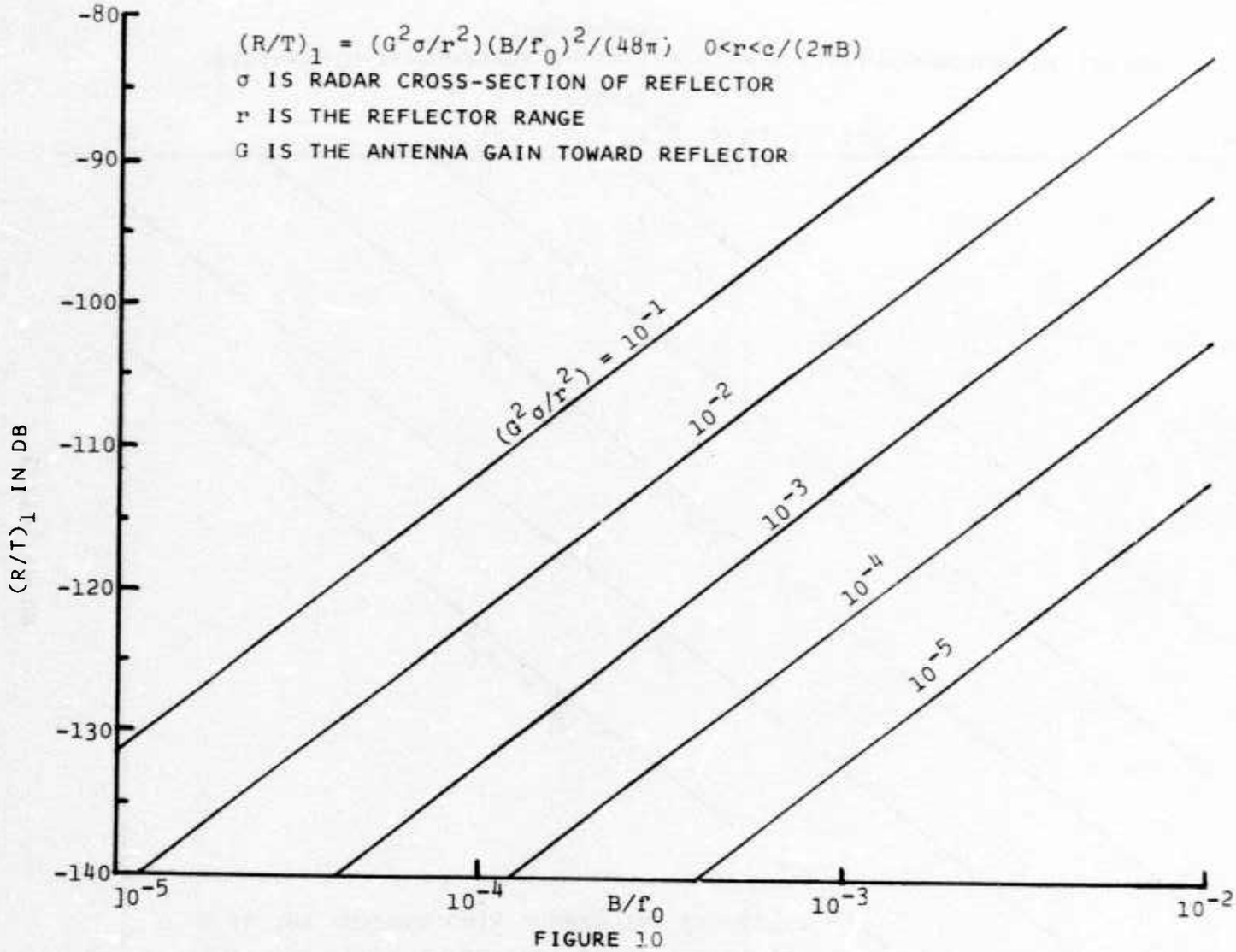

FIGURE 10

RECEIVER-TO-TRANSMITTER ISOLATION WITH A SINGLE SPECULAR REFLECTOR
(ONE-CHANNEL ICS)

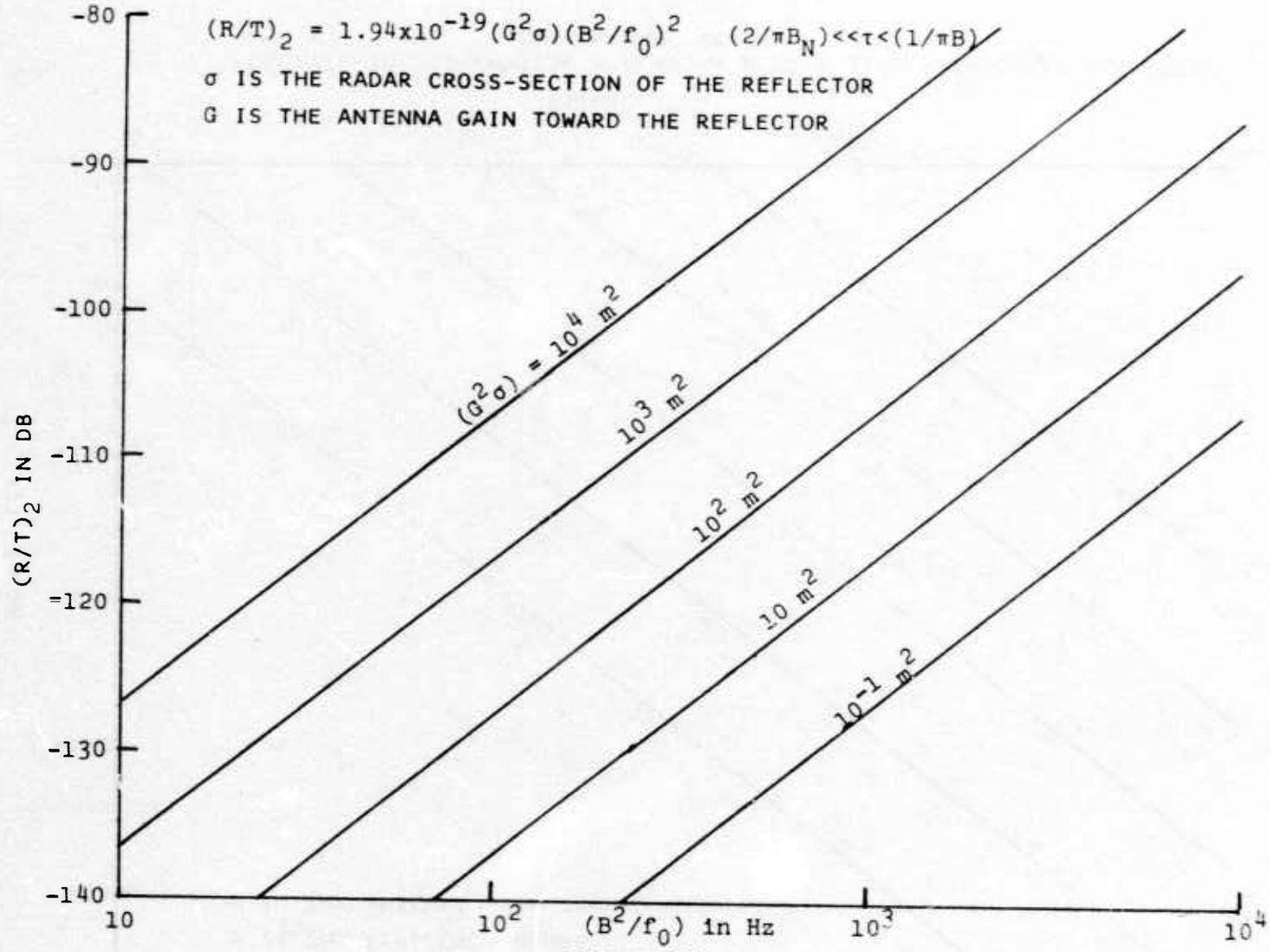

FIGURE 11

RECEIVER-TO-TRANSMITTER ISOLATION WITH A SINGLE SPECULAR REFLECTOR
(TWO-CHANNEL ICS)

$$\sigma_1 = \sigma_0 \Delta A_i$$
$$= \sigma_0 r_i \Delta r_i \Delta \psi_i$$
$$= \frac{c^2 \sigma_0}{4} \tau_i \Delta \tau_i \Delta \psi_i \qquad (101)$$

where ψ is the azimuthal angle. We will now approximate the summations in (99) and (100) by integration over the variables τ and ψ, using (99) for $\tau \leq 1/\pi B$ and (100) for $\tau > 1/\pi B$. Thus,

$$(R/T)_1 \simeq \frac{B^2 G^2 \sigma_0}{48\pi f_0^2} \int_{\tau_{min}}^{1/\pi B} \int_0^{2\pi} \frac{d\psi}{\tau} d\tau + \frac{G^2 \sigma_0}{16\pi^3 f_0^2} \int_{1/\pi B}^{\infty} \int_0^{2\pi} \frac{d\psi}{\tau^3} d\tau \qquad (102)$$

where τ_{min} is the round-trip propagation delay to the nearest scatterers. Evaluating the integrals gives

$$(R/T)_1 \simeq \frac{G^2 \sigma_0}{16} \left(\frac{B}{f_0}\right)^2 \left[1 + \frac{2}{3} \ln\left(\frac{1}{\pi B \tau_{min}}\right)\right] \qquad (103)$$

The reflectivity σ_0 is larger for ground clutter than for sea clutter [13], so that ground clutter will be used as a worst-case environment. From [13], we use

$$\sigma_0 = 3.2 \times 10^{-4} / \lambda$$
$$= 1.07 \times 10^{-12} f_0 \qquad (104)$$

Inserting (104) into (103) gives

$$(R/T)_1 \simeq 6.67 \times 10^{-14} G^2 \left(\frac{B}{f_0}\right) B \left[1 + \frac{2}{3} \ln\left(\frac{1}{\pi B \tau_{min}}\right)\right] \qquad (105)$$

where f_0 = the carrier frequency in Hz
B = the signal bandwidth in Hz
τ_{min} = the round-trip propagation delay to the nearest scatterers in seconds
G = the numerical value of the antenna gain.

Following a similar development for the two-channel ICS in a clutter environment, we have from (85), (91) and (92),

$$(R/T)_2 \simeq \frac{\pi B^4 G^2}{180 c^2 f_0^2} \sum_i \frac{\sigma_i}{\tau_i^2} \left(\tau_i - \frac{2}{\pi B_N}\right)^2, \quad \text{for } \pi B \tau_i \ll 1 \qquad (106)$$

and

---

[13] Barton, D.K. and H.R. Ward, *Handbook of Radar Measurement*, Prentice-Hall Book Co., 1968, p. 138.

$$(R/T)_2 \simeq \frac{1}{4\pi^3 c^2 f_o^2} \sum_i \frac{G^2}{\tau_i^2}, \quad \text{for } \pi B\tau_i > 1 \tag{107}$$

Passing to the integral approximations, we have

$$(R/T)_2 \simeq \frac{\pi B^4 G^2 \sigma_0}{720 f_0^2} \int_{\tau_{min}}^{1/\pi B} \int_0^{2\pi[\tau-(2/\pi B_N)]^2} \frac{}{\tau} d\psi d\tau$$

$$+ \frac{G^2\sigma_0}{16\pi^3 f_0^2} \int_{1/\pi B}^{\infty} \int_0^{2\pi} \frac{d\psi}{\tau^3} d\tau \tag{108}$$

Using

$$\tau_{min} << \frac{2}{\pi B_N} << \frac{1}{\pi B} \tag{109}$$

evaluation of the integrals results in

$$(R/T)_2 \simeq \frac{G^2\sigma_0}{16}\left(\frac{B}{f_0}\right)^2\left[1 + \frac{8}{45}\left(\frac{B}{B_N}\right)^2 \ln\left(\frac{1}{\pi B\tau_{min}}\right)\right] \tag{110}$$

Finally, applying (104) to (110) results in

$$(R/T)_2 \simeq 6.67\text{x}10^{-14} G^2 \left(\frac{B}{f_0}\right) B\left[1 + \frac{8}{45}\left(\frac{B}{B_N}\right)^2 \ln\left(\frac{1}{\pi B\tau_{min}}\right)\right] \tag{111}$$

d. Antenna Effects on the Multichannel ICS

The SFR antenna, being a tuned device, will reflect the transmitted signal with a reflection coefficient that is frequency dependent. The antenna is modelled by a resonant circuit shown in Figure 12. The reflection coefficient for this model is given by

$$\rho(\omega) = \frac{Z_{in}-R}{Z_{in}+R} = \frac{(X_C+X_L)^2+2jR(X_C+X_L)}{4R^2+(X_C+X_L)^2} \tag{112}$$

where $X_L = \omega L$ and $X_C = -\omega C$. Note that at center frequency $\omega_0 = 1/\sqrt{LC}$, the antenna is matched so that $\rho(\omega_0) = 0$.

As done previously, we will expand $\rho(\omega)$ in a Taylor series about ω_0, and determine the single-channel and two-channel ICS performance from the coefficients of $H_c(f)$, where $H_c(t) = \rho(2\pi[f+f_0])$

$$C_1 = 2\pi\rho'(\omega_0)$$
$$C_2 = 2\pi^2\rho''(\omega_0) \tag{113}$$

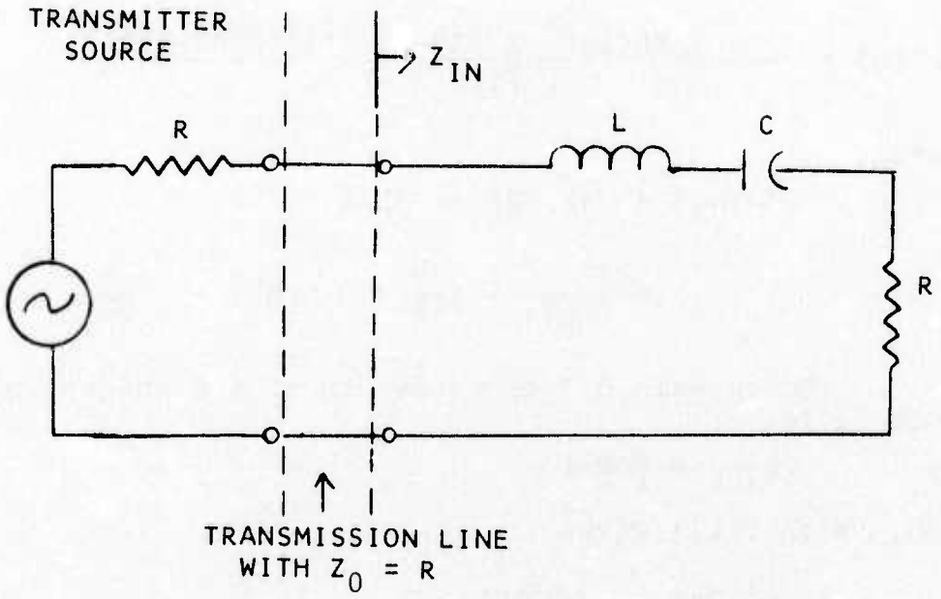

FIGURE 12

RESONANT CIRCUIT MODEL OF SFR ANTENNA

Differentiating (112) gives

$$\rho'(\omega) = \frac{8R^2XX' + 2jRX'(4R^2 - X^2)}{(4R^2+X^2)^3} \tag{114}$$

where

$$X = X_C + X_L = -1/\omega C + \omega L \tag{115}$$

Differentiating (114) gives

$$\rho''(\omega) = \frac{8R^2\{(4R^2+X^2)[(X')^2+XX''] - 4X^2(X')^2\}/(4R^2+X^2)^3}{2jR[(16R^4-X^4)X'' - X(X')^2(20R^2-3X^2)]} \tag{116}$$

$$(4R^2+X^2)^3$$

At $\omega=\omega_0$,

$$\rho'(\omega_0) = jX'/2R = jL/R$$

$$\rho''(\omega_0) = \frac{(X')^2}{2R^2} - j\frac{X''}{2R} = 2(L/R)^2 - j\frac{L}{R\omega_0} \tag{117}$$

The two-sided 3 dB bandwidth of the antenna model in Figure 12 is

$$B_{ant} = \frac{1}{\pi}(R/L) \tag{118}$$

which, with (117) gives

$$\rho'(\omega_0) = j\frac{1}{\pi B_{ant}}$$

$$\rho''(\omega_0) = \frac{2}{\pi^2 B_{ant}^2} - j\frac{1}{\pi B_{ant}\omega_0}$$

$$\simeq \frac{2}{\pi^2 B_{ant}^2}, \quad \text{for } B_{ant} << \omega_0 \tag{119}$$

Inserting (119) into (113) gives

$$C_1 = j^2/B_{ant}$$

$$C_2 = 4/B_{ant}^2 \tag{120}$$

Using (120) in (73) with $B/B_{ant} << 1$ gives

$$(R/T)_1 \approx |C_1|^2 B^2/12 + |C_2|^2 B^4/180$$

$$\approx \frac{1}{3}(B/B_{ant})^2 + \frac{4}{45}(B/B_{ant})^4$$

$$\approx \frac{1}{3}(B/B_{ant})^2 \qquad (121)$$

for the single-channel ICS. Using (120) in (80) with $B/B_{ant} << 1$ gives

$$(R/T)_2 \approx |C_2 + j2(C_1/B_N)|^2 B^4/180$$

$$= \frac{4}{45}(B/B_{ant})^4[(B_{ant}/B_N)-1]^2 \qquad (122)$$

for the two-channel ICS.

e. Numerical Examples

(1) Single-Channel ICS

Let us consider a single-channel ICS with the following design parameters:

$f_0 = 3 \times 10^8$ Hz
$B = 10^5$ Hz
$G = 1$
$B_{ant} = 5 \times 10^7$ Hz

We assume the following environmental conditions:

$(\sigma/r^2)_{max} = 10^{-1}$ for dominant specular reflector
$\tau_{min} = 20$ ns (closest reflectors 10 feet away)

Using Figure 10, the isolation achievable with the specular reflector is

$$(R/T)_1 = -101 \text{ dB (specular reflector)} \qquad (123)$$

The isolation achievable in the presence of ground clutter is determined from (105) to be

$$(R/T)_1 \approx -110 \text{ dB (ground clutter)} \qquad (124)$$

The isolation limitation due to the antenna reflection is

$$(R/T)_1 = -59 \text{ dB (antenna reflection)} \qquad (125)$$

It is clear from the above results that the antenna is the limiting factor.

(2) Two-Channel ICS

We now consider a two-channel ICS with the following design parameters:

$f_0 = 3 \times 10^8$ Hz
$B = 10^5$ Hz
$G = 1$
$B_{ant} = 5 \times 10^7$ Hz
$B_N = 5 \times 10^6$ Hz

} same as for single-channel ICS example

We assume the following environmental conditions:

$(\sigma/r^2)_{max} = 10^{-1}$ for nearby dominant specular reflector ($\tau < 2/\pi B_N$)

$\sigma = 10^3$ meters^2 for distant dominant specular reflector ($\tau > 2/\pi B_N$)

$\tau_{min} = 20$ ns (closest reflectors 10 feet away)

From Equation (96) and Figure 10 the isolation achievable with the nearby specular reflector is

$$(R/T)_2 = -140 \text{ dB (nearby specular reflector)} \quad (126)$$

The isolation achievable with the distant specular reflector is determined from Figure 11 to be

$$(R/T)_2 = -127 \text{ dB (distant specular reflector)} \quad (127)$$

The isolation achievable in the presence of ground clutter is determined from (111) to be

$$(R/T)_2 = -116.5 \text{ dB (ground clutter)} \quad (128)$$

The isolation limitation due to the antenna reflection is

$$(R/T)_2 = -99 \text{ dB (antenna reflection)} \quad (129)$$

Once again the antenna is the limiting factor, but the achievable isolation of the two-channel ICS is 40 dB better than that for the single-channel ICS.

f. Discussion of Analytical Results

In both the one-channel and the two-channel ICS numerical results, the antenna reflection is the major limitation to the amount of achievable transmitter-to-receiver isolation. However, the isolation with the two-channel ICS is about 40 dB better than with the one-channel ICS.

An attempt has been made to anticipate the analytical results for a three-channel ICS by examining the results for the one- and two-channel ICS's. It is anticipated that the antenna reflection limitation would drop by approximately another 40 dB from that for the two-channel ICS. However, almost no improvement is expected on the limitation imposed by ground

clutter, since the primary ground clutter contributions for the two-channel ICS are beyond the range for which $\pi B\tau=1$. Thus, ground clutter becomes the major limiting factor for the three-channel ICS, allowing transmitter-to-receiver isolation of about -117 dB. The same limitation holds for any multichannel ICS with more than three channels.

With a design goal of 120 dB for SFR forward gain, conservative design requires transmit-to-receive isolation well below -120 dB. The above results, although approximate, leave doubt whether 120 dB of useful forward gain is achievable at 300 MHz with a 100 kHz bandwidth in a ground-based situation. Since the achievable isolation is close to -120 dB, the SFR breadboard design will incorporate a three-channel ICS with 120 dB forward gain capability to allow future field testing of SFR operation with the full gain capability.

2. MULTICHANNEL NOTCH FILTER ICS EXPERIMENT

A laboratory experiment was conducted early in the program to verify the multichannel notch filter ICS concept. The experiment used the General Atronics MX-200 two-channel VHF ICS developed previously on internal R&D funds.

The MX-200 was constructed with two identical channels, intended for cancelling two independent interferences simultaneously. For this experiment, the reference input to the second channel was obtained by passing the first channel reference input through a notch filter and amplifiers. In this way a two-channel notch filter ICS was synthesized with the intention of improved cancellation of a single broadband interference with delay, compared to that obtainable with a single-channel ICS.

The experimental setup is shown in Figure 13. The interference was provided by a sinusoidally modulated FM signal generator operating at 125 MHz with a 600 kHz bandwidth. It is connected to the ICS antenna input through a delay of 200 feet of coaxial cable. It is supplied at high level to Reference #1 with no frequency shaping. The input to Reference #2 is shaped in frequency by a notch filter centered at 125 MHz with a bandwidth much greater than 600 kHz. Both an L-C notch and a quarter-wave delay line notch were used. Following the notch filter is 36 dB of gain. The ICS output is monitored on a spectrum analyzer.

The cancellation results for the L-C notch and the delay line notch were indistinguishable. Figure 14 shows the cancellation results by a sequence of spectrum analyzer photographs of the ICS output. The upper photo is the ICS output with References #1 and #2 disconnected, showing the uncancelled interference. The center photo shows the ICS output with only Reference #1 connected, the single-channel ICS configuration giving the expected M-shaped residue spectrum. The lower photo shows the ICS output with both References #1 and #2 connected.

The photos show a band edge cancellation ratio of 30 dB with the single-channel ICS and 55 dB with the two-channel ICS. As shown in Equations (88) and (89), cancellation in the single-channel ICS is proportional to $(B\tau)^2$, and in the two-channel ICS it is proportional to $(B\tau)^4$. That is, cancellation in dB with the two-channel ICS should be approximately double that with the single-channel ICS. The measured performance roughly verifies the improvement expected.

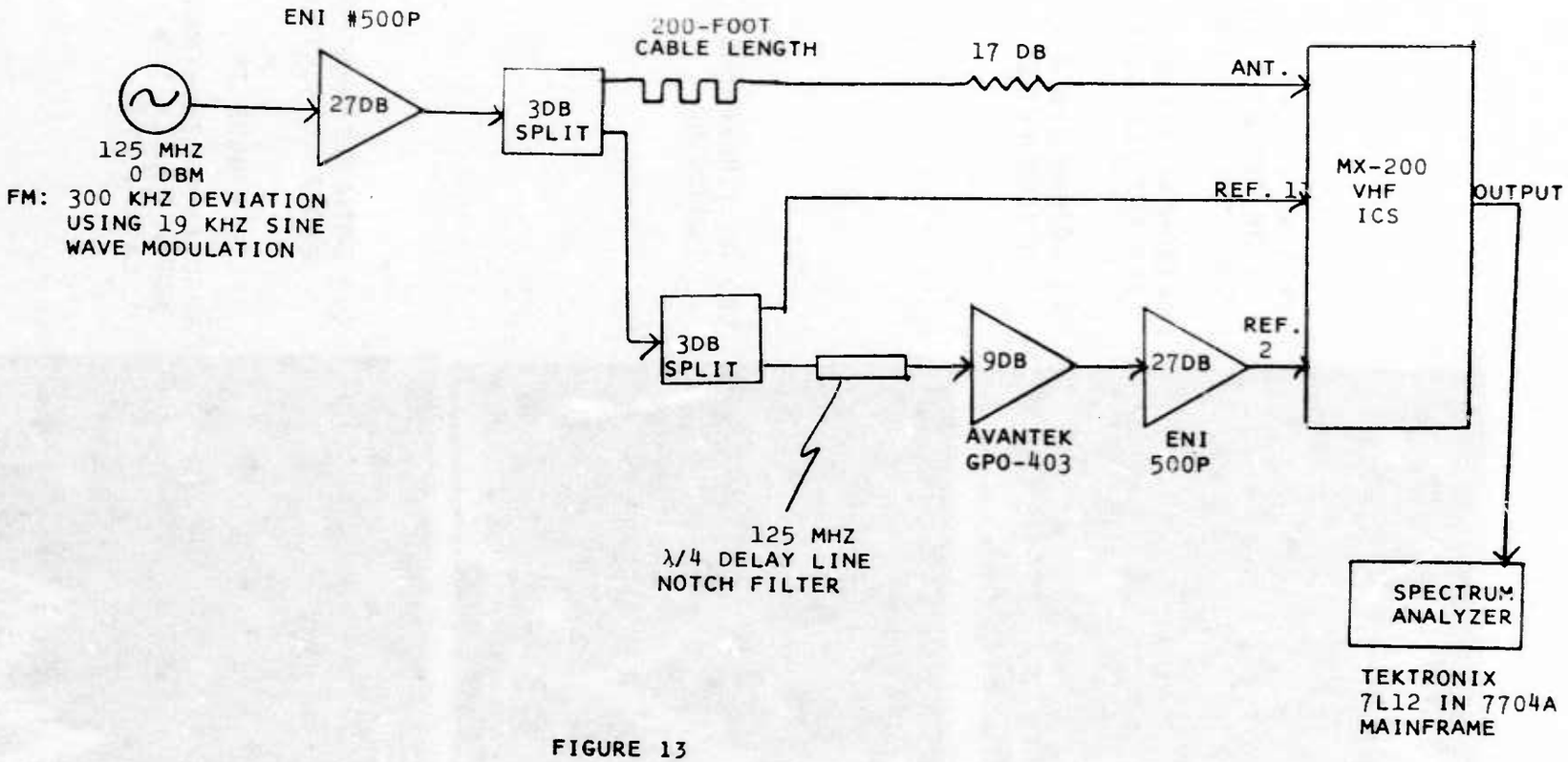

FIGURE 13

TWO-CHANNEL NOTCH FILTER ICS EXPERIMENTAL SETUP

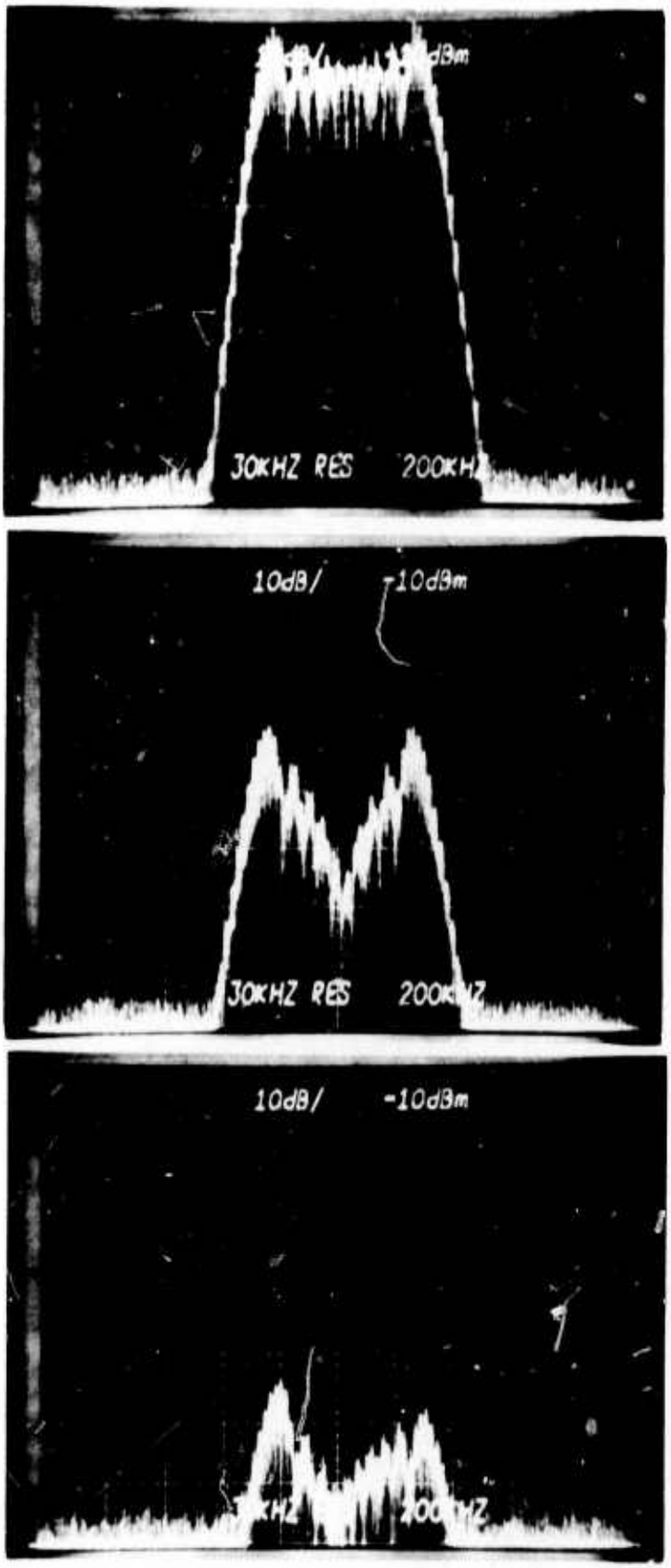

VERTICAL SCALE:
10 DB PER DIVISION
TOP LINE = 10 DBM

HORIZONTAL SCALE:
200 KHZ PER DIVISION

(A) REFERENCES 1 AND 2 DISCONNECTED

(B) ONLY REFERENCE 1 CONNECTED

(C) BOTH REFERENCES 1 AND 2 CONNECTED

FIGURE 14

RESULTS OF TWO-CHANNEL NOTCH FILTER ICS EXPERIMENT

SECTION III

PILOT-DIRECTED MULTICHANNEL ICS

1. SYSTEM CONCEPT

The multichannel ICS discussed in Section 2 derives its weight-control voltages by correlating the input to each weight with a feedback error signal which is proportional to the cancellation residue. An ICS designed in this fashion will provide the desired degree of cancellation in the presence of other input signals as long as those signals do not cause any significant output from the correlators in the weight control units. In the SFR application, the transmitted signal is essentially a delayed replica of the received signal. Thus, an undesired correlator output which causes errors in the weights and thereby degrades cancellation would be unavoidable.

The means to be used in this program to maintain ICS performance in the SFR is to use an additive pilot signal to control the ICS. The ICS thus is modified from the "transmit-signal-directed" form to a "pilot-directed" form. A block diagram showing the concept in a single-channel ICS is given in Figure 15.

A pilot signal is added to the transmitted signal before the directional tap is taken to provide the reference signal input to the complex weight. Instead of using this same reference signal as an input to the weight control unit (see Figure 1), the pilot signal alone is used. The weight control is based on the correlation of the ICS output with the pilot signal alone, rather than with the transmitted signal. The pilot signal must be designed to have low correlation with the received signal, and hence with the transmitted signal. The complex weight value W established by pilot direction is that which optimizes coupled pilot cancellation, and hence coupled signal cancellation as well.

When a pilot-directed multichannel notch filter ICS is used, the pilot supplied to the weight control units must undergo the same notch filter processing as the weight inputs do. A block diagram of the pilot-directed multichannel notch filter ICS is shown in Figure 16. The differences required by pilot direction may be seen by comparison with Figure 5.

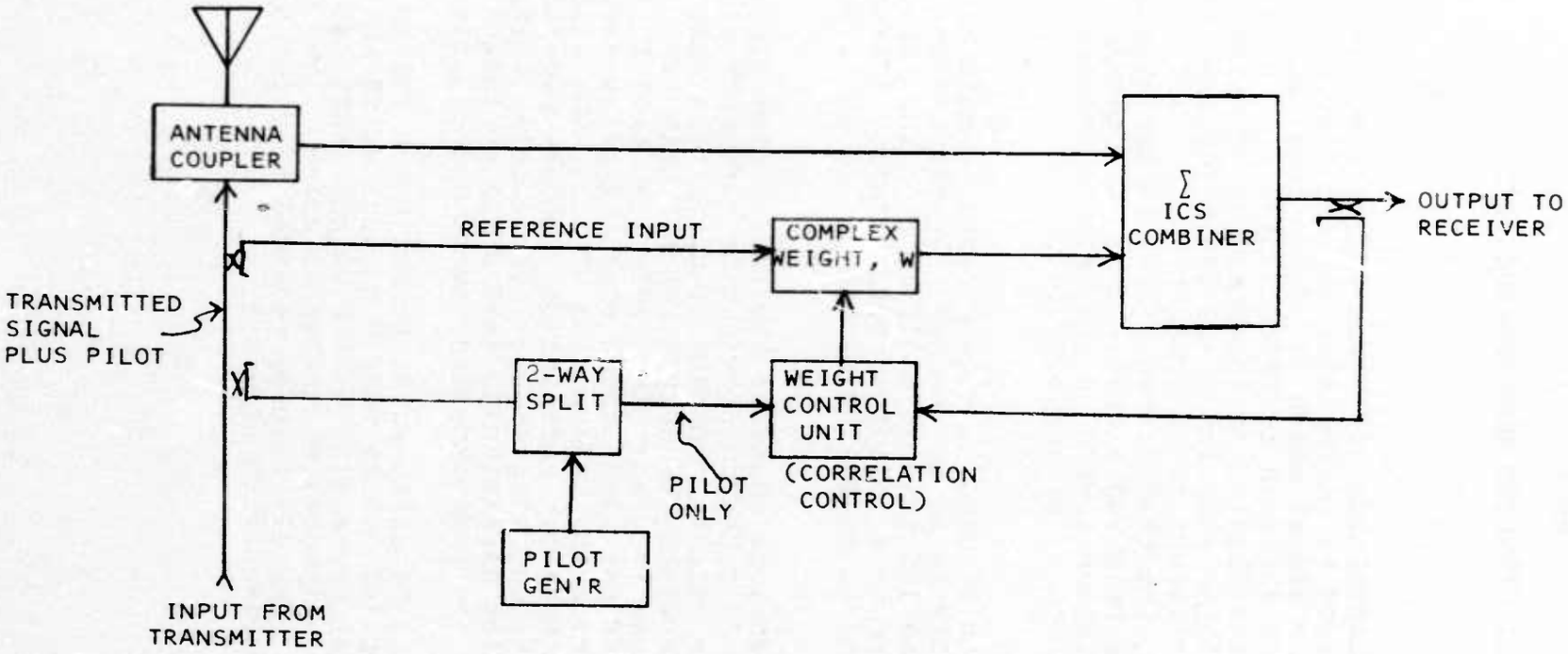

FIGURE 15

PILOT-DIRECTED SINGLE-CHANNEL ICS

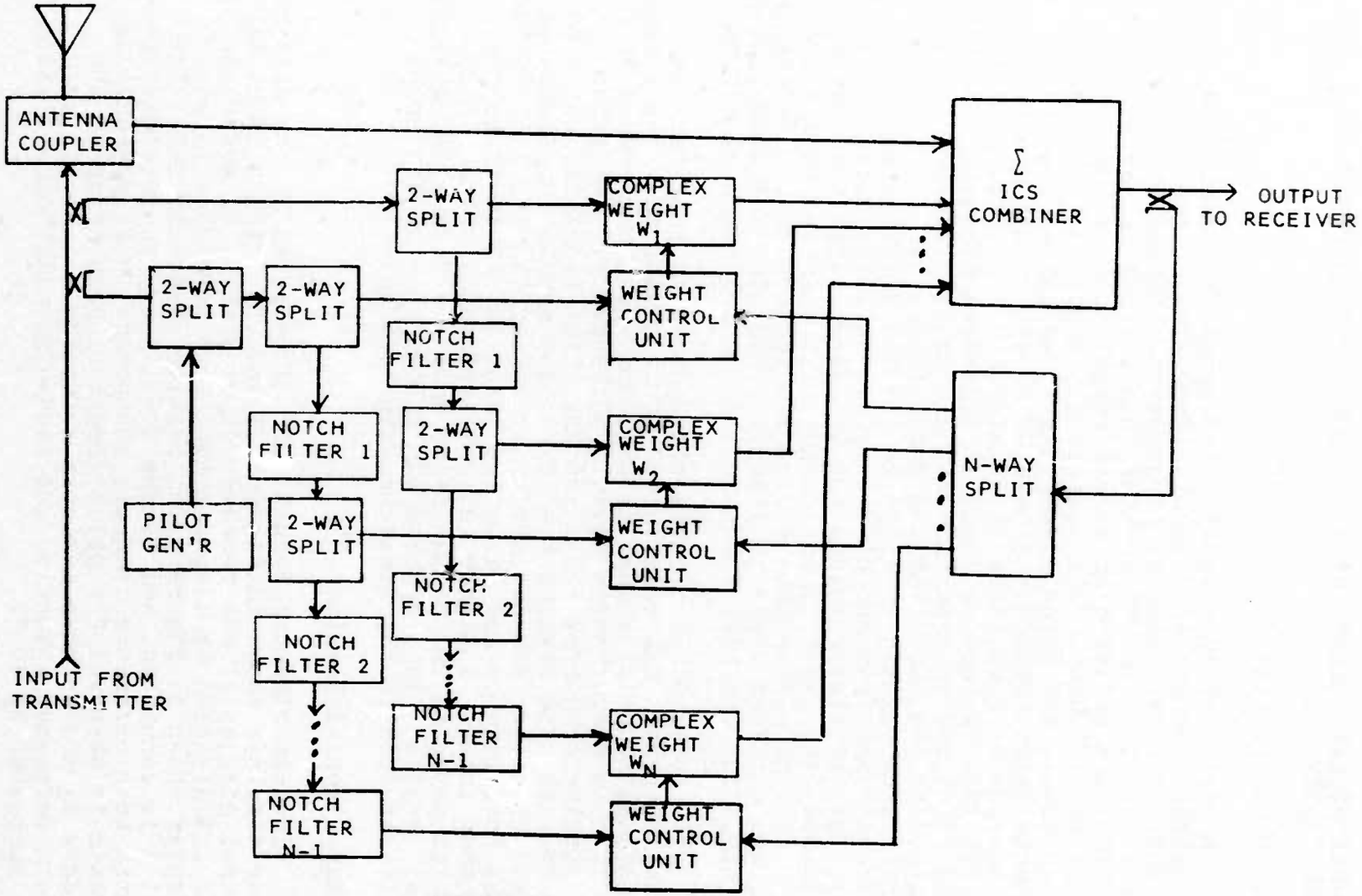

FIGURE 16

PILOT-DIRECTED MULTICHANNEL NOTCH FILTER ICS

2. LABORATORY EXPERIMENTS WITH A PILOT-DIRECTED TWO-CHANNEL NOTCH FILTER ICS

a. Test Description

A series of laboratory experiments have been conducted to demonstrate the use of a pilot signal with a two-channel notch filter ICS. The experimental arrangement utilized is shown in Figures 17 and 18. The MX-200 VHF Interference Cancellation System (ICS) was modified to permit correlation of the error signal at the ICS output with externally supplied pilot signals. The interference and pilot signal are added and applied to the ICS antenna input through a simulated coupling path consisting of the cascade of a variable attenuator and a 0.26 us delay coaxial cable (200 ft). Reference input 1 is derived directly from the combined pilot and interference signals while reference input 2 is obtained at the output of L-C notch filter no. 1. The correlator reference signals utilized in the ICS weight control circuits are derived from the pilot signal, as illustrated in Figure 17. The correlator inputs for the first reference channel are obtained directly from the output of the Anaren quadrature hybrid. The correlator inputs required for the second reference channel are obtained after additional processing using the notch filter-amplifier cascades shown in the lower portion of Figure 17.

The performance of this pilot-directed interference cancellation system has been tested for the case in which a frequency-modulated pilot signal is used and the interference is either CW or a pseudorandom noise (PN) waveform. The pilot signal carrier frequency = 141.185 MHz. The modulation is sinusoidal FM with peak deviation = 50 kHz and modulation frequency = 3 kHz. The interference carrier frequency is also 141.185 MHz and both interference and pilot are identical in level at the ICS antenna input. A higher level interference caused intermodulation products in the amplifier added in Figure 18, obscuring the test results. This problem can be overcome by different gain distribution in the final repeater design.

b. Experimental Results

The experimental results are illustrated by the spectrum analyzer displays shown in Figures 19 and 20. Figure 19(a) is a spectral display of the receiver input with CW interference and the ICS disabled by disconnecting both reference inputs. The display shown in Figure 19(b) results when only reference channel 1 is connected, and Figure 19(c) shows the residue spectrum with both reference channels connected. A 24 dB cancellation ratio is observed for pilot frequency components at the band edges f_1 and f_2 when a single reference channel is used; with both reference channels, the band edge pilot cancellation ratio increases to 46 dB.

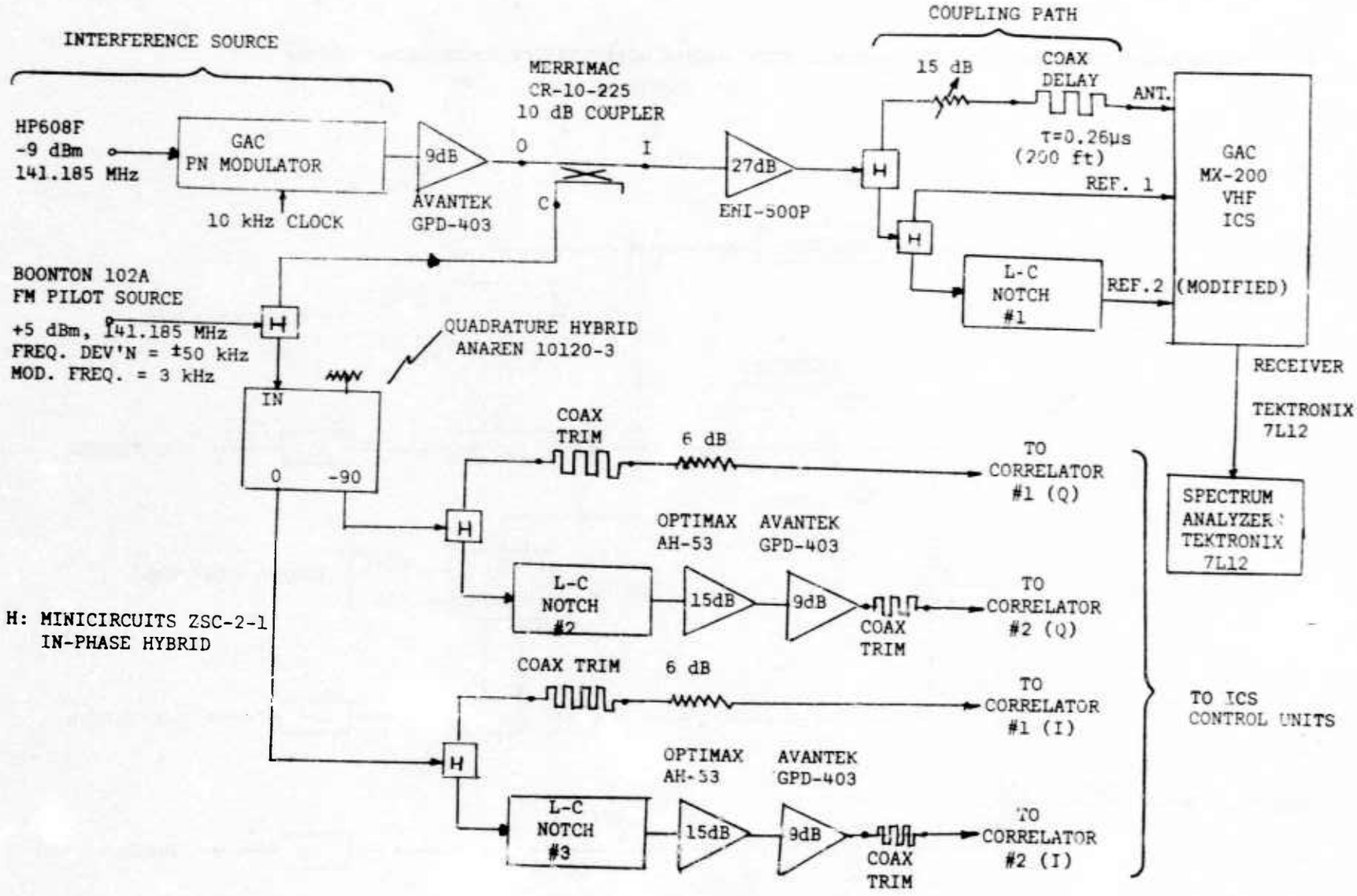

FIGURE 17
DUAL CHANNEL PILOT-DIRECTED INTERFERENCE CANCELLATION EXPERIMENT

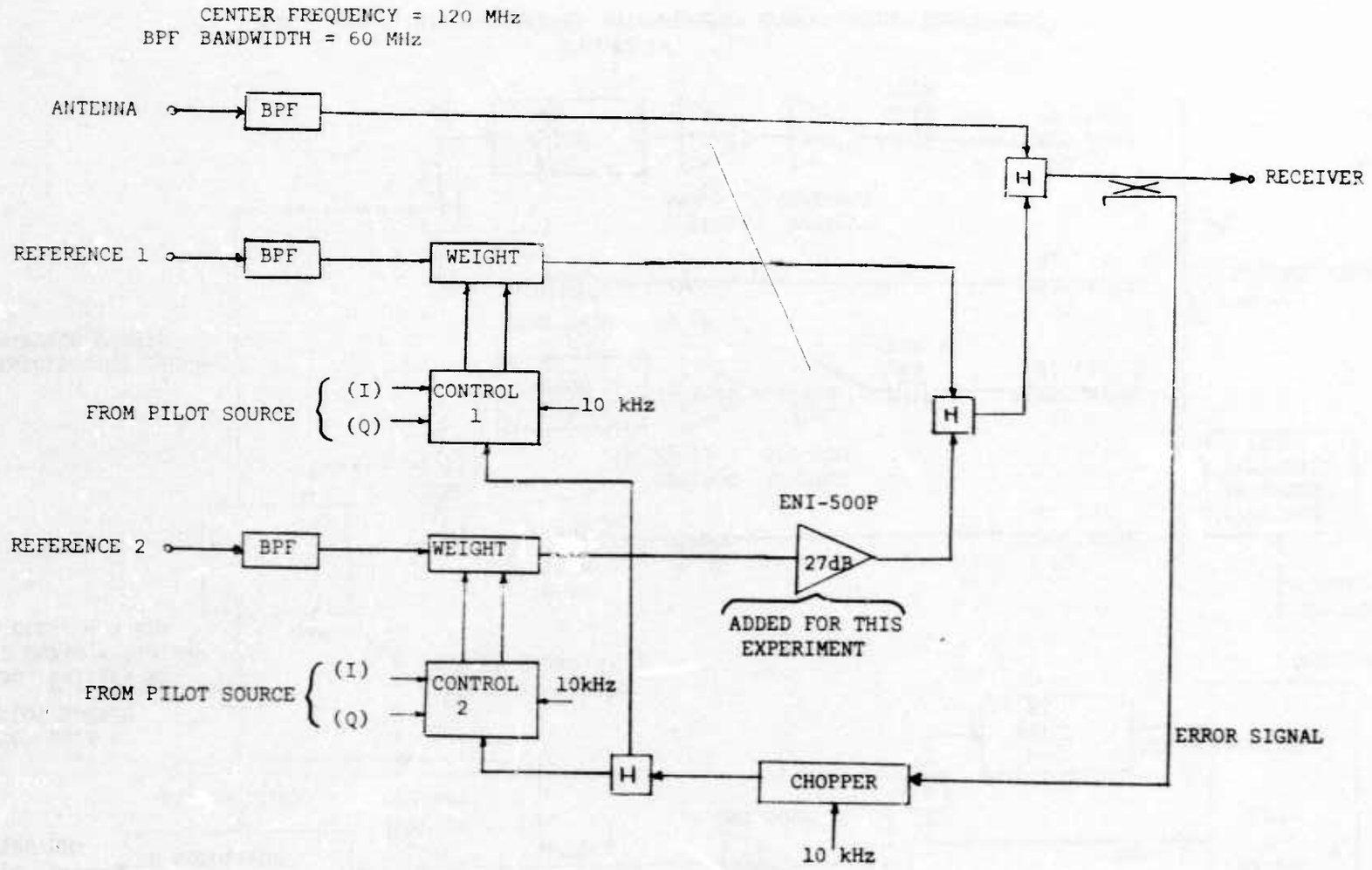

FIGURE 13

MX-200 INTERFERENCE CANCELLATION SYSTEM BLOCK DIAGRAM (MODIFIED FOR THIS EXPERIMENT)

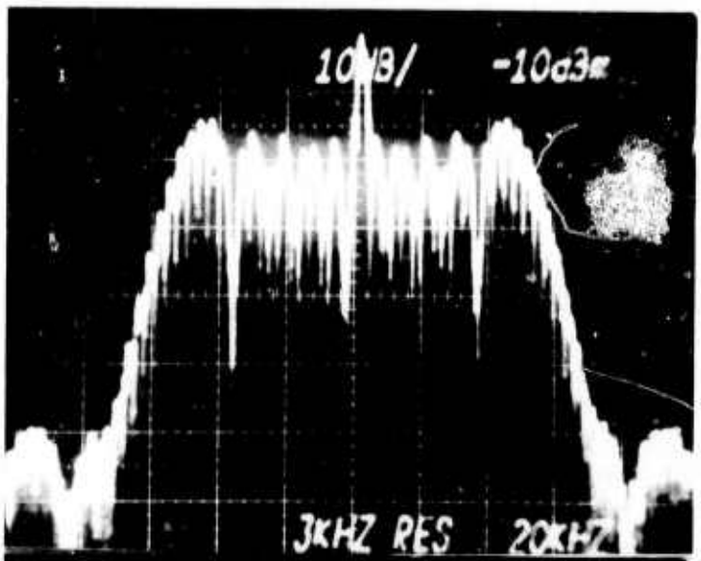

-10 DBM

VERTICAL: 10 DB/DIV

FIGURE 19(A)

CW INTERFERENCE + FM PILOT REFERENCE INPUTS DISCONNECTED (NO CANCELLATION)

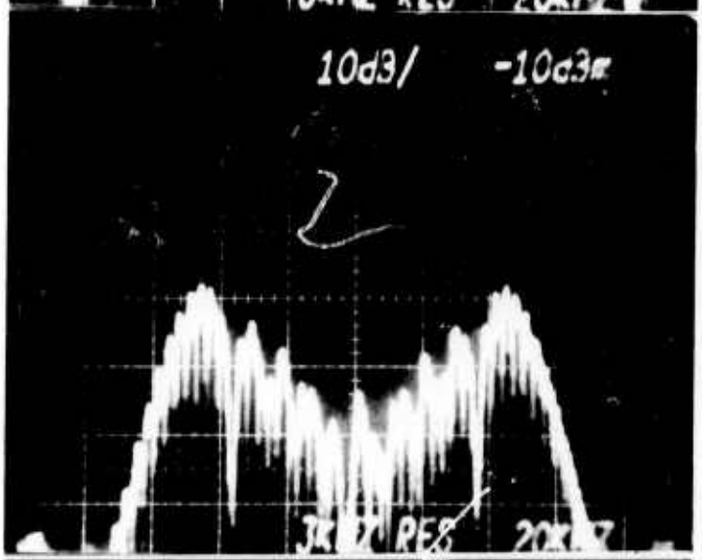

-10 DBM

FIGURE 19(B)

CW INTERFERENCE + FM PILOT REFERENCE 1 CONNECTED

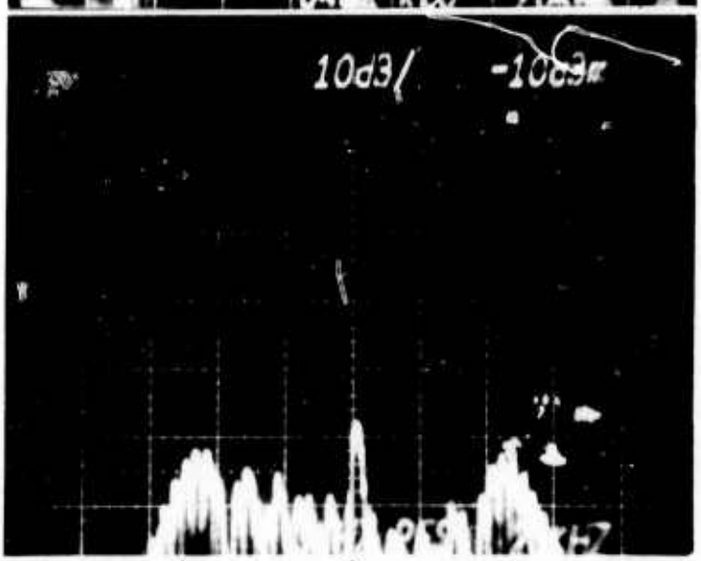

-10 DBM

FIGURE 19(C)

CW INTERFERENCE + FM PILOT BOTH REFERENCE CHANNELS CONNECTED

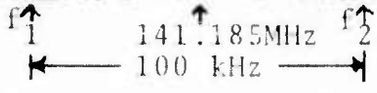

Similar results are shown in Figure 20 when the interference carrier is biphase modulated by a pseudorandom sequence at 20 kilobits/sec. The same FM waveform again is used as the pilot. In this case the band edge pilot cancellation ratio is 25 dB using reference channel 1 only and increases to 48 dB when both reference inputs are connected. It should be noted that at each frequency the interference spectral component is cancelled by the same amount as the pilot spectral component.

c. Conclusions

The results described provide experimental confirmation of the pilot-directed interference cancellation concept to be employed in the single frequency repeater design. The test results indicate that both pilot and interference signals are cancelled equally well. These results hold for both single and dual channel interference cancellation systems.

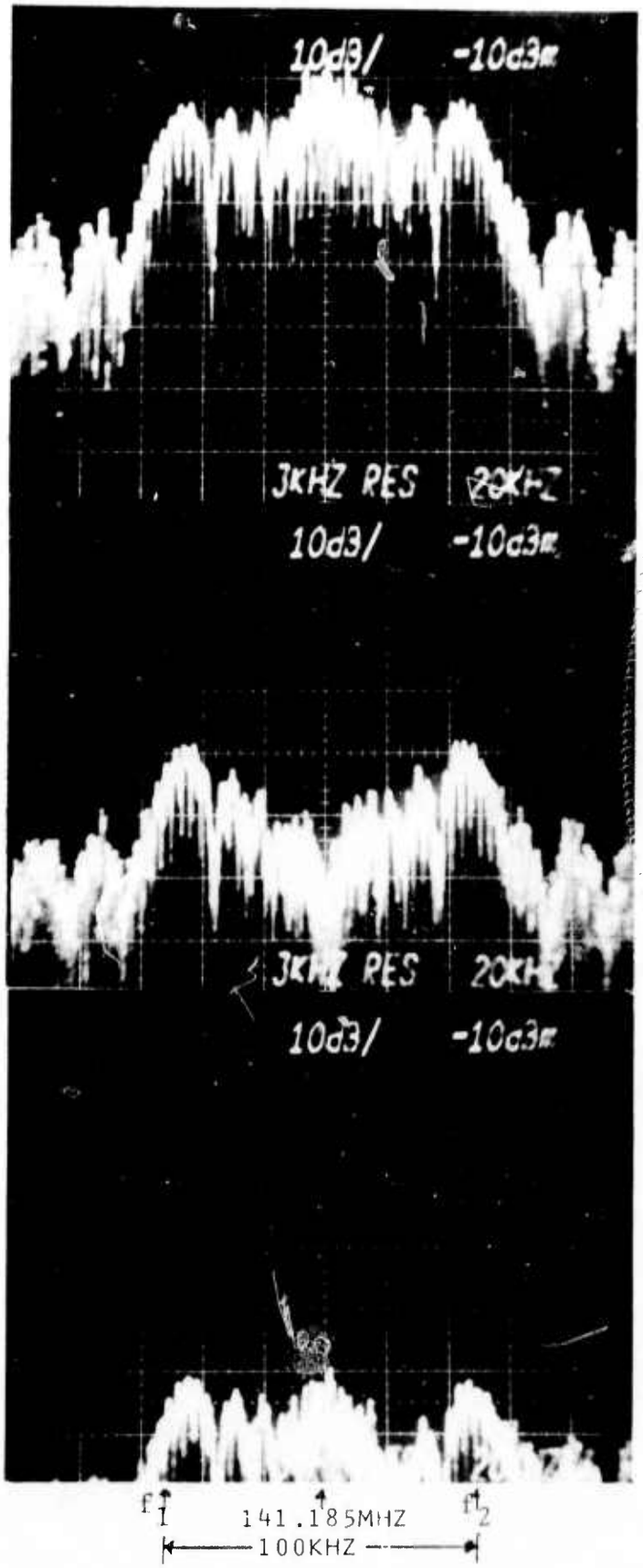

-10 DBM

VERTICAL: 10 DB/DIV

FIGURE 20(A)

PN* INTERFERENCE + FM PILOT REFERENCE INPUTS DISCONNECTED (NO CANCELLATION)

-10 DBM

FIGURE 20(B)

PN* INTERFERENCE + FM PILOT REFERENCE 1 CONNECTED

-10 DBM

FIGURE 20(C)

PN* INTERFERENCE + FM PILOT BOTH REFERENCE CHANNELS CONNECTED

*BIPHASE CARRIER MODULATION BY A PSEUDORANDOM SEQUENCE

SECTION IV

ICS WEIGHT LINEARITY

The complex weight circuit used in the ICS must be highly linear with respect to the reference input. Any nonlinearity will cause nonlinear distortion on the weighted interference which will not be cancelled. Nonlinear distortion in the complex weight thus has the same effect as limiting the achievable ICS cancellation. The level of in-band third-order intermodulation products resulting from a two-tone input is used here as a measure of nonlinear distortion caused by the weight.

The weight design intended for use in the SFR breadboard consists of two bipolar attenuators, one in each of two quadrature channels, as shown in Figure 21. Each bipolar attenuator is DC-controlled to effect amplitude scaling with or without phase inversion.

A PIN diode network has been developed at General Atronics for use as a bipolar attenuator. The circuit offers the following features: high power handling capability with low distortion, low return loss, and low minimum insertion loss. This section will review the efforts carried out to date on this program to minimize the nonlinear distortion in the PIN diode bipolar attenuator.

1. PIN DIODE DISTORTION THEORY

The resistance R_d of a PIN diode is controlled by a DC bias current I_{DC}, with the two approximately reciprocally related:

$$R_d = K_1/I_{DC} \tag{129}$$

where K_1 is a constant depending on the particular diode. Distortion in the diode monotonically increases with the distortion factor

$$F_D = I_{AC}/I_{DC} \tag{130}$$

where I_{AC} is the peak AC current through the diode. Low distortion performance requires that F_D be much less than the $f_0\tau_L$ product, where f_0 is the AC operating frequency and τ_L is the minority carrier lifetime of the diode.

Let us now consider a PIN diode network coupled to input and output by 1:n and n:1 impedance transformers, respectively. (See Figure 22) Let the source and load impedances be fixed, but let N be variable. Let us define the network attenuation as the ratio of the power delivered to the load divided by the maximum power available from the source. The attenuation can always be expressed in terms of ratios of impedances found in

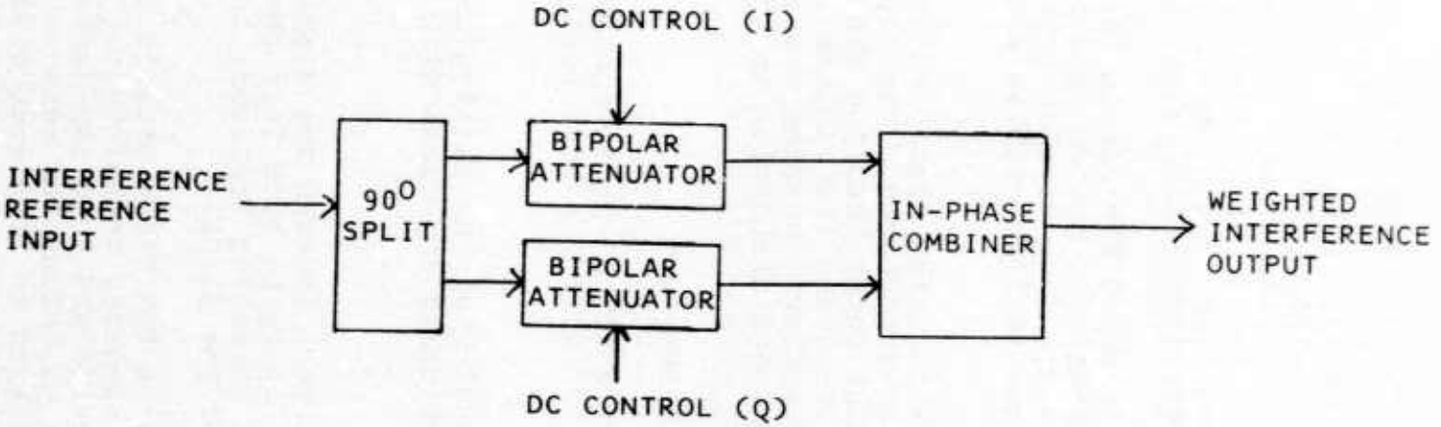

FIGURE 21
STRUCTURE OF COMPLEX WEIGHT

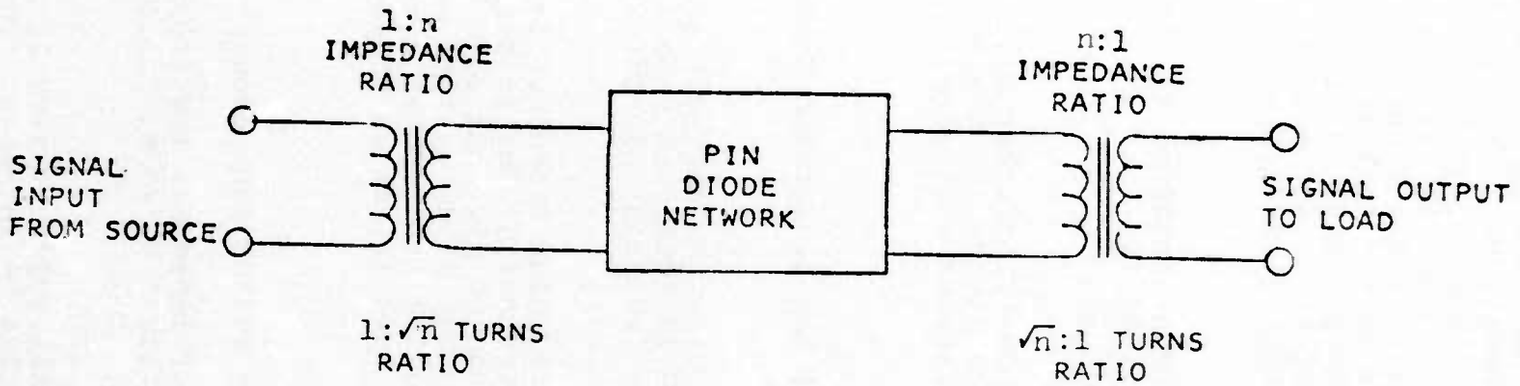

FIGURE 22

GENERAL PIN DIODE ATTENUATOR

the network, where the source and load impedances appear multiplied by the impedance transformation n. Thus, for the attenuation from input to output of Figure 22 to be constant as n varies, the resistance of every diode in the network must be proportional to n. For example, if the input transformer is changed from a 1:1 transformer to one that steps up the source impedance by 1:4, then the same attenuation is obtained if the diode resistances are increased by a factor of 4. Thus, R_d should be proportional to n for constant attenuation:

$$R_d = K_2 n \tag{131}$$

From (129) and (131), the DC current required to obtain the desired resistance in any particular diode is

$$I_{DC} = K_1/R_d = K_1/(K_2 n) \tag{132}$$

The 1:n input impedance transformer will step down the AC input current by $\sqrt{n}$. If the diodes are biased according to (132), then each diode in the network will carry an AC current proportional to $1/\sqrt{n}$, i.e.,

$$I_{AC} = K_3/\sqrt{n} \tag{133}$$

Thus, from (130), (132) and (133) the distortion factor is given by

$$F_D = K_2 K_3 \sqrt{n}/K_1 \tag{134}$$

Thus, we see that reducing F_D requires making n as small as possible. That is, the source impedance as seen by the diode network should be stepped down (AC-input current stepped up) for reduced distortion.

A second distortion-reducing technique is to replace each diode in the network by several diodes in series. If m identical series diodes are used to give the same total resistance, then the resistance of each diode must be reduced by n. This is accomplished by increasing its DC bias current by a factor of m. The AC current, however, is unchanged, so that F_D is proportional to 1/m, i.e.,

$$F_D \propto 1/m \tag{135}$$

Thus, distortion is reduced by adding more diodes in series.

The combined effect of impedance transformation and series diodes makes F_D proportional to $\sqrt{n}/m$, i.e.,

$$F_D \propto \sqrt{n}/m \tag{136}$$

As n is made very small and/or m very large, the minimum attenuation of the network begins to increase. That is, there is a tradeoff between minimum attenuation and distortion. There is also a tradeoff between drive power and distortion. These

two tradeoffs will set the eventual limit on how low the distortion can be made.

2. EXPERIMENTAL RESULTS

A number of experiments have been conducted to measure two-tone intermodulation in the PIN-diode circuit using various circuit modifications. Two different methods were used to isolate the third-order intermodulation product generated in the circuit to permit measurement of its level. One circuit was tested with both methods, and the results were substantially the same.

The first method is diagrammed in Figure 23, in which the third-order intermodulation product is isolated by cancellation. Two CW tones are generated, amplified, and combined so that each is at a level of +15 dBm at the D.U.T. input. Some of the D.U.T. input is tapped off in a 10 dB coupler to a path which is manually adjusted in phase and amplitude to cancel the D.U.T. output. In this way, the two tones and the intermods produced ahead of the D.U.T. are cancelled to a very low level at the input to the spectrum analyzer. This allows the intermods caused by the test setup to be at a very low level compared to those generated in the D.U.T., so that the intermods seen on the spectrum analyzer are those caused by the D.U.T. as long as they exceed the calibration level. The calibration level is found by replacing the D.U.T. with a 6 dB pad and manually adjusting phase and amplitude to cancel the test signals on the spectrum analyzer display.

The second method, diagrammed in Figure 24, uses filtering to isolate the third-order intermodulation product. The two tones are separated by 5 MHz, and their generators are isolated from each other by a hybrid combiner and by bandpass filters #1 and #2. The third-order intermodulation product is selected by bandpass filter #3 for display on the spectrum analyzer.

A summary of the worst-case intermodulation levels found from a two-tone test on the different bipolar attenuator implementations is given in Table 1. The first column shows the date on which each test was conducted. The second column refers to the test setup -- either Figure 23 or Figure 24. The third column of Table 1 describes the structure of the D.U.T. -- the type of input transformer used, the number of series diodes in each leg of the network and the diode type. The fourth column shows the principal test result -- the highest level of the output intermods over the full range of attenuation of the D.U.T.

Several conclusions can be drawn from these results. First, as long as the DC drive is optimized for low intermodulation performance at the frequency of operation, there is very little dependence on frequency in the 225 MHz to 400 MHz range.

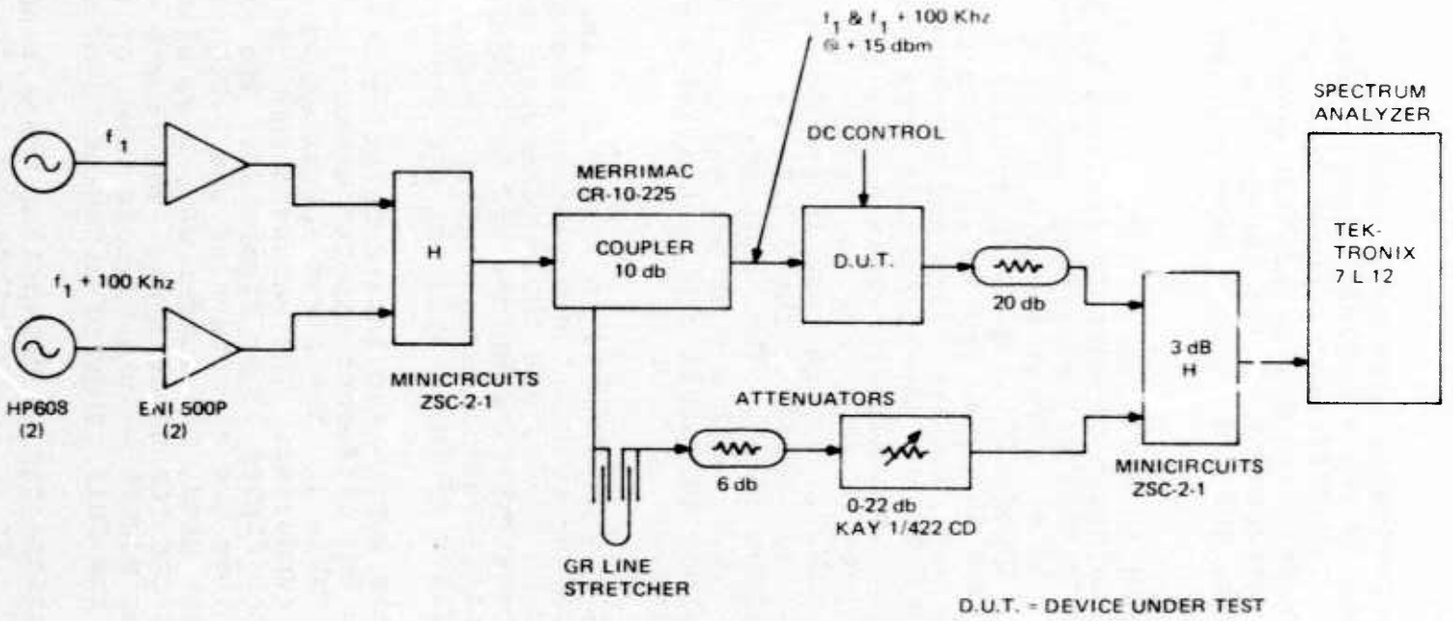

FIGURE 23

TEST SETUP BIPOLAR ATTENUATOR

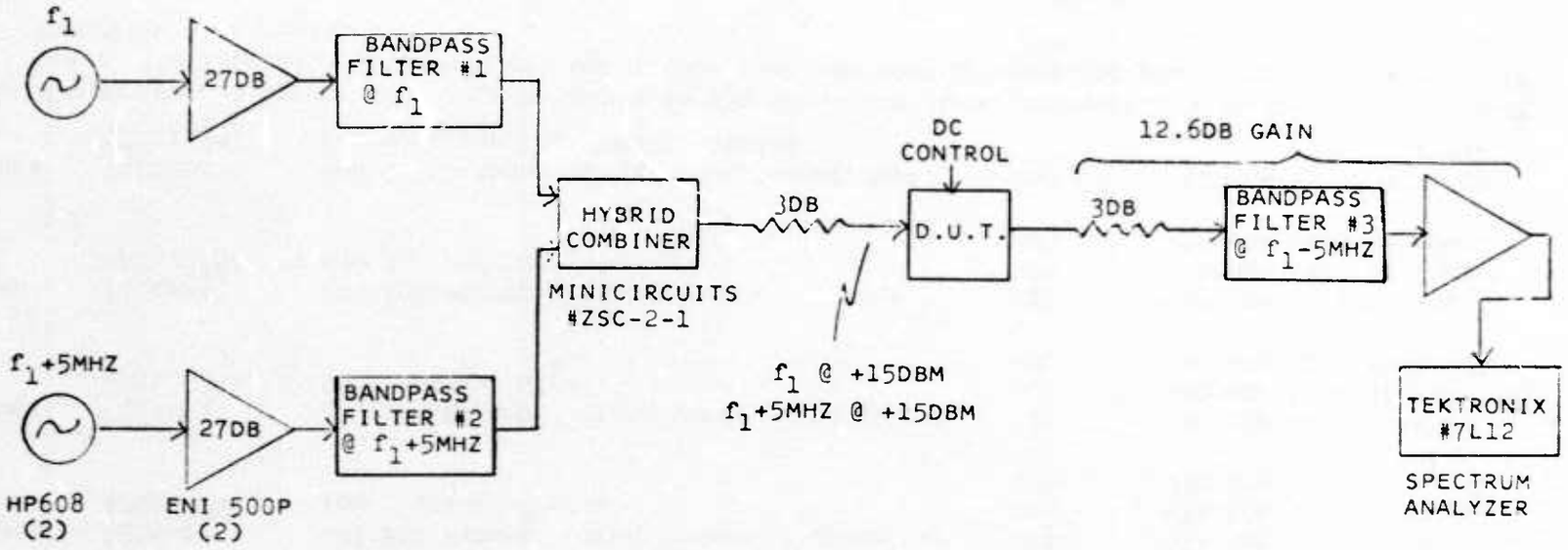

D.U.T. = DEVICE UNDER TEST

FIGURE 24

ALTERNATE TEST SETUP FOR BIPOLAR ATTENUATOR

TABLE 1
INTERMODULATION DISTORTION DATA SUMMARY FOR BIPOLAR ATTENUATOR

Test Data (1974)	Test Method	D.U.T. Structure	Test Frequency (MHz)	Output Intermod with Two-Tone Input, each +15 dBm
20 Aug	Canceller (Fig. 23)	50Ω:50Ω autotransformer, 1 diode per leg, DC driver with nonlinear shaping to optimize 300 MHz intermod performance. UM6601 diodes.	300 125 400	-71 dBm -47 dBm (not optimum drive) -67 dBm (not optimum drive)
27 Aug	Canceller (Fig. 23)	50Ω:12.5Ω transmission line transformer, 2 diodes per leg, optimized DC drive, UM6601 diodes.	260	-95 dBm
28 Aug	Filters (Fig. 24)	50Ω:12.5Ω transmission line transformer, 2 diodes per leg, optimized DC drive. UM6601 diodes	300	-95 dBm
5 Sept	Filters (Fig. 24)	50Ω:12.5Ω transmission line transformer, 1 diode per leg, optimized DC drive. UM6601 diodes	300	-86 dBm
17 Sept	Filters (Fig. 24)	50Ω:50Ω Ruthroff transformer, 1 diode per leg. UM6601 diodes.	225 300 400	-74 dBm -74 dBm -70 dBm
23 Sept	Filters (Fig. 24)	50Ω:50Ω Ruthroff transformer, 1 diode per leg. UM9303 dioes.	225 300 400	-87 dBm (1.8 dB min. -98 dBm (1.2 dB insertion -94 dBm (1.8 dB loss)
24 Sept	Filters (Fig. 24)	50Ω:50Ω Ruthroff transformer, 2 diodes per leg. UM9303 dioes,	225 300 400	-99 dBm (2.2 dB min. -106dBm (1.8 dB insertion -105dBm (1.8 dB loss)
26 Sept	Filters (Fig. 24)	50Ω:12.5Ω transmission line transformer, 2 diodes per leg. UM9303 diodes	260	-110dBm (5 dB min.ins. loss)

NOTE: The minimum insertion loss figures given in the table are those achievable with the circuit under test. The tabulated intermods are worst-case over the full attenuation range, not at the minimum insertion loss setting.

Secondly, the intermod products can be reduced by about 10 dB by using a 50Ω:12.5Ω input transformer instead of a 50Ω:50Ω transformer. (The same transformer with primary and secondary interchanged is used on the output as well.) Finally, the same 10 dB improvement can be gained by replacing each PIN diode by two PIN diodes in series and keeping the transformer fixed.

SECTION V

SFR SYSTEM DESIGN

The concepts described in the preceding sections form the basis for the formulation of the SFR block diagram. A conceptual block diagram of the SFR is given in Figure 25. It shows a single antenna used for both transmission and reception, with a 6 dB hybrid as the antenna coupler. The received signal passes through a single-channel pilot-directed ICS at RF. The RF ICS is expected to provide 55 dB of transmit-to-receive isolation, sufficient to allow RF amplification and RF-to-IF conversion with negligible distortion. An experiment with a simulated antenna supporting the 55 dB figure is described in Section V.2 below.

Following RF-to-IF conversion, the signal is amplified and inserted into a three-channel pilot-directed notch filter ICS at IF. At this point the full $(R/T)_3$ isolation is obtained. The signal then passes through an IF filter and amplifier with AGC for output level control. The detected video output of the amplifier is used to indicate signal presence to control the DC power supplied to the RF transmitter amplifier.

The pilot is generated at IF and added to the signal. It is also supplied to the IF ICS as well as to the RF ICS after up-conversion. The combined signal plus pilot are up-converted to RF and amplified to a 1 watt level for transmission.

A more detailed block diagram showing functional units is given in Figure 26. This diagram follows the form of Figure 25. The extra detail shows the distribution of gain throughout the system.

1. FEATURES OF THE SYSTEM DESIGN

The SFR has been designed to provide the following design features:

Operating frequency	300 MHz (nominal)
Bandwidth	100 kHz
Minimum detectable signal	-90 dBm
Signal-to-noise ratio for minimum detectable signal	+17 dB for 100 kHz bandwidth +23 dB for 25 kHz bandwidth
Forward gain on minimum signal	+120 dB
Output power level[1]	+30 dBm (PEP)
Input dynamic range	60 dB

[1] The output power level is expressed in terms of peak effective power since the AGC detector which controls the output power level is a peak detector.

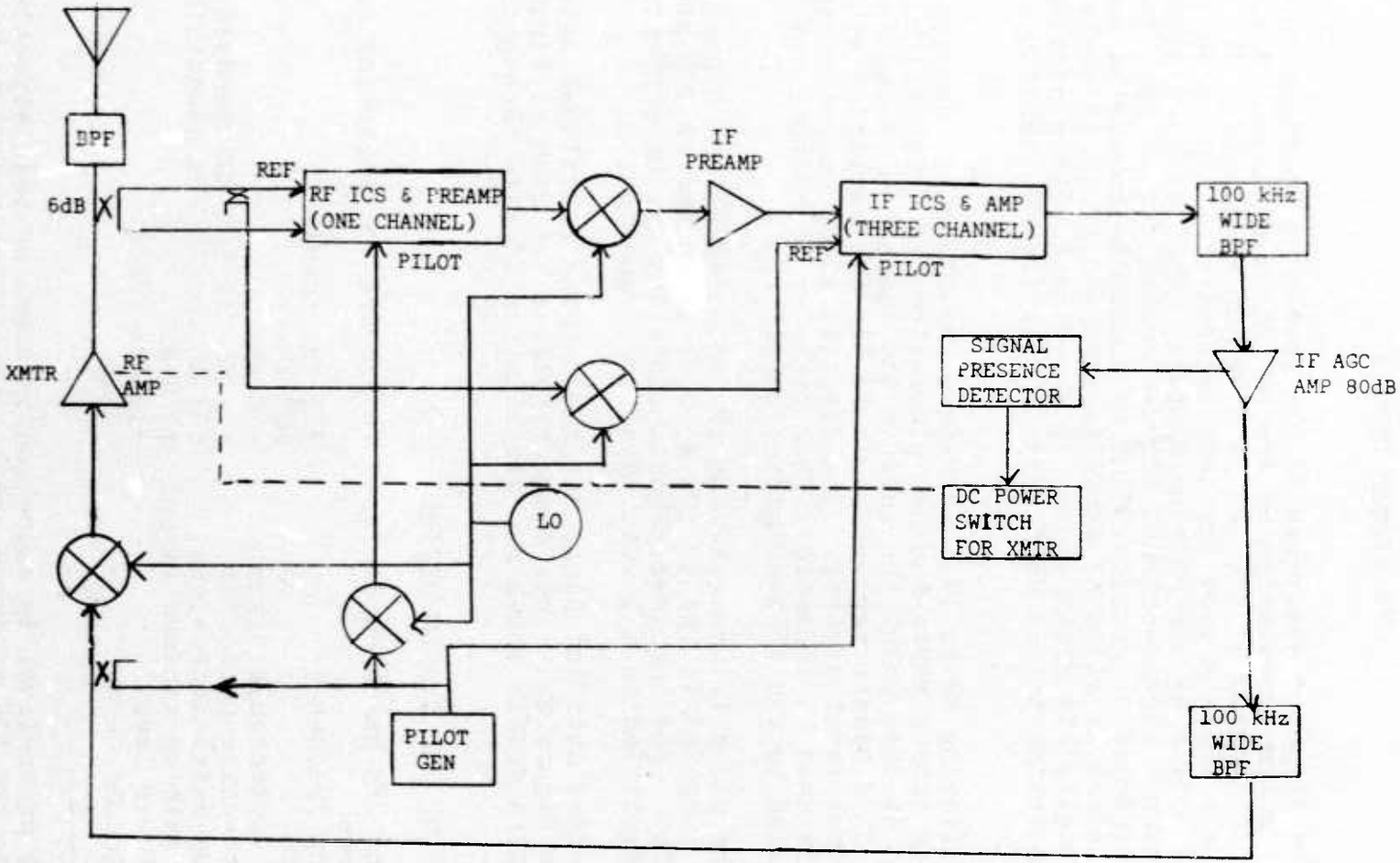

FIGURE 25

SFR CONCEPTUAL BLOCK DIAGRAM

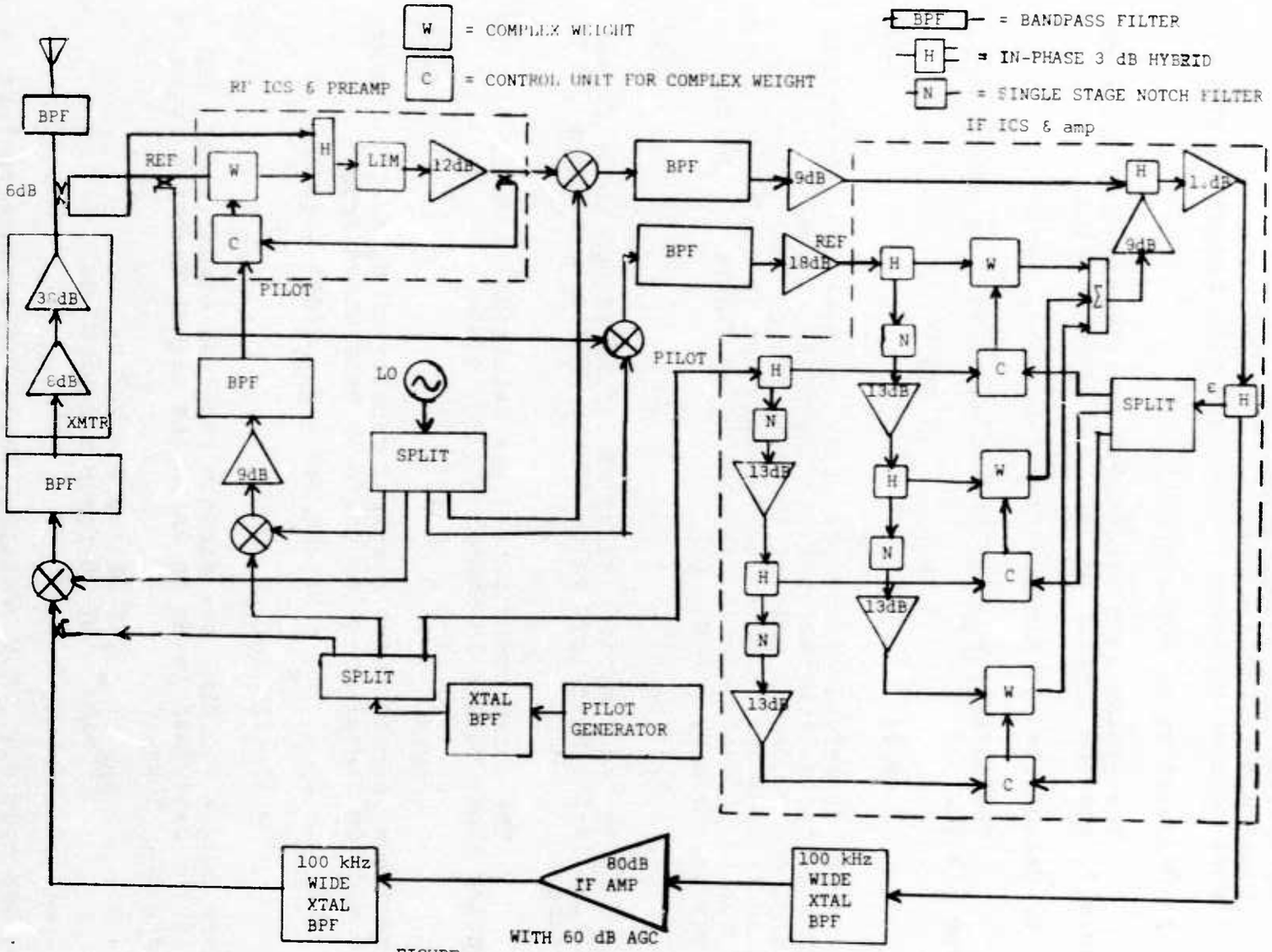

FIGURE 26
SFR BLOCK DIAGRAM SHOWING FUNCTIONAL UNITS

Signal-to-Intermodulation ratio (two-tone output with minimum detectable signal)	+20 dB
Signal modulation types	any with bandwidth ≤100 kHz

a. Calculation of Forward Gain

The system gain (and loss) distribution is tabulated in Table 2, showing a total of 120 dB of forward gain.

b. Calculation of Minimum Signal-to-Noise Ratio

The noise figure of the receiver will be calculated from [14,Eq. 53]

$$F_{RCVR} = F_1 + \frac{(F_2-1)}{g_1} + \frac{(F_3-1)}{g_1 g_2} \tag{137}$$

where the numerical subscripts index the receiver gain stages in order of their occurrence, F_i is the noise figure of the i-th stage, and g_i is the gain of the i-th stage. All gains and noise figures are in numerical ratios, not in decibels. Because of the RF losses preceding it, the noise figure of the first stage is given by [14,Eq. 61]

$$F_1 = L_{RF} F_1' \tag{138}$$

where F_1' is the numerical value of the RF preamp noise figure and L_{RF} is the numerical value of the RF loss preceding the preamp.

The noise contributors are tabulated in Table 3. Inserting those values in Equation (137) gives

$$F_{RCVR} = 53.5 \simeq 17 \text{ dB} \tag{139}$$

Assuming a thermal noise spectral density of $N_0 = -174$ dBm/Hz, the minimum signal-to-noise ratio is determined from

$$\begin{aligned} SNR_{min} &= S_{min}(\text{dBm}) - N_0(\text{dBm/Hz}) - F_{RCVR}(\text{dB}) - 10 \log_{10} B \\ &= 67 - 10 \log_{10} B \end{aligned} \tag{140}$$

where $S_{min} = -90$ dBm, the minimum received signal level, and B is the bandwidth in Hz in which the signal-to-noise ratio is measured. Thus,

$$SNR_{min} = \begin{cases} 17 \text{ dB for } B = 10^5 \text{ Hz} \\ 23 \text{ dB for } B = 2.5 \times 10^4 \text{ Hz} \end{cases}$$

---

[14] Mumford, W.W., E.H. Scheibe, *Noise Performance Factors in Communications System,* Horizon House-Microwave, Inc., Dedham, Mass., 1968.

TABLE 2

SYSTEM GAIN DISTRIBUTION

Gain or Loss Contributor (re: Fig. 26)	Gain (in dB)
BPF	-1
6 dB Coupler	-7
RF ICS	+7
RF-IF Mixer and BPF	-7
First IF Amplifier	+9
IF ICS	+10
XTAL BPF (2)	-8
IF AGC Amplifier	+80 (max)
IF-RF Mixer and BPF	-7
Transmitter RF Amp	+46
6 dB Coupler	-1
BPF	-1
Overall System Gain	120 dB (max)

TABLE 3

SYSTEM NOISE FIGURE CONTRIBUTORS

Item	Decibel Value	Numerical Value
L_{RF}, RF losses	12 dB	15.85
F_1', noise figure of RF preamp	5 dB	3.16
g_1, gain from input of RF preamp with image filter to input of IF amp #1	5 dB	3.16
F_2, noise figure of IF amp #1	5 dB	3.16
g_2 gain from input of IF amp #1 to input of IF amp #2	6 dB	3.98
F_3, effective noise figure of IF amp #2	5 dB plus IF ICS added noise	35.84

c. Impact of Signal-to-Intermodulation Ratio on Weight Linearity

A minimum level signal at -90 dBm at the SFR input appears at the input to the RF ICS at a level of -98 dBm. Thus, the third-order intermodulation products coming out of the RF ICS weight must be at a level not exceeding -118 dBm in order to meet the signal-to-intermodulation ratio of 20 dB.

When the SFR transmits two equal strength tones, they are both at a level of +24 dBm (+30 dBm PEP). Assuming that the return loss of the SFR antenna is at least 15 dB, the two tones are coupled to the antenna input of the RF ICS at a level of +1 dBm each. If they are to be cancelled, the RF ICS weight must provide the same +1 dBm output level. Thus, the weight is required to put out two tones at +1 dBm each with third-order intermod products not exceeding -118 dBm. This corresponds to a third-order intercept requirement of +59.5 dBm on the weight. The data of September 24 and 26 in Section IV.2 show that this goal has been met.

2. ICS EXPERIMENT WITH A SIMULATED ANTENNA

a. Test Description

A single-channel pilot-directed ICS was tested using a tuned circuit to simulate an antenna as configured in the single frequency repeater. The experiment was conducted to verify that a single-channel ICS at RF can provide sufficient cancellation of the transmitted signal for RF amplification and RF-IF conversion to take place. Further cancellation will then be achieved at IF with a multichannel notch filter ICS.

The tuned circuit was built and adjusted to simulate the input impedance of an antenna with a bandwidth of 50 MHz, and a return loss of 15 dB at the frequency of operation. A schematic diagram of this circuit is given in Figure 27.

Figure 28 shows a block diagram of the test setup. It is based on the block diagram of Figure 17 used for tests with a two-channel ICS, with those portions for the second channel unused. The antenna simulator was connected as shown at the top of the figure, using a 10 dB directional coupler to simulate the antenna coupler in the repeater.

The repeater output consists of the repeated signal and an additive pilot. The repeated signal (the interference) is simulated by a CW tone from the HP 608F Signal Generator passing through the PN Modulator, but in this test no modulation was applied. An FM signal source (Boonton #102A) was used to generate the pilot signal, which is coupled with the interference in a 10 dB coupler. The repeated signal (interference) plus pilot are fed to the antenna simulator and to the Reference 1

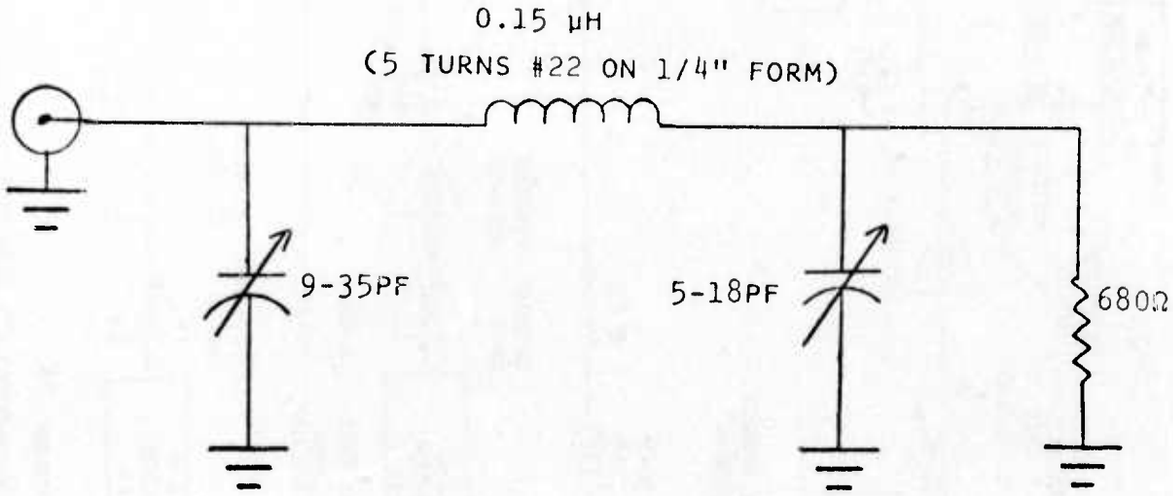

FIGURE 27
SIMULATED ANTENNA NETWORK

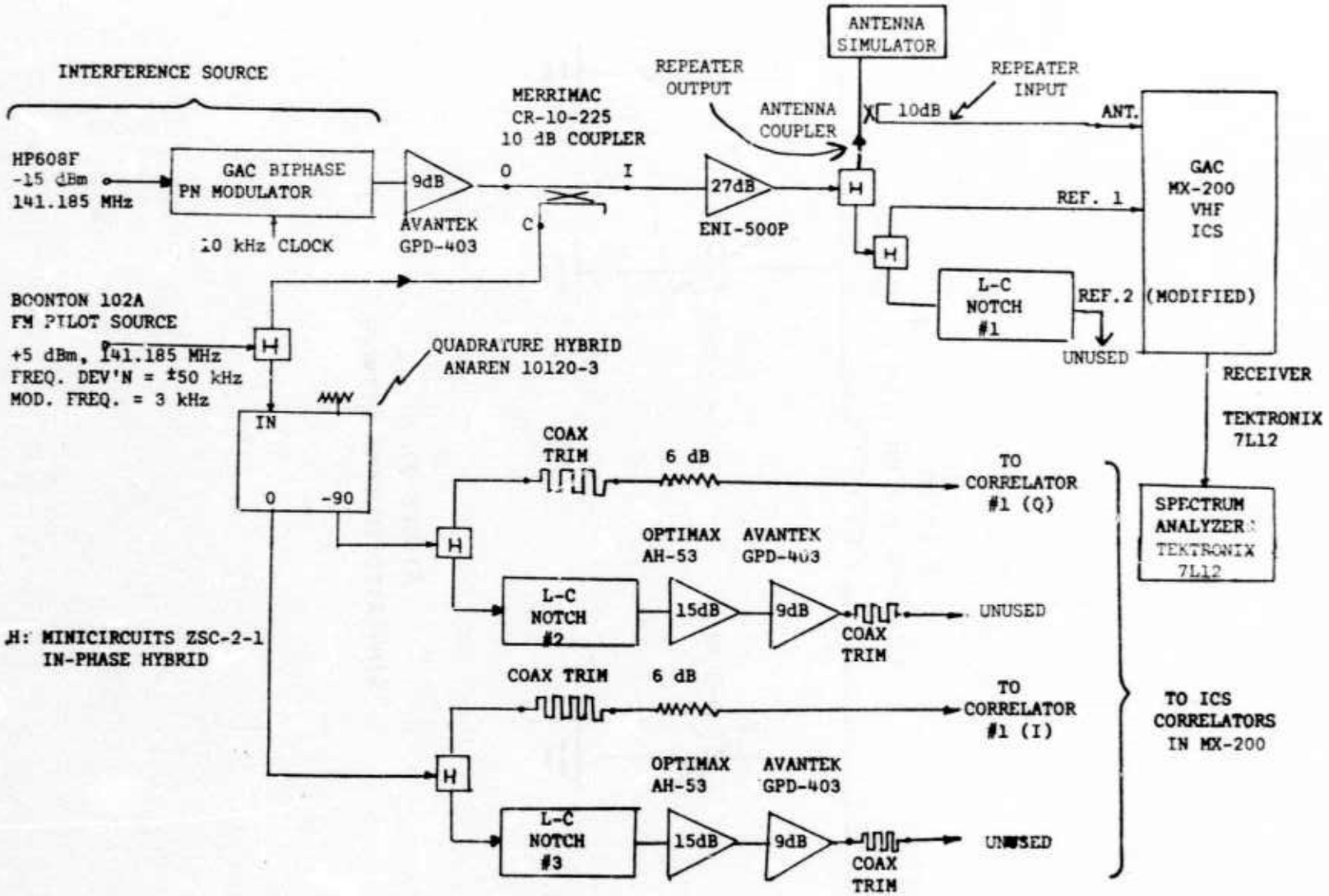

FIGURE 28

SINGLE CHANNEL PILOT-DIRECTED ICS WITH ANTENNA SIMULATOR

input of the modified MX-200 VHF ICS. The MX-200 modifications are identical to those discussed in Section IV.2.

A portion of the pilot is taken and split into two quadrature components which are adjusted in delay and amplitude to drive the I and Q correlators in Channel #1 of the MX-200. The notch filter processing used with Channel #2 in Section III.2 is not used in this experiment.

The antenna simulator was connected to the antenna coupler in two ways: with a BNC barrel (approximately 2 inches long), and with a six-foot length of coax. Cancellation results were obtained for both connections. The reference level for 0 dB return loss was obtained by disconnecting the antenna port of the antenna coupler and leaving it open.

b. Test Results

The test results are shown in the photographs of Figures 29 through 32. Figure 29 shows the output of the ICS with no cancellation and the antenna simulator disconnected. The 100 kHz wide FM pilot is shown with the CW transmitter signal near the center of the screen. Figure 29 is the return loss reference.

When the antenna simulator is connected on a two-inch cable, Figure 30 shows the ICS output is reduced by 15 dB from Figure 29. No ICS cancellation has yet taken place.

When the ICS reference is connected, the ICS cancels, producing the output spectrum shown in Figure 31(a). The CW transmitter signal at the center of the screen is in a deep null in excess of 70 dB from the return loss reference. When the CW frequency is moved to the pilot edge in Figure 31(b), the interference rejection is seen to be 55 dB from the reference level.

A similar sequence of photographs is shown in Figure 32, for which the antenna simulator is connected at the end of a six-foot cable. Figure 32(a) shows the uncancelled ICS output down 15 dB from the reference level. Figure 32(b) shows the cancelled ICS output with the CW interference at band center nulled by more than 70 dB. Figure 32(c) shows the cancelled ICS output with the CW interference at band edge nulled by 60 dB.

c. Discussion of Results

The combination of 15 dB return loss and single-channel ICS cancellation is seen to provide a worst-case (band edge) transmitter-to-receiver isolation of 55-60 dB with a 50 MHz wide simulated antenna. This isolation is felt to be sufficient for repeater RF front end to operate properly. Further transmitter rejection will then be accomplished at IF with a multichannel notch filter ICS.

HORIZONTAL: 20 KHZ/DIV; VERTICAL: 10 DB/DIV, -10 DBM TOP

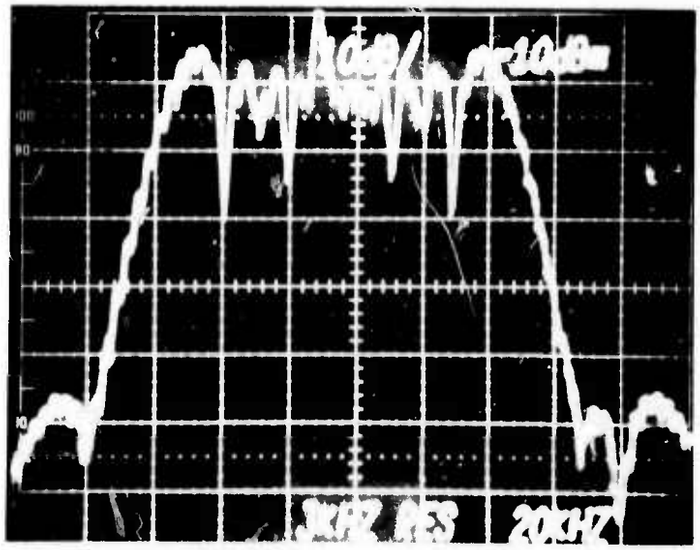

FIGURE 29- RETURN LOSS REFERENCE - ICS OUTPUT WITH ANTENNA PORT OPEN AND NO CANCELLATION

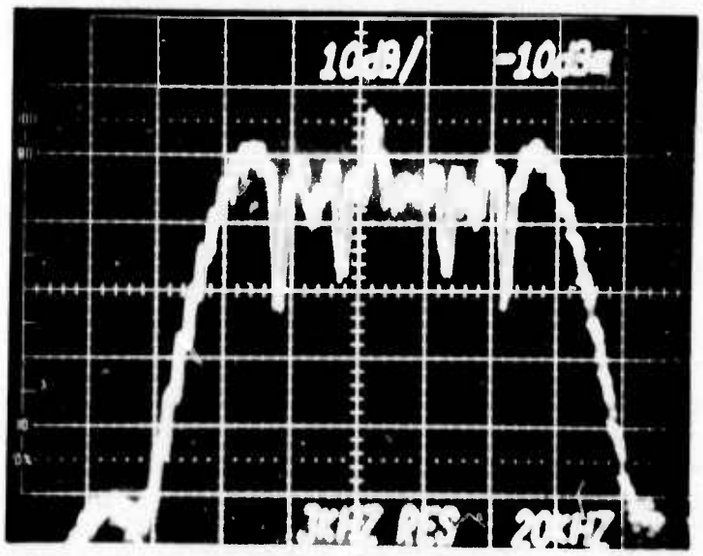

FIGURE 30 - UNCANCELLED ICS OUTPUT WITH ANTENNA SIMULATOR ON TWO-INCH CABLE

HORIZONTAL: 20 KHZ/DIV; VERTICAL: 10DB/DIV, -10 DBM TOP

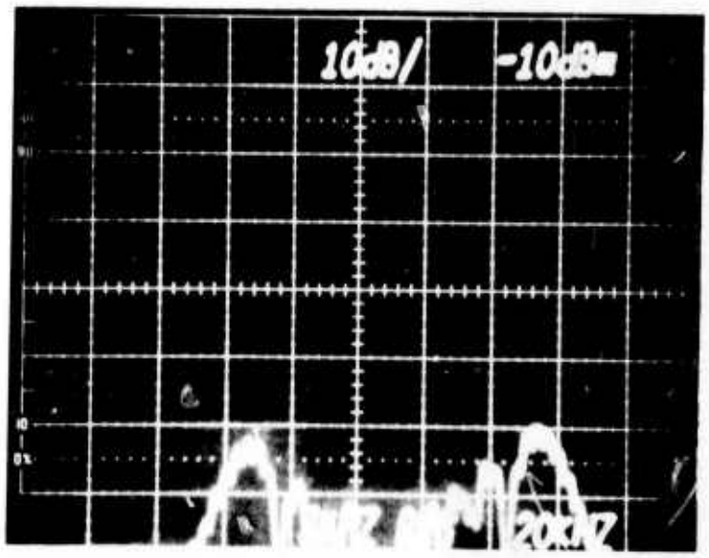

(A) CW INTERFERENCE COMPONENT AT BAND CENTER

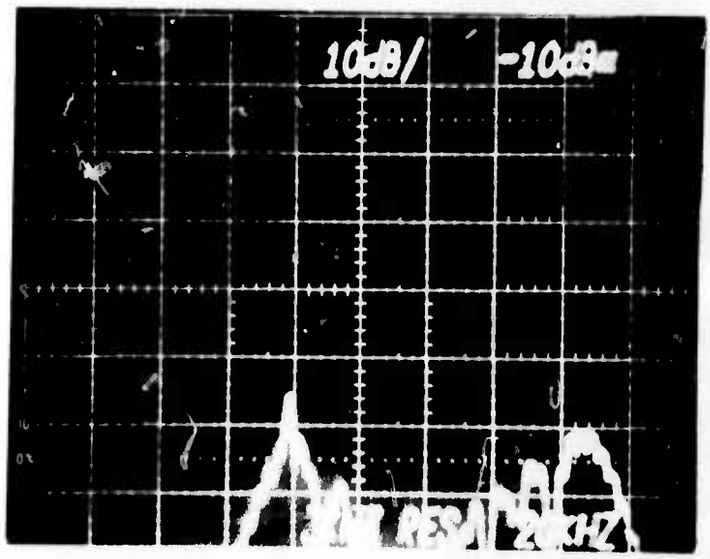

(B) CW INTERFERENCE COMPONENT LOW FREQUENCY BAND EDGE

FIGURE 31 - SINGLE-CHANNEL CANCELLED ICS OUTPUT WITH ANTENNA SIMULATOR ON TWO-INCH CABEL (15 DB RETURN LOSS)

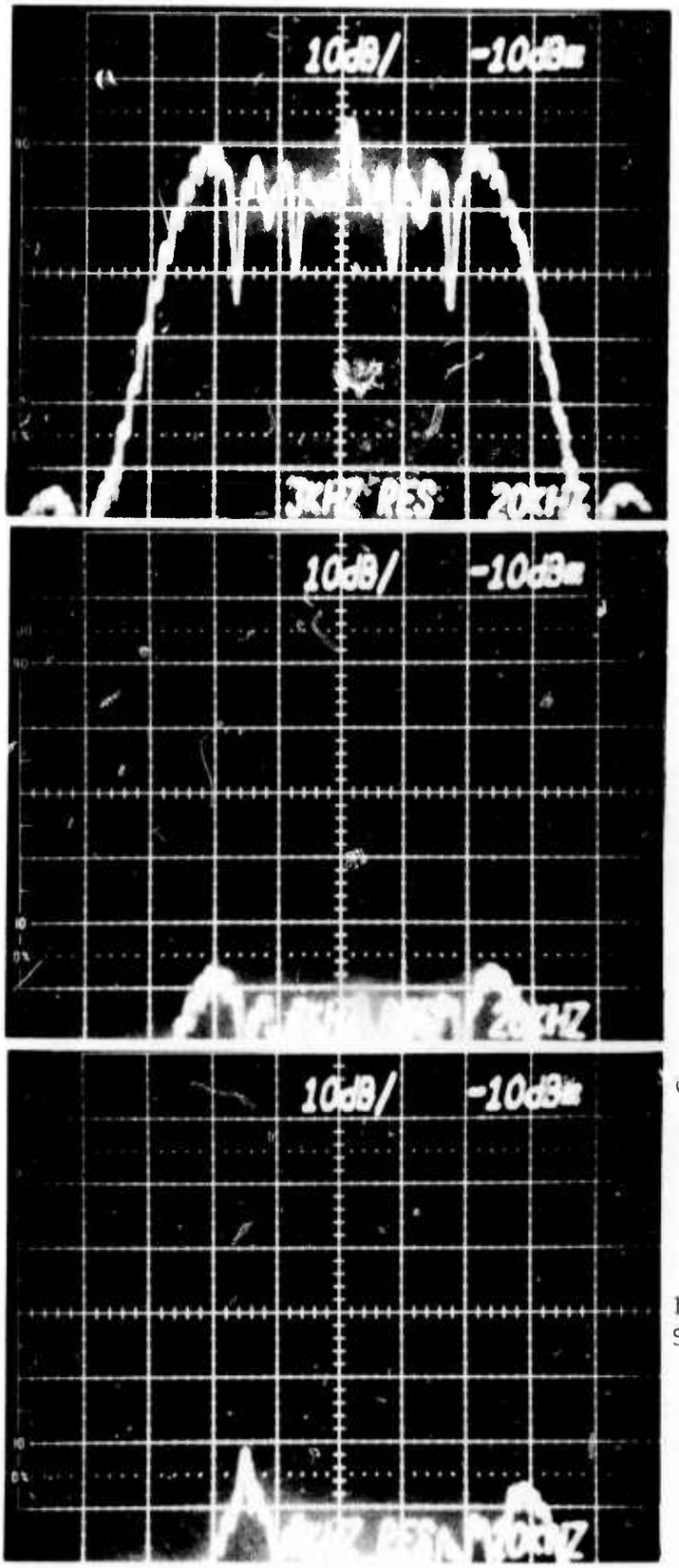

HORIZONTAL: 20 KHZ/DIV
VERTICAL: 10 DB/DIV,
-10 DBM TOP

(A) UNCANCELLED OUTPUT

(B) CANCELLED OUTPUT WITH CW INTERFERENCE COMPONENT AT BAND CENTER

(C) CANCELLED OUTPUT WITH CW INTERFERENCE COMPONENT AT BAND EDGE

FIGURE 32

ICS OUTPUTS WITH ANTENNA SIMULATOR ON SIX-FOOT CABLE (15 DB RETURN LOSS)

SECTION VI

SFR BREADBOARD DESIGN

An SFR breadboard system was built based on the design concept presented in Figures 25 and 26. It was designed to operate at a 291.8 MHz RF, with a power output of 1 watt. The details of the implementation are presented in this section.

A block diagram of the SFR breadboard is given in Figure 33 which shows the system functions performed in each subassembly, identified by the letter in the upper left-hand corner of each block. Figure 34 is a block diagram illustrating the electrical implementation of each of these subassemblies.

Both the RF and IF ICS's have their complex weights controlled by correlation of the ICS error signal with a pilot signal. This pilot signal is added to the SFR transmission so that it is present on the transmitted signal as discussed previously. The pilot supplied to the IF ICS correlators is at 30 MHz. while the pilot supplied to the RF ICS correlator is first up-converted to the RF.

1. BLOCK DIAGRAM DESCRIPTION (Figure 34)

An input signal from the antenna is coupled into the Antenna Input of Box A through a 6 dB coupler. Also present on this input are coupled components of the transmitted signal and the pilot. The fourth port of the same 6 dB coupler serves to provide a portion of the transmitted signal and the pilot to the Reference Input of Box A. The Reference Input, attenuated by 26 dB, is outputted from Box A for down-conversion to IF and further use in the IF ICS. A larger portion of the Box A Reference Input (attenuated by 5 dB) is adjusted by the RF weight to effect cancellation of the coupled RF transmitted signal and pilot in a 3 dB hybrid combiner. The RF weight is designed to impart very low intermodulation distortion upon the reference signal.

After RF cancellation, the received signal and cancellation residue are provided to Box B where they are amplified and down-converted to 30 MHz and outputted to Box D. A sample of the RF ICS output is extracted for use as the RF ICS feedback error signal. It is chopped at a 455 kHz rate. Chopping sidebands that appear in the main line of the error coupler are at multiples of 455 kHz from the RF, and will subsequently be rejected by 100 kHz wide filters at IF.

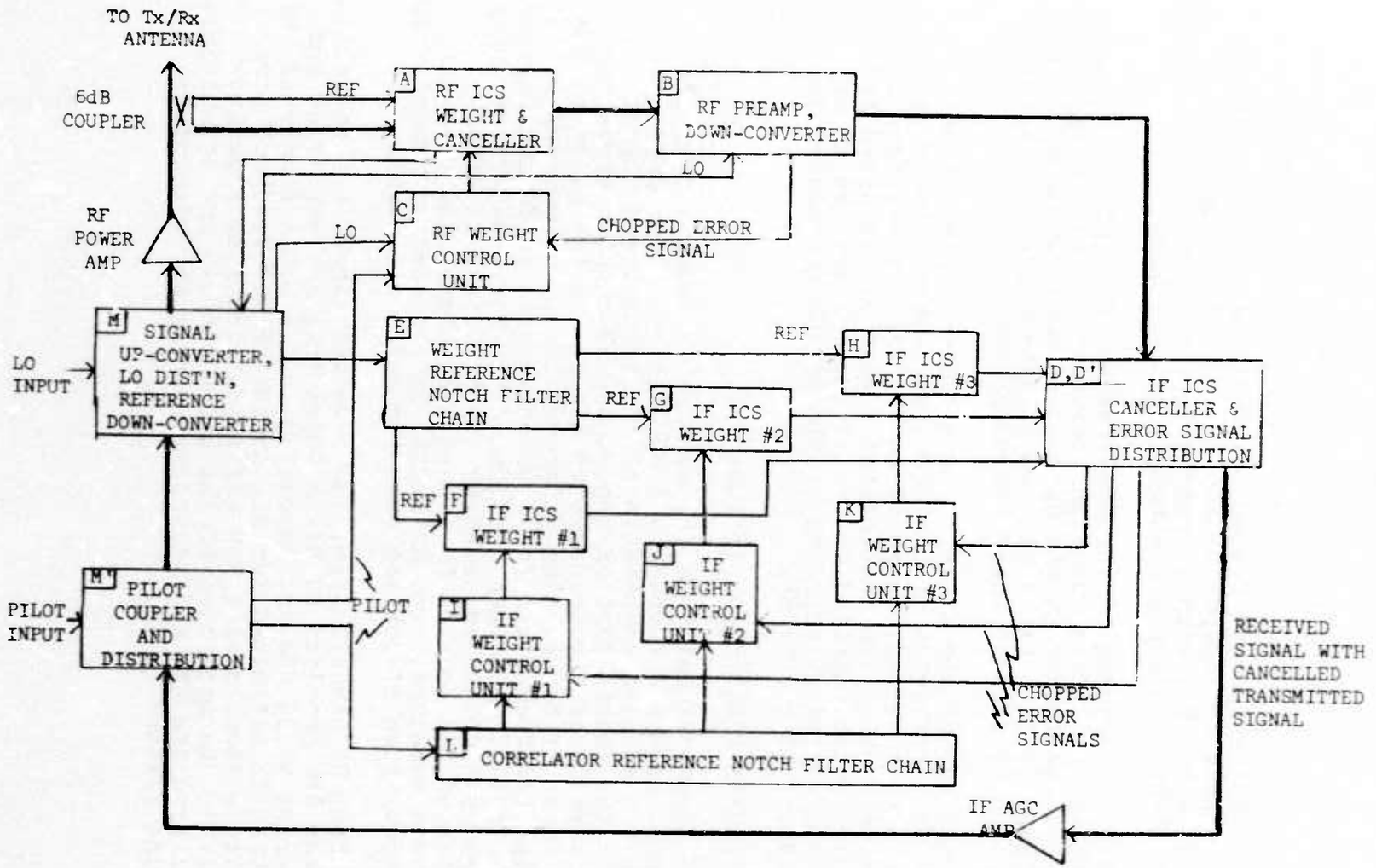

FIGURE 33

SFR BREADBOARD BLOCK DIAGRAM BY SUBASSEMBLIES

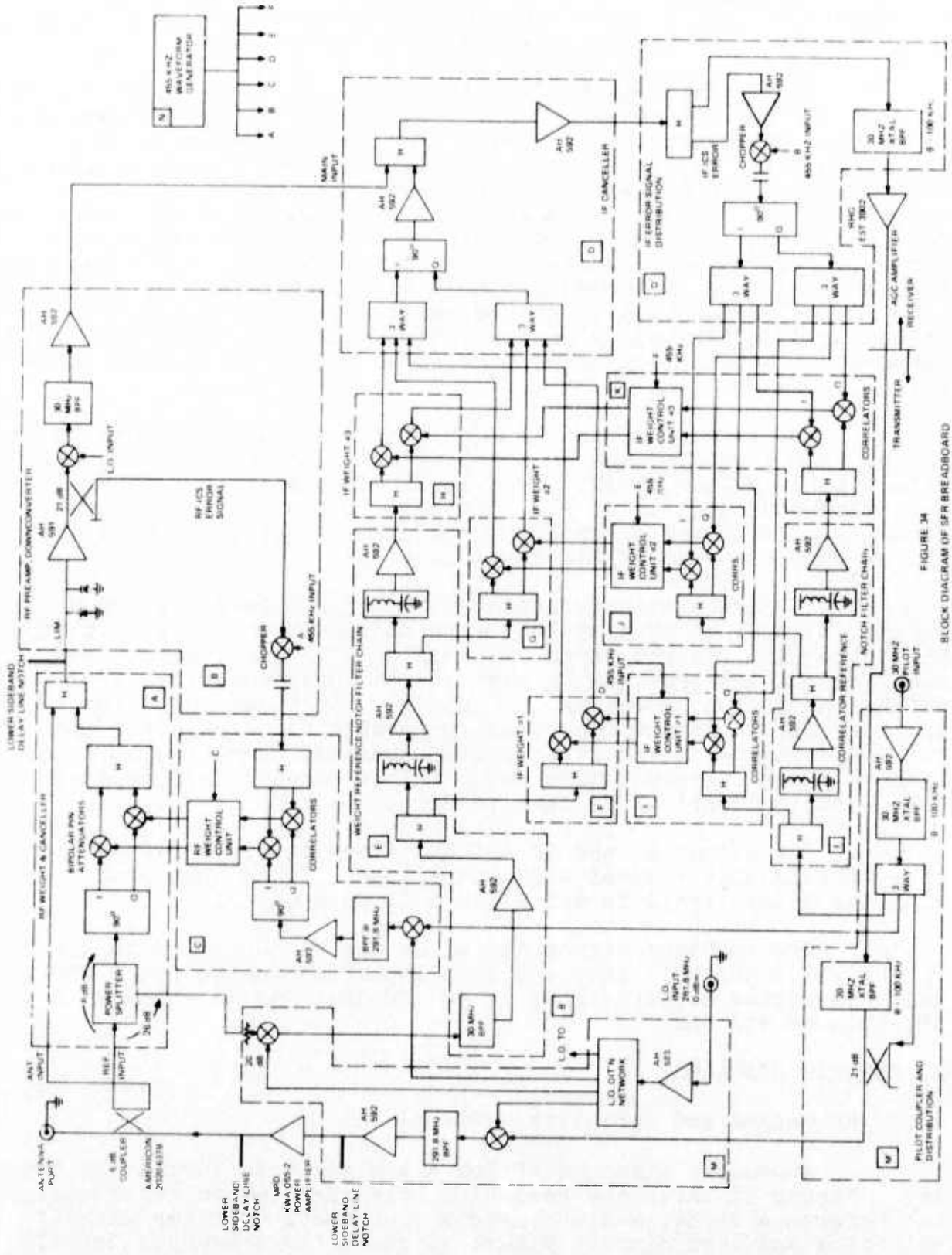

FIGURE 34
BLOCK DIAGRAM OF SFR BREADBOARD

The chopped preamp output is fed to Box C, where it is correlated with I and Q versions of the up-converted pilot to generate the I and Q control signals for the RF weight.

The output from Box A carrying the 26 dB attenuated version of the Box A Reference Input is connected to Box M where it is further attenuated by 20 dB and then down-converted to IF. The attenuation is necessary to avoid generating intermodulation distortion in the down-converting mixer. The resulting signal, containing the transmitted signal and pilot at IF, forms the reference input for the IF ICS weights. It is provided to the three IF ICS weights, located in Boxes F, G and H, from output taps on a cascade of 30 MHz notch filters located in Box E. The taps are extracted by 3 dB hybrid splitters. Each stage of notch filtering is separated by an amplifier to provide isolation between the notches and to restore some gain to the notched signals.

The outputs of the IF ICS weights are all combined in Box D, then amplified and combined with the IF Main Input to effect cancellation at IF. The resulting signal is further amplified and supplied to Box D', where it is split into two paths. One path passes through a 100 kHz wide crystal bandpass filter and out to an IF AGC amplifier.

The other path, serving as the IF ICS feedback error signal, is chopped at a 455 kHz rate and split into six outputs, three in-phase (I) and three quadrature (Q). One I output and one Q output are provided to each of the three identical IF weight control units (Boxes I, J and K). In these units the I and Q weight control voltages are generated by correlating the I and Q inputs with the pilot signal obtained from taps on a cascade of notch filters. This notch filter cascade is located in Box L and is identical to that in Box E.

The output of the IF AGC amplifier is further filtered by a 100 kHz wide crystal bandpass filter. It is then combined with the pilot signal in Box M' in a 21 dB coupler.

The combined signal and pilot are up-converted in Box M to the 291.8 MHz RF. They are then amplified to the point where the transmitted output signal is at +30 dBm, and the transmitted pilot is at +10 dBm.

2. CIRCUIT DIAGRAMS

a. RF Weight and Canceller - Box a

Schematic diagrams of Box A are given in Figures 35 and 36. Figure 35 shows the resistive networks used to attenuate the Reference Input, and the hybrid components used for signal splitting and combining. Figure 36 shows the schematic details

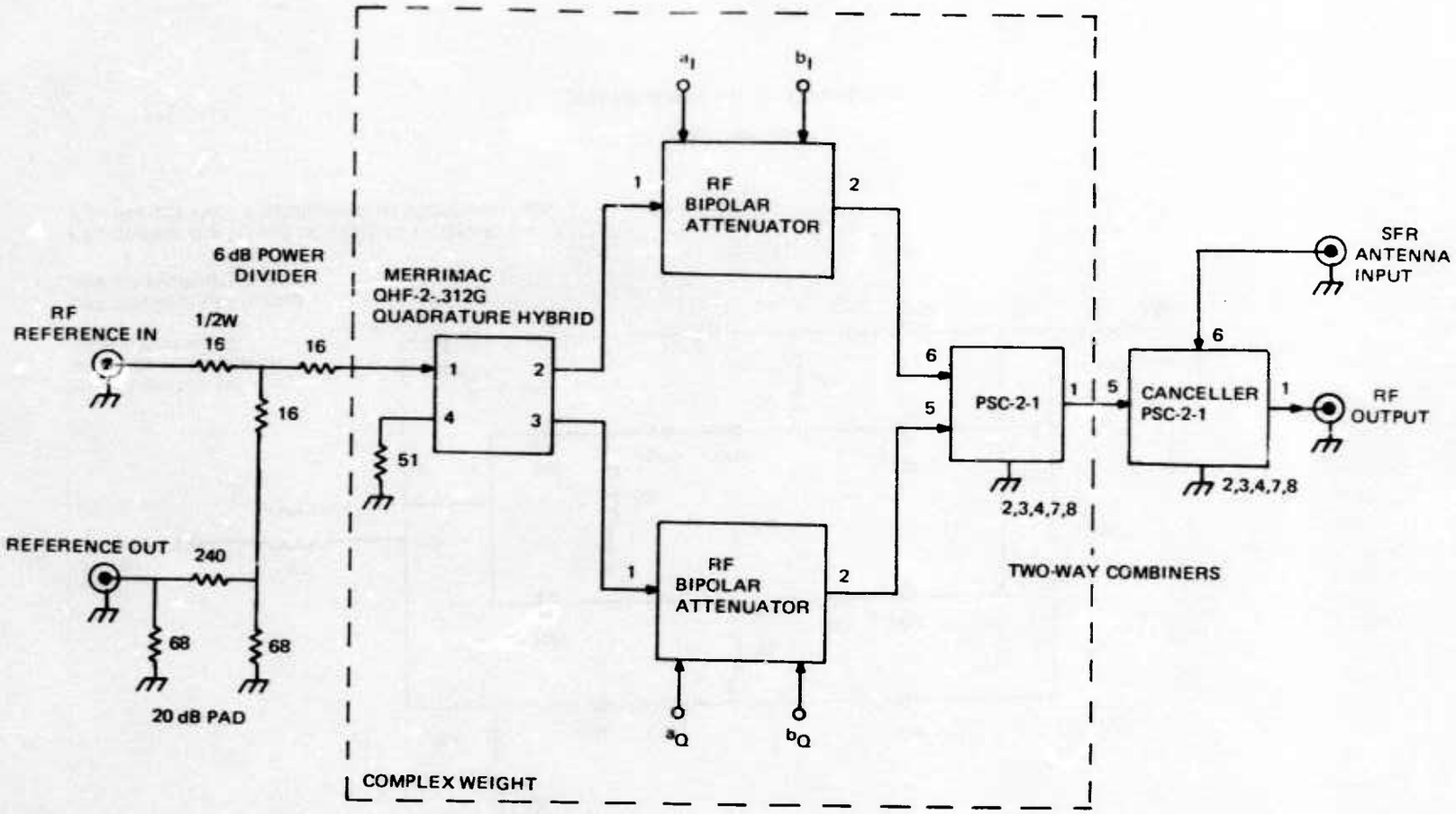

FIGURE 35

RF ICS' COMPLEX WEIGHT AND CANCELLER [A]

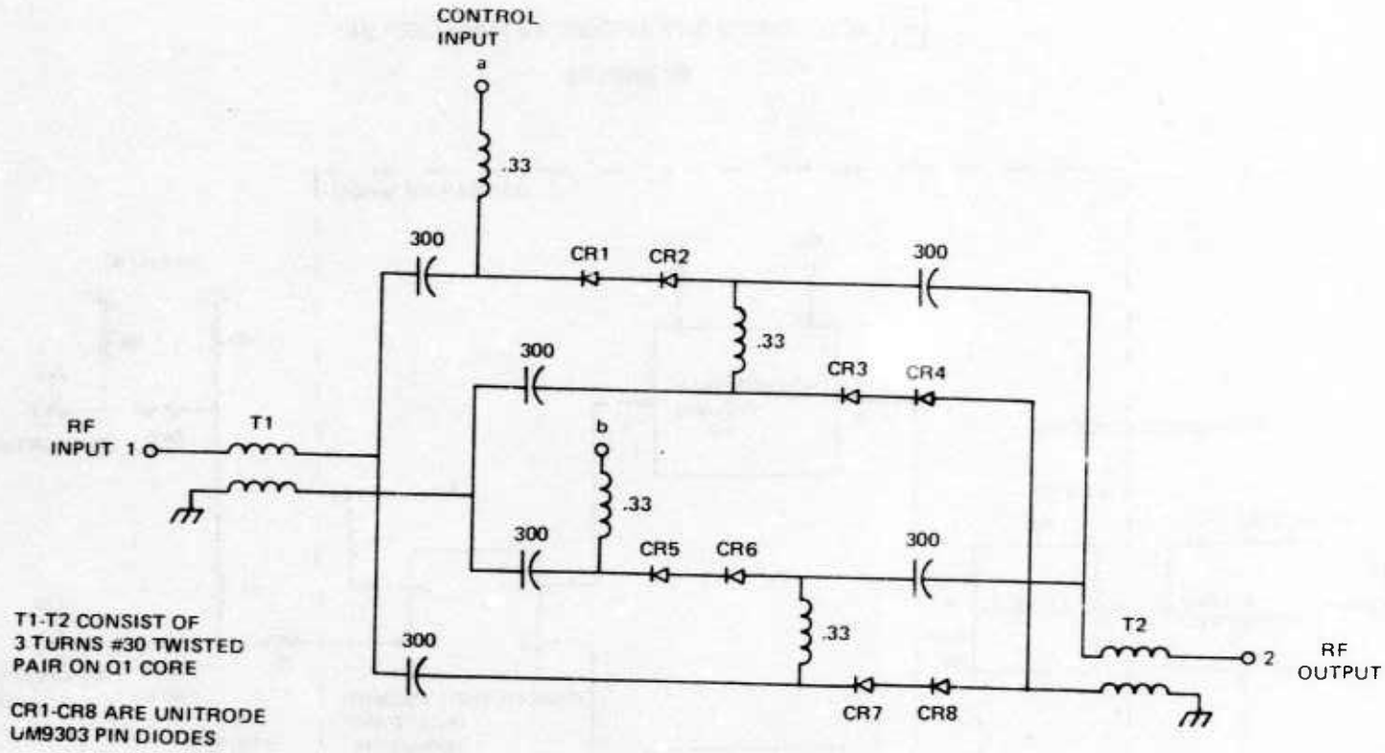

FIGURE 36

SFR RF BIPOLAR ATTENUATOR

of the RF bipolar attenuator, designed for low intermodulation distortion.

b. RF Preamp and Down-Converter - Box B

A schematic diagram of Box B is given in Figure 37. Care has been taken to isolate the RF amplifier (AH-591) and the IF amplifier (AH-592) from stray coupling through the +15V DC power line. The input to the AH-591 is protected by a Schottky diode limiter, so that if excessive power is reflected at the SFR antenna terminal, it will not destroy the amplifier.

c. RF Weight Control Unit - Box C

Schematic diagrams of Box C are given in Figures 38 through 41. Box C contains five circuit cards. With reference to Figure 38, the circuitry is subdivided in the following manner: the first card contains the pilot up-converter, the two hybrid splitters, and the two correlators (I and Q); the second and third cards are the synchronous detector/lowpass filter, I and Q respectively; the fourth and fifth cards are the bipolar attenuator drivers, I and Q respectively. A test jack is included between each lowpass filter and driver to allow the feedback loop to be opened and an external DC weight-control voltage inserted, or to monitor the DC weight control voltages under closed-loop operation.

Figure 39 shows a schematic of the correlator. It takes the form of a diode-quad double-balanced mixer, except that the diodes are biased with a low DC current to maintain linearity with respect to both inputs without sacrificing sensitivity at low input levels. The output is at the chopped frequency, 455 kHz.

Figure 40 shows a schematic of the synchronous detector/lowpass filter. The 455 kHz input from the correlator is stepped up in voltage in a tuned transformer, amplified in a μA733 video amplifier, and further amplified in a CA3100 wideband op amp. It is synchronously detected against the 455 kHz chopping signal by the combination of a CD4016D analog switch and a CA3100 op amp, in which the analog switch alternately puts the op amp in the unity gain inverting mode and the unity gain noninverting mode. A 741 op amp is then used as a lowpass filter to establish the open loop feedback time constant of 1.5 seconds.

Figure 41 shows the schematic of the driver for the RF bipolar attenuator. A 741 op amp is used as an input buffer, after which the driving voltage is split into two paths, one the inversion of the other. These voltages are converted nonlinearly into the drive currents, I_a and I_b, required by the bipolar attenuator to maintain low intermodulation distortion over the range of attenuation while maintaining linear control of the RF output voltage. The crossover currents, where $I_a=I_b$

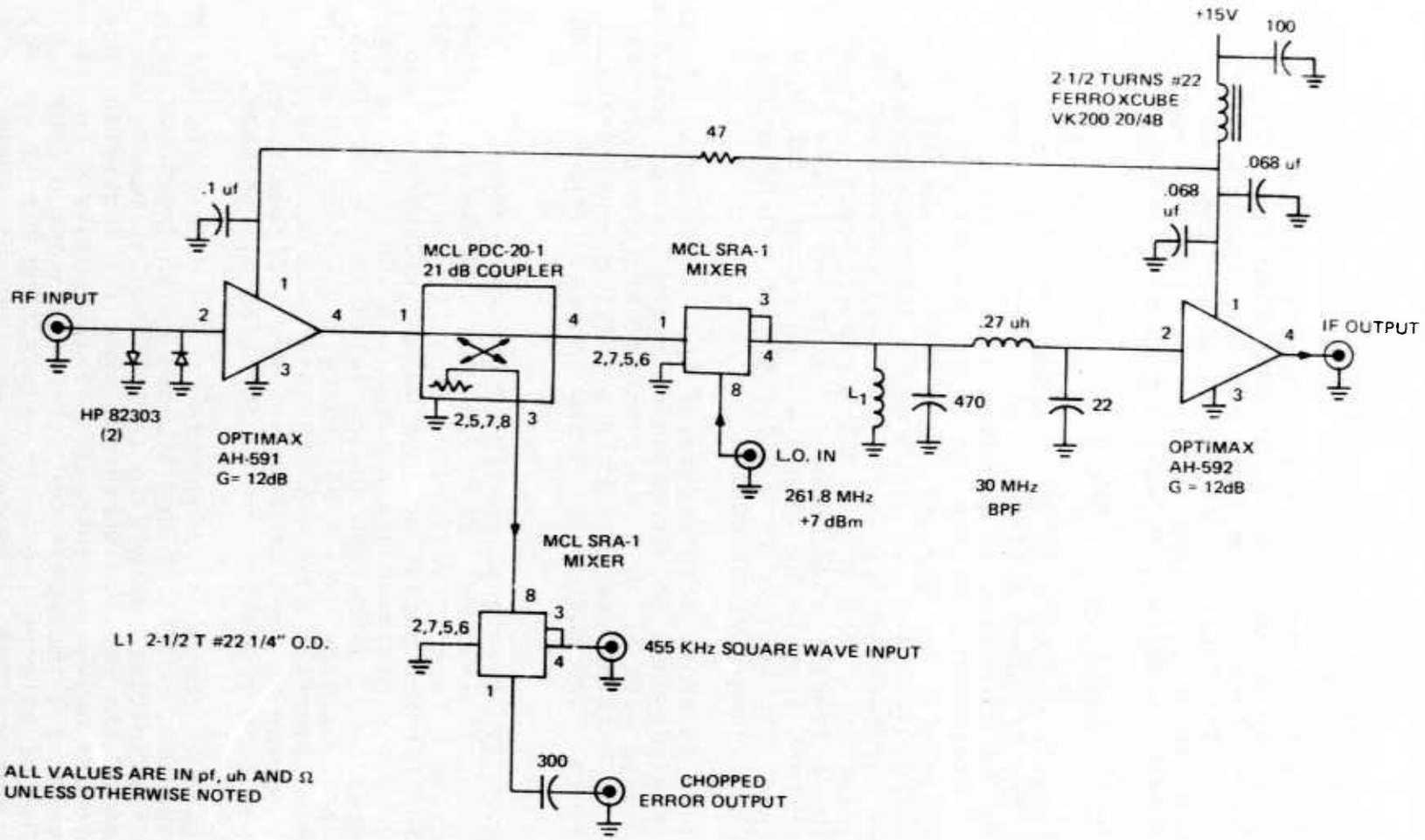

FIGURE 37

RF PREAMP AND DOWN-CONVERTER B

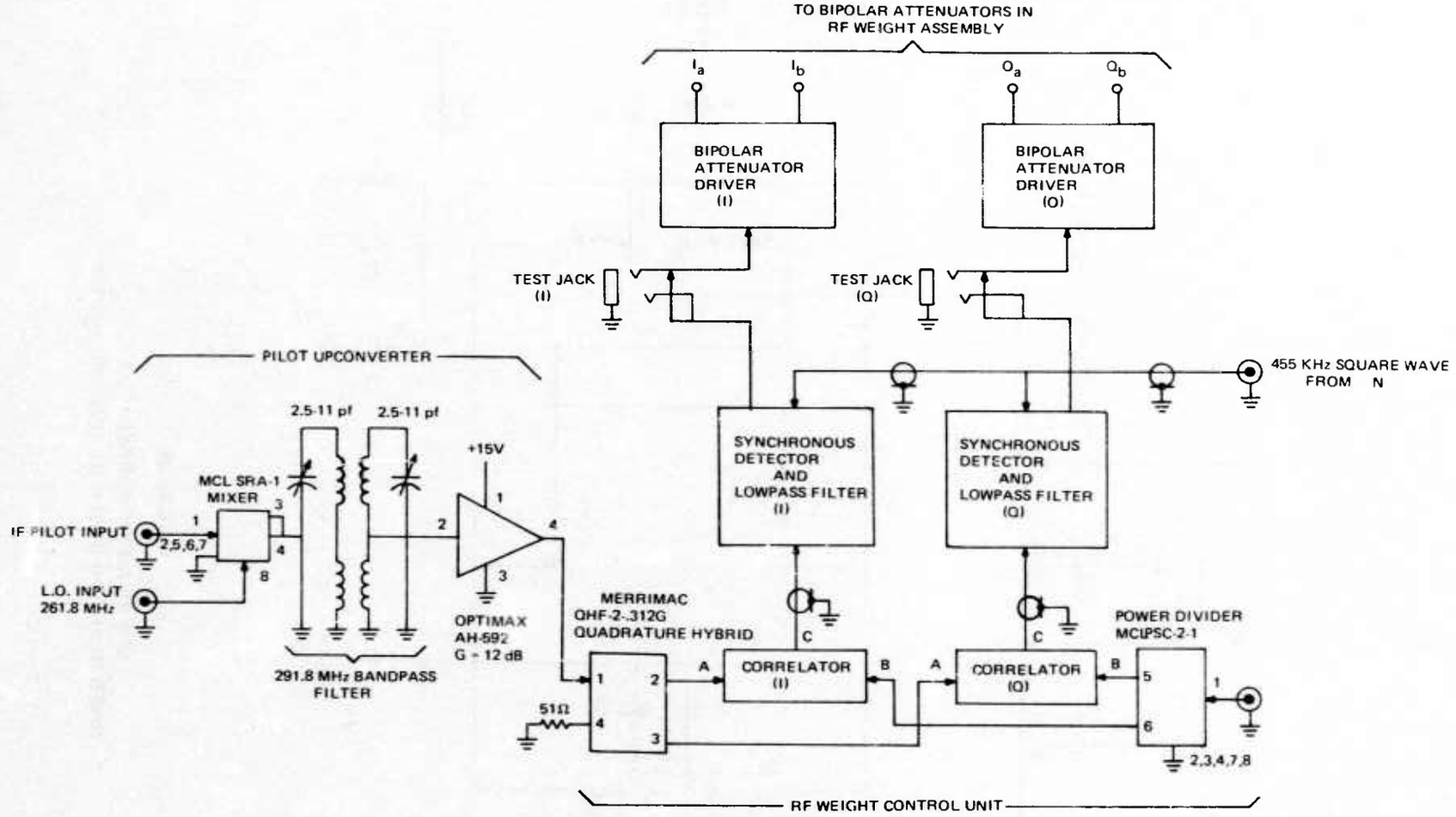

FIGURE 38

SFR PILOT UP-CONVERTER AND
RF WEIGHT CONTROL UNIT C

COMPONENT	VALUE	
	RF CORRELATOR	IF CORRELATOR
C1	300 pf	1000 pf
C2	.15 uf	.15 uf
C3	.15 uf	.15 uf
C4	.15 uf	.15 uf
C5	300 pf	1000 pf
C6	.15 uf	.15 uf
C7	300 pf	1000 pf

CR1 - CR4 ARE FAIRCHILD FH1100

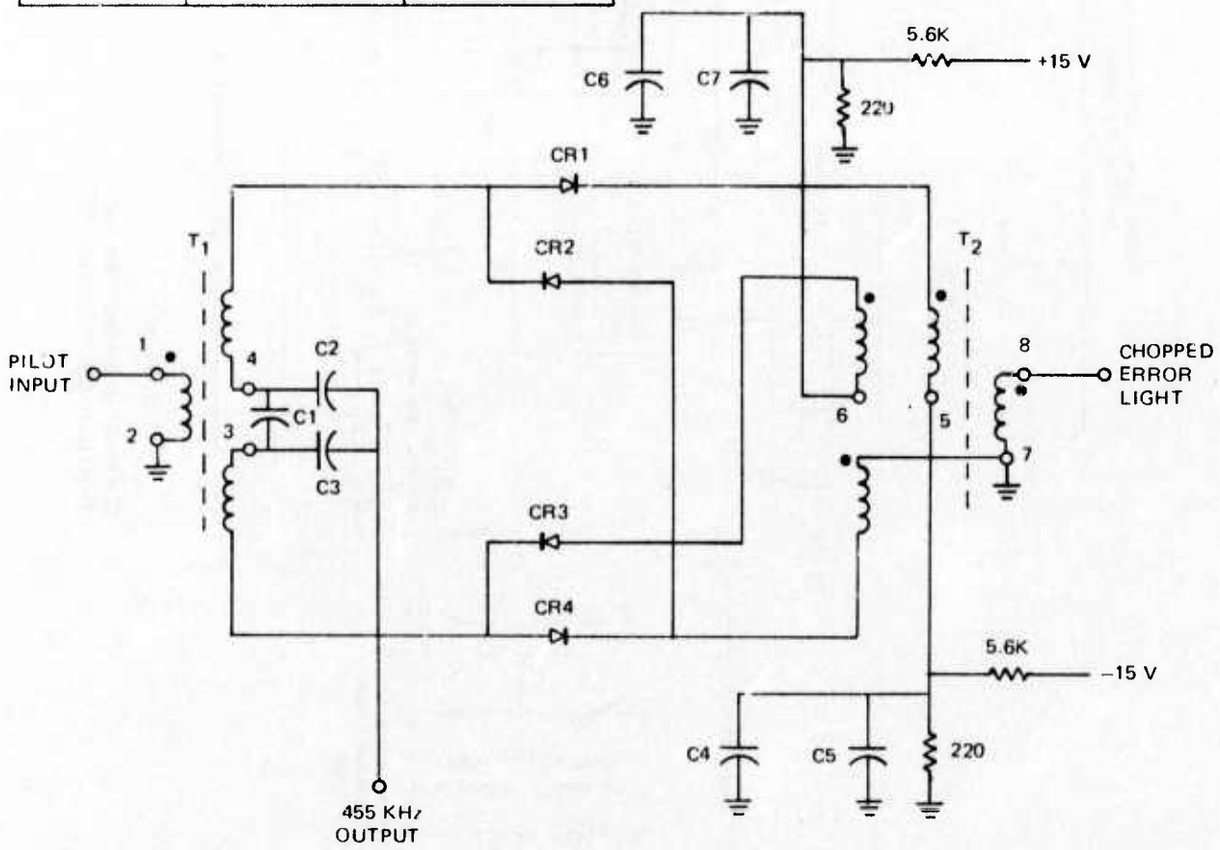

FIGURE 39

SFR RF AND IF CORRELATORS
(USED IN RF AND IF WEIGHT CONTROL UNITS)

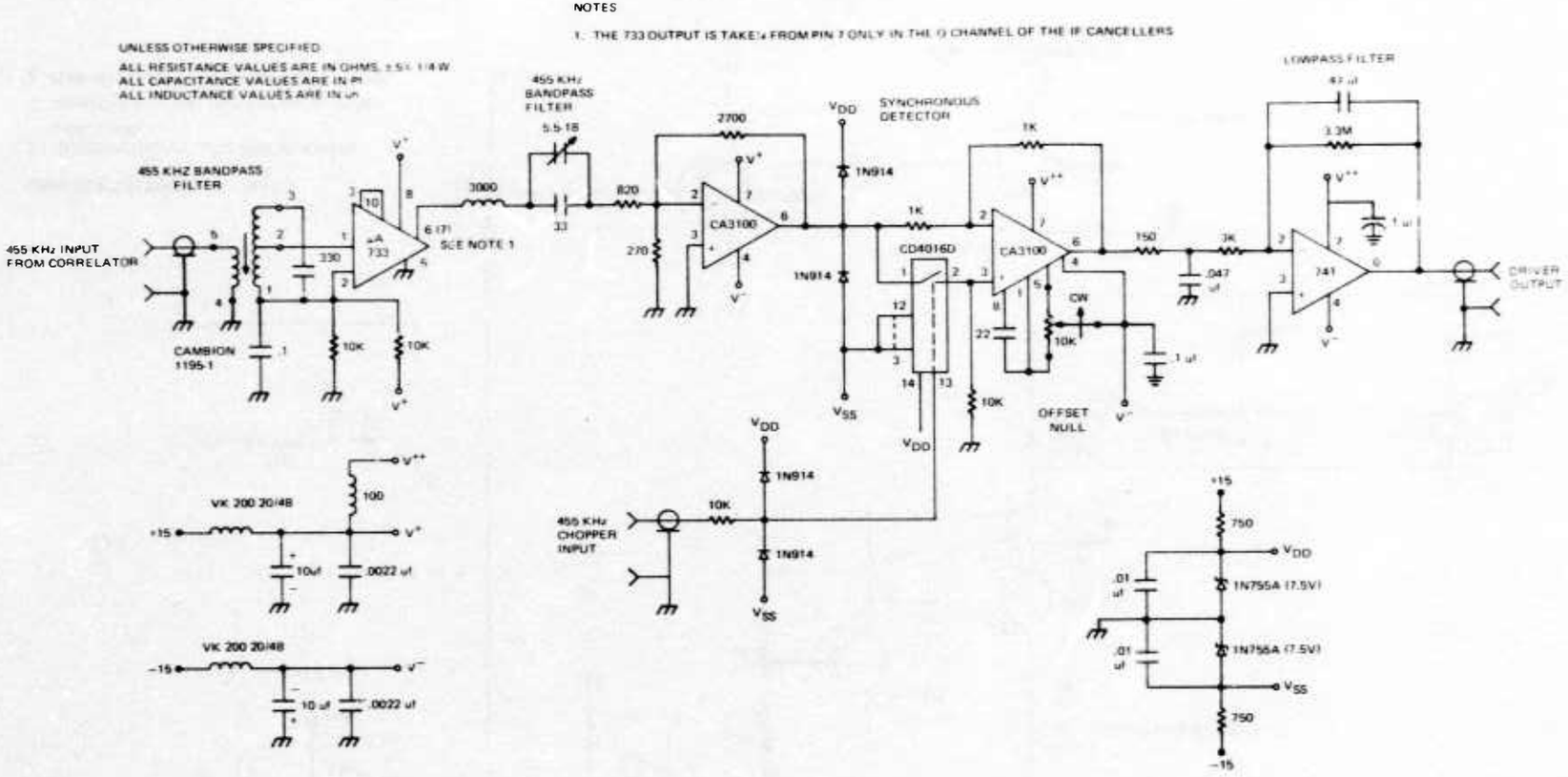

FIGURE 40

SFR SYNCHRONOUS DETECTOR AND LOWPASS FILTER

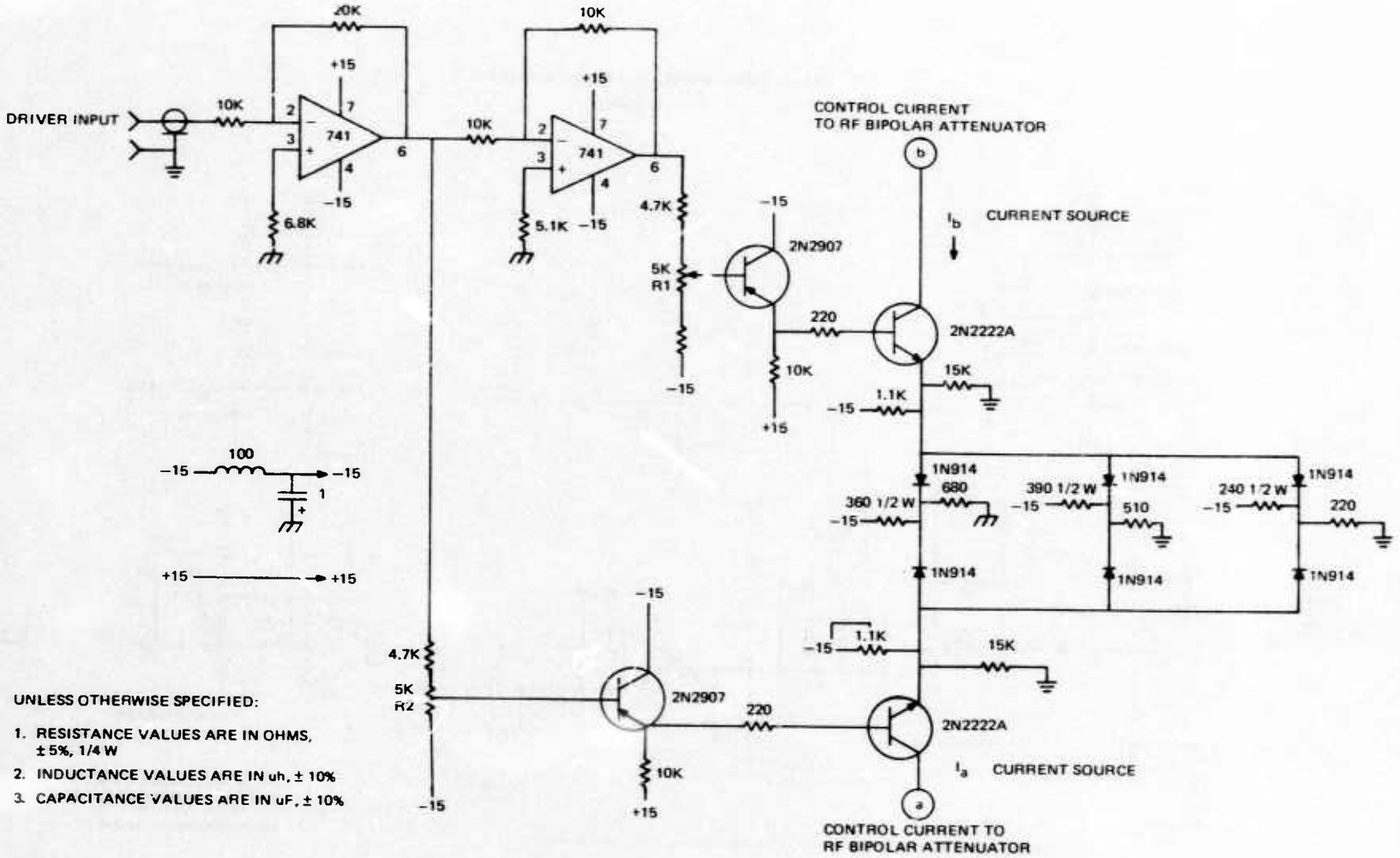

FIGURE 41

SFR RF BIPOLAR ATTENUATOR DRIVER

and the attenuation is greatest, are set by the two pot adjustments. The nonlinear characteristic of output current vs input voltage, which compensates for the control nonlinearity of the PIN diode bipolar attenuator, is determined by the diode-resistor networks in emitters of the two current source transistors. The resulting linearization of the overall control is shown in Figure 42.

d. IF Canceller and Error Signal Distribution - Boxes D and D'

Figure 43 gives the schematic diagram of Boxes D and D'. In Box D the I outputs and Q outputs of the three IF ICS weights are combined using a single quadrature hybrid combiner for all three weights. The combined weight outputs are amplified, combined with the main IF input from Box B for cancellation, and then further amplification provides the output to Box D'.

The input to Box D' is split into two paths. The upper path is amplified, chopped by 455 kHz, and split into three I and three Q outputs to be used as chopped error signal inputs to the IF ICS correlators. The lower path is passed through a two-pole crystal filter with L-C impedance matching networks at its input and output. The input matching network is enclosed in a copper can to prevent it from radiating out-of-band signals around the crystal filter into the output network.

e. Notch Filter Chains, Boxes E and L

Figure 44 gives a schematic diagram of the notch filter chains in Boxes E and L that provide the tapped outputs of tandem notch filters. The inductors L_1 and L_2 are high-Q components, made by winding 22 turns of #30 wire on a Micrometals #T30-6 ferrite toroid. The resulting 3 dB bandwidth of the notch filters is 2.1 MHz, and the notch depth is 20 dB. Several passive notch filter configurations were tried, and this one gave the narrowest bandwidth with the same notch depth.

f. IF Weight Assemblies, Boxes F, G, H

As shown in Figure 45, the three identical IF weight assemblies in Boxes F, G and H consist of an in-phase power splitter and two bipolar attenuators, one for the in-phase (I) component and one for the quadrature (Q) component. The schematic diagram of the IF bipolar attenuators is given in Figure 46. It is similar in form to the RF bipolar attenuators drawn in Figure 36, but intermodulation distortion is less important because the IF bipolar attenuators are operating at input levels at least 38 dB below the RF bipolar attenuator input level.

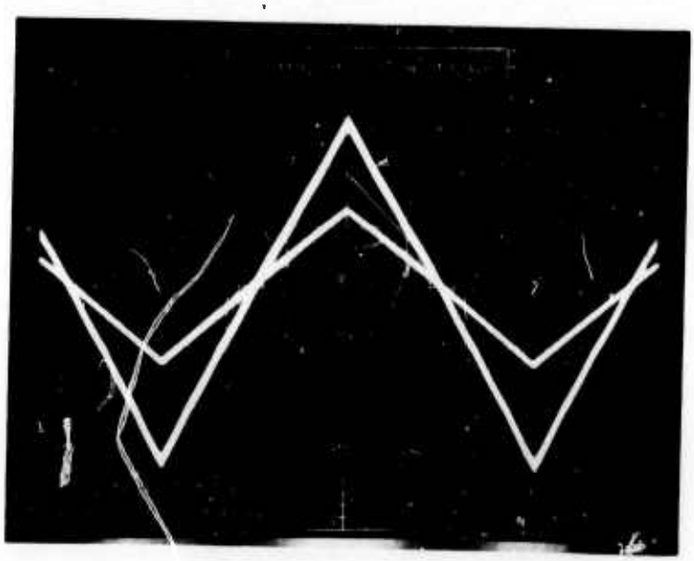

FIGURE 42

RF BIPOLAR ATTENUATOR-DRIVER CHARACTERISTIC:
DETECTED RF OUTPUT VOLTAGE VS INPUT CONTROL VOLTAGE

UNLESS OTHERWISE SPECIFIED:

ALL RESISTANCE VALUES ARE IN OHMS, ± 5% 1/4 W
ALL CAPACITANCE VALUES ARE IN PICOFARADS

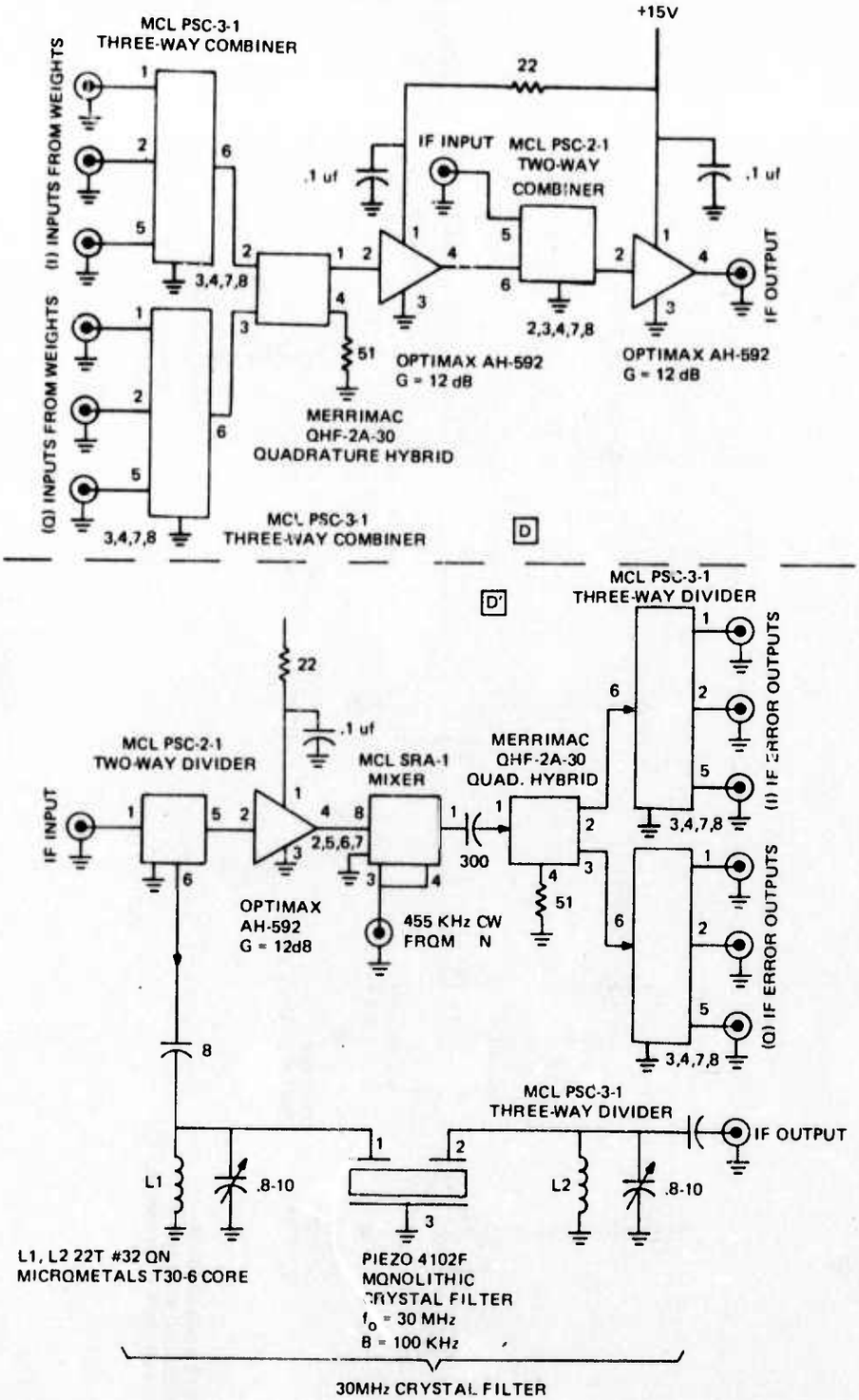

FIGURE 43

SFR IF CANCELLER AND ERROR SIGNAL DISTRIBUTION

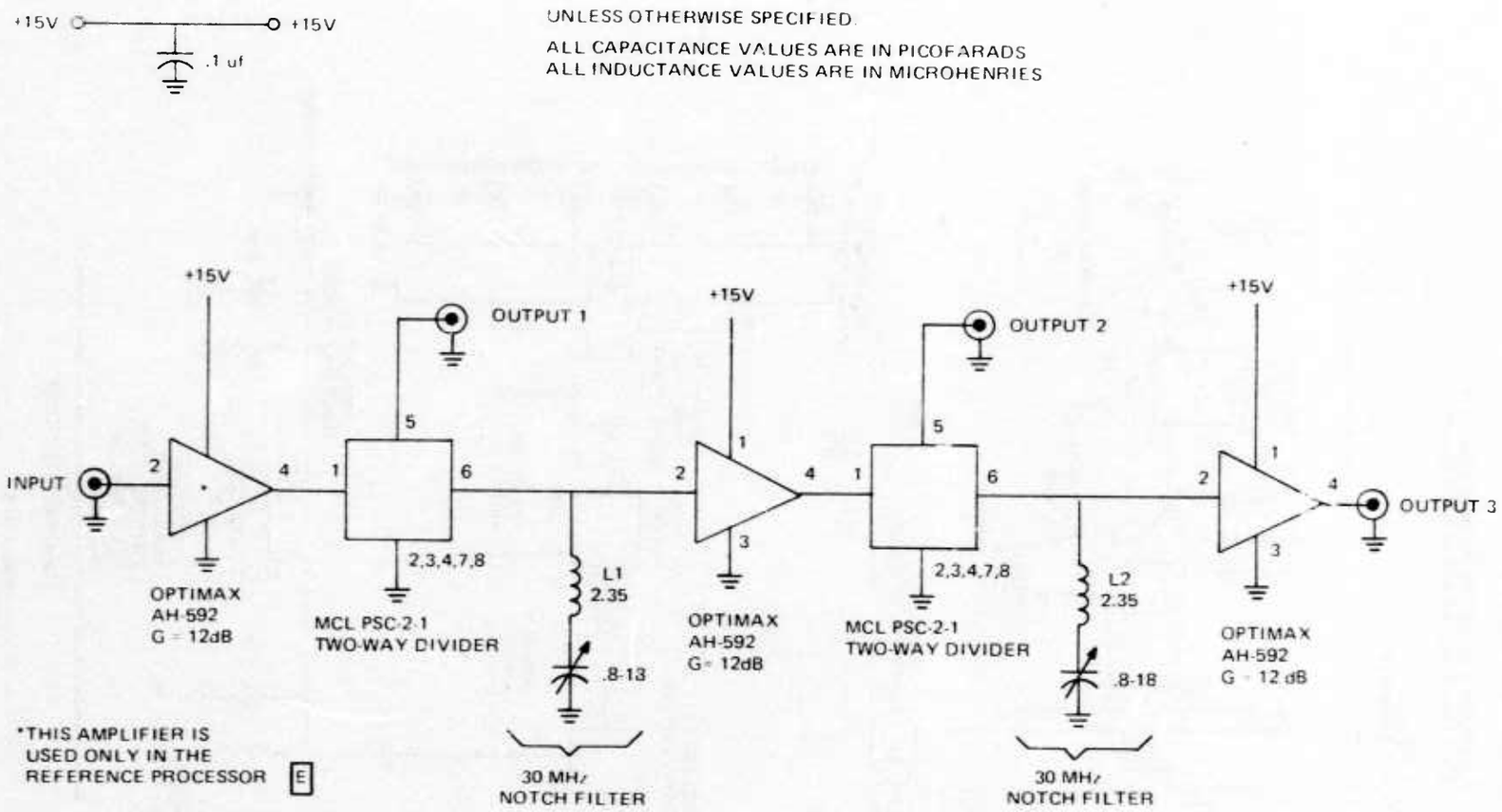

FIGURE 44

SFR [E] AND [L] . NOTCH FILTER CHAINS FOR IF WEIGHT AND CORRELATOR REFERENCES

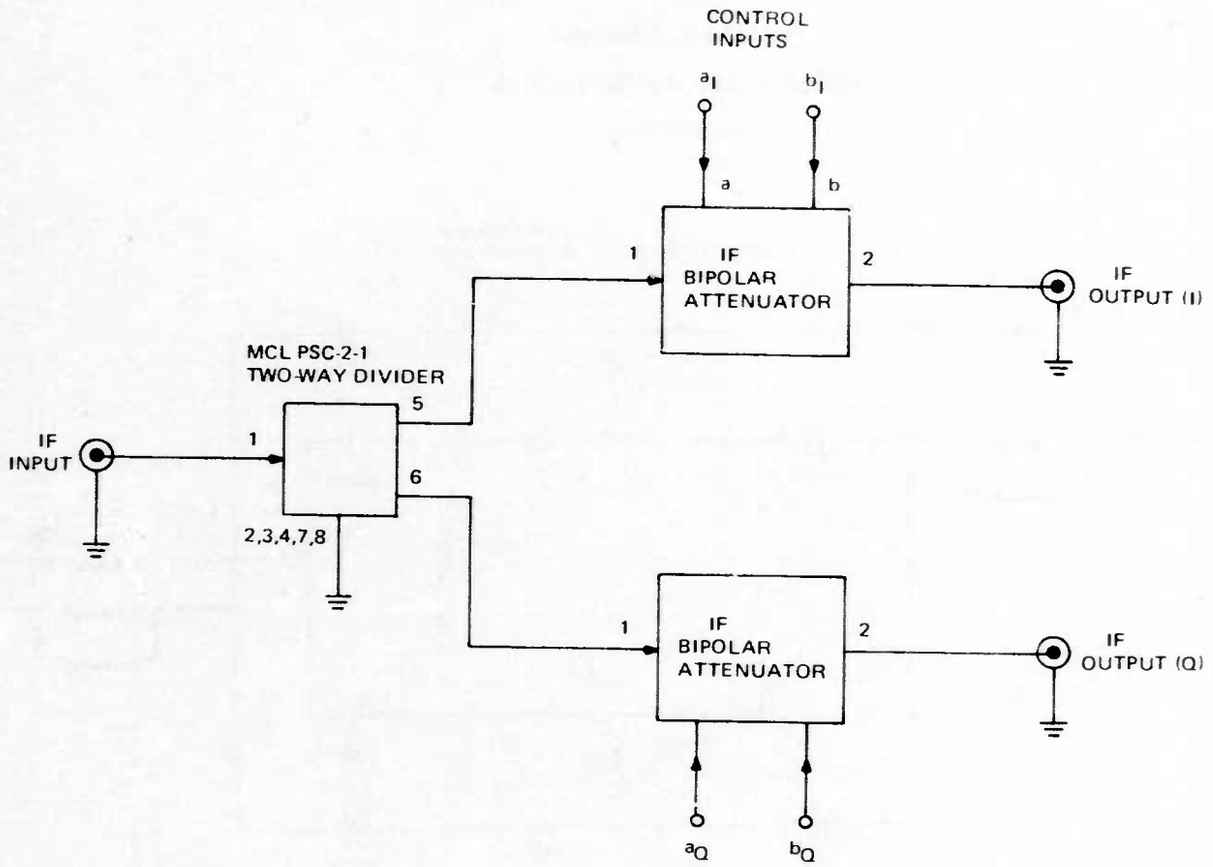

FIGURE 45

F G H SFR IF WEIGHT ASSEMBLY

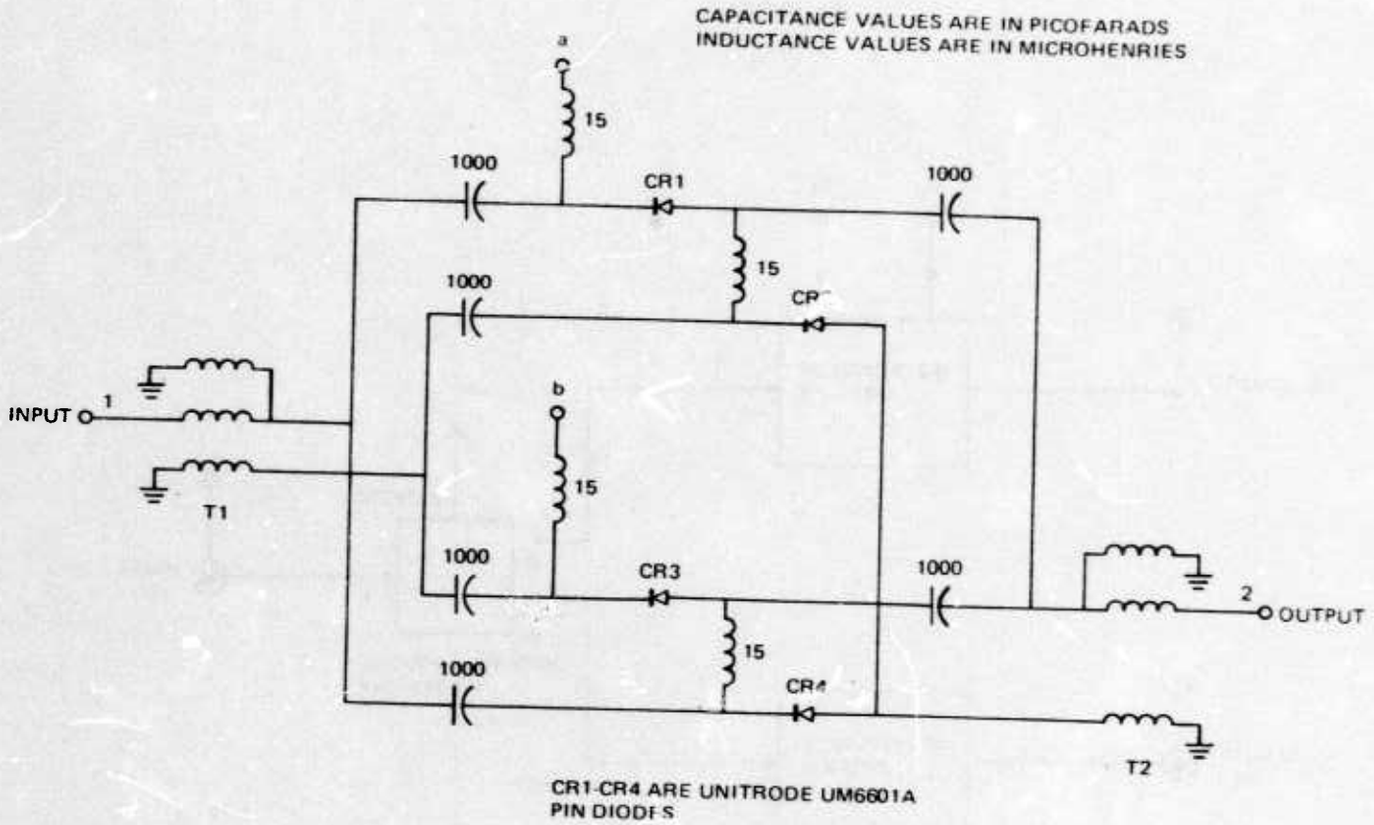

FIGURE 46

SFR IF BIPOLAR ATTENUATOR

CIRCUIT DIAGRAM

g. IF Weight Control Units, Boxes I, J, K

Boxes I, J and K contain three identical control units for the IF weights. A block diagram of these control units is given in Figure 47. These units are built in a fashion very similar to that used in the RF weight control units discussed earlier. There are five circuit cards. The first contains the power divider and two (I and Q) correlators, whose schematic is shown in Figure 39. The second and third cards contain the I and Q synchronous detector/lowpass filters, whose schematic is shown in Figure 40. The fourth and fifth cards contain the I and Q bipolar attenuator drivers, which are each preceded by a test jack for monitoring the DC control voltages and for inserting external DC voltages under open loop test conditions.

Since the IF bipolar attenuators are slightly different from the RF ones, their drivers are slightly different as well. A schematic of the IF bipolar attenuator driver is given in Figure 48. Its operation is basically the same as that of the RF bipolar attenuator driver of Figure 41. The difference between the two lies in the resistor values used in the resistor-diode network on the emitters of the I_a and I_b current source transistors that compensate for the control nonlinearity of the bipolar attenuators. The 30 MHz attenuator output voltage waveform is shown in Figure 49 as a function of a sawtooth driver input waveform.

h. IF AGC Amplifier

The IF AGC amplifier is used to provide gain at IF with AGC action through a peak detector. This keeps the final transmitted output power at 1W so that multichannel inputs are relayed with the same relative power. The IF AGC amplifier is manufactured by RHG Electronics Laboratory, Inc., Model #EST3002. Its performance is summarized in Table 4.

i. IF Bandpass Filter and Pilot Distribution System, Box M'

A schematic diagram of Box M' is given in Figure 50. The AGC amplifier output is bandpass filtered in box M' in a two-pole crystal filter of 100 kHz bandwidth at 30 MHz, with L-C input and output impedance matching networks. The same type of filter is used to constrain the spectrum of the pilot signal before it is split and combined with the transmitted signal in Box M'. The pilot is used as the reference input in the RF and IF ICS correlators.

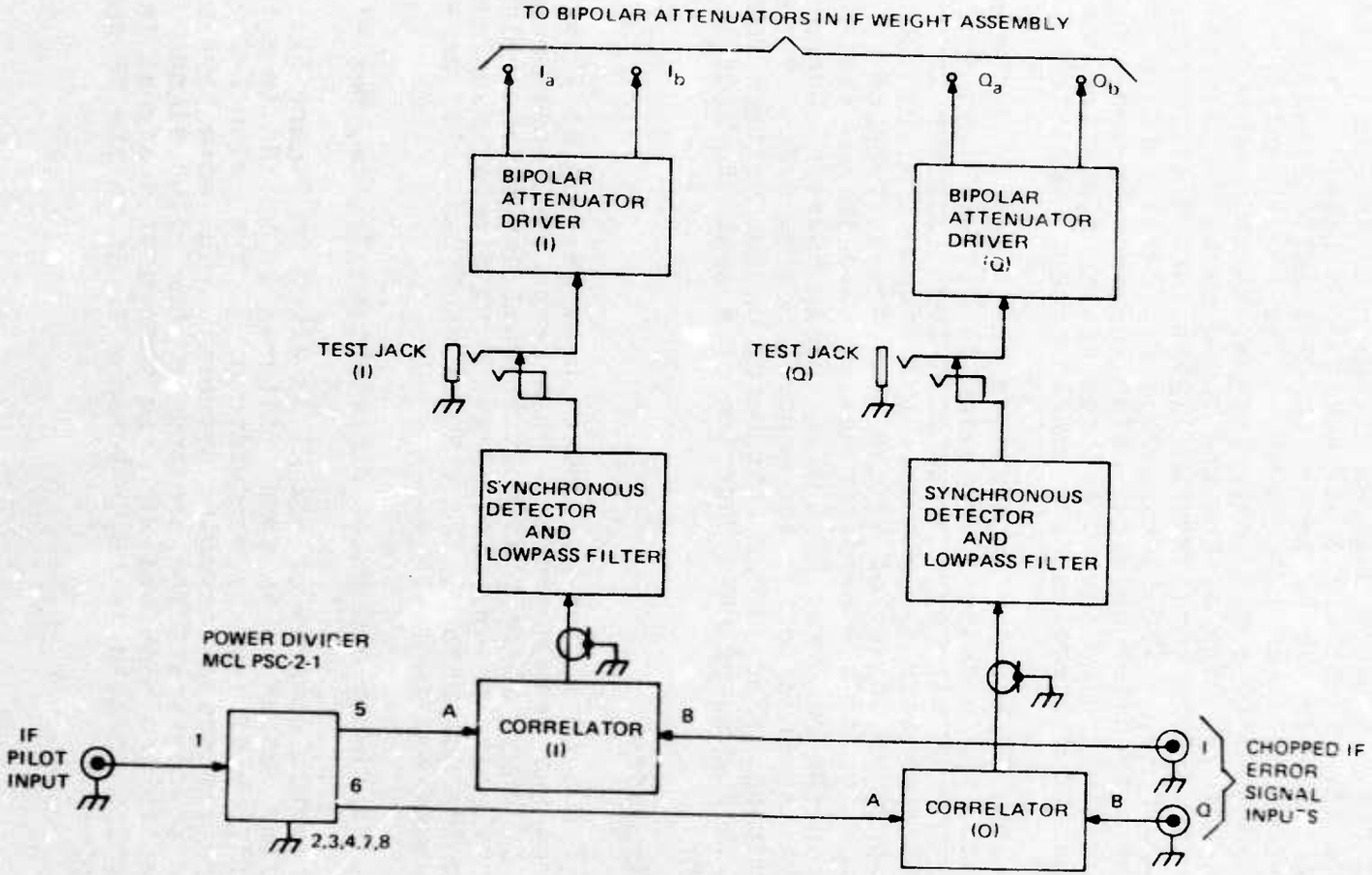

FIGURE 47

SFR IF WEIGHT CONTROL UNITS I J K

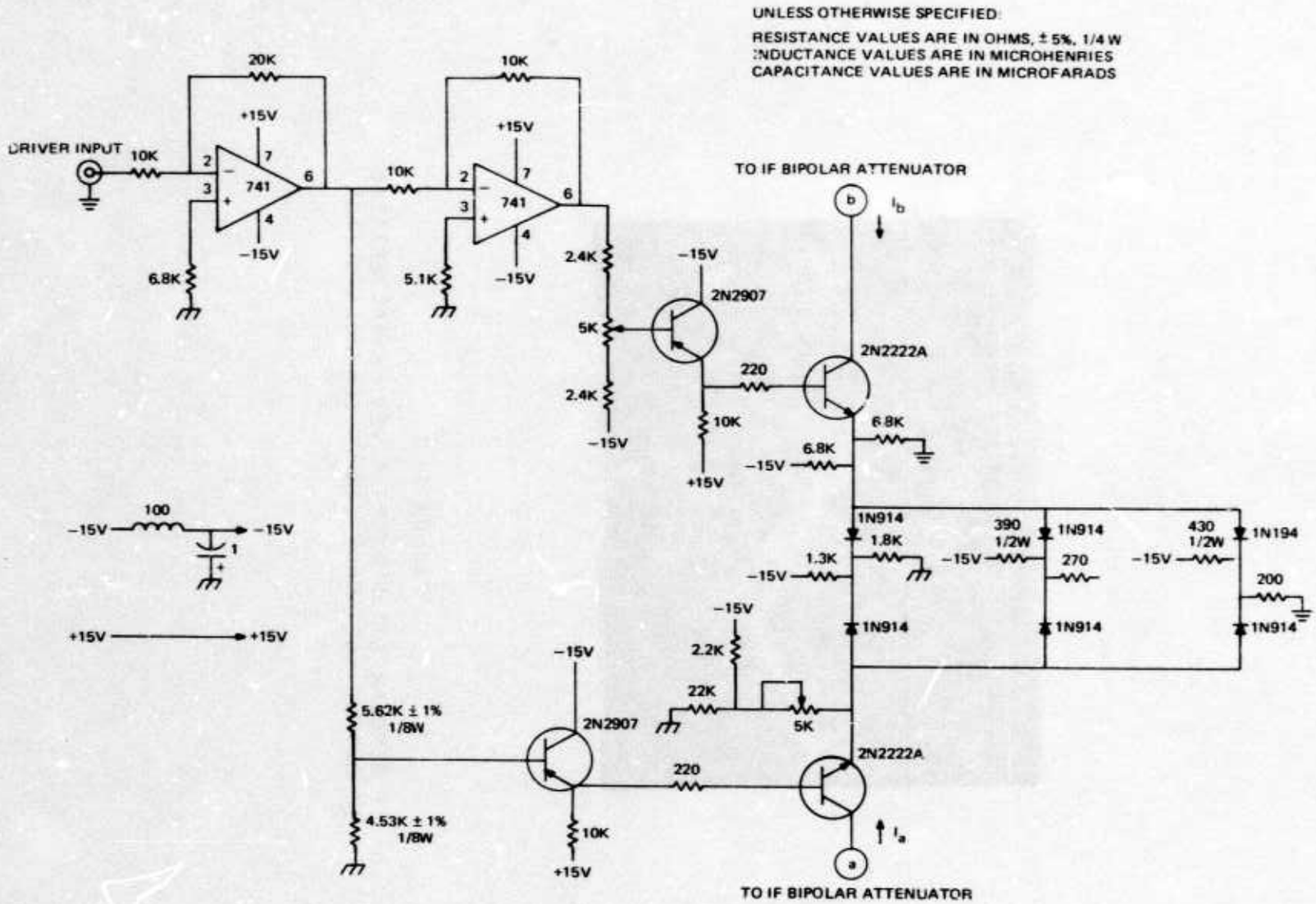

FIGURE 48

SFR IF BIPOLAR ATTENUATOR DRIVER

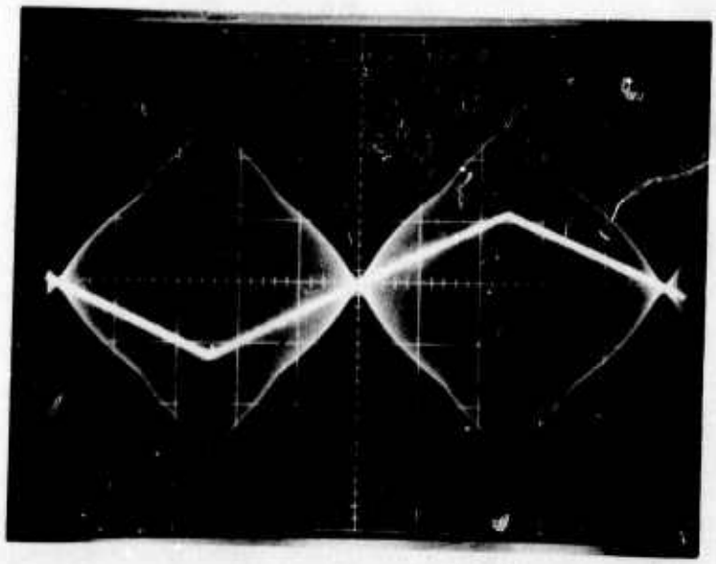

FIGURE 49

IF BIPOLAR ATTENUATOR-DRIVER CHARACTERISTIC
IF OUTPUT VOLTAGE VS INPUT CONTROL VOLTAGE

Table 4

IF AGC Amplifier
(RHG #EST3002) Performance Characteristics

Center Frequency	30 MHz
3 dB Bandwidth	2.8 MHz
Maximum Power Gain	83 dB
1 dB Compression Point	+15 dBm
Maximum Saturated Power Out	+20 dBm
Noise Figure	1.8 dB
Max. Voltage Gain (AGC loop)	103 dB
Maximum Voltage Out (video)	7.4 V P-P
Voltage Required for 60 dB of AGC Range	-4.65 V
AGC Time Constant	15 µs
AGC Compression Ratio	60 dB/<3 dB
Rise Time	0.50 µs
Power Required	+12 VDC at 110 mA -12 VDC at 45 mA

L1 – L4: 22T #32 WIRE ON
MICROMETALS T30-6 CORE

ALL CAPACITANCE VALUES ARE IN PICOFARADS

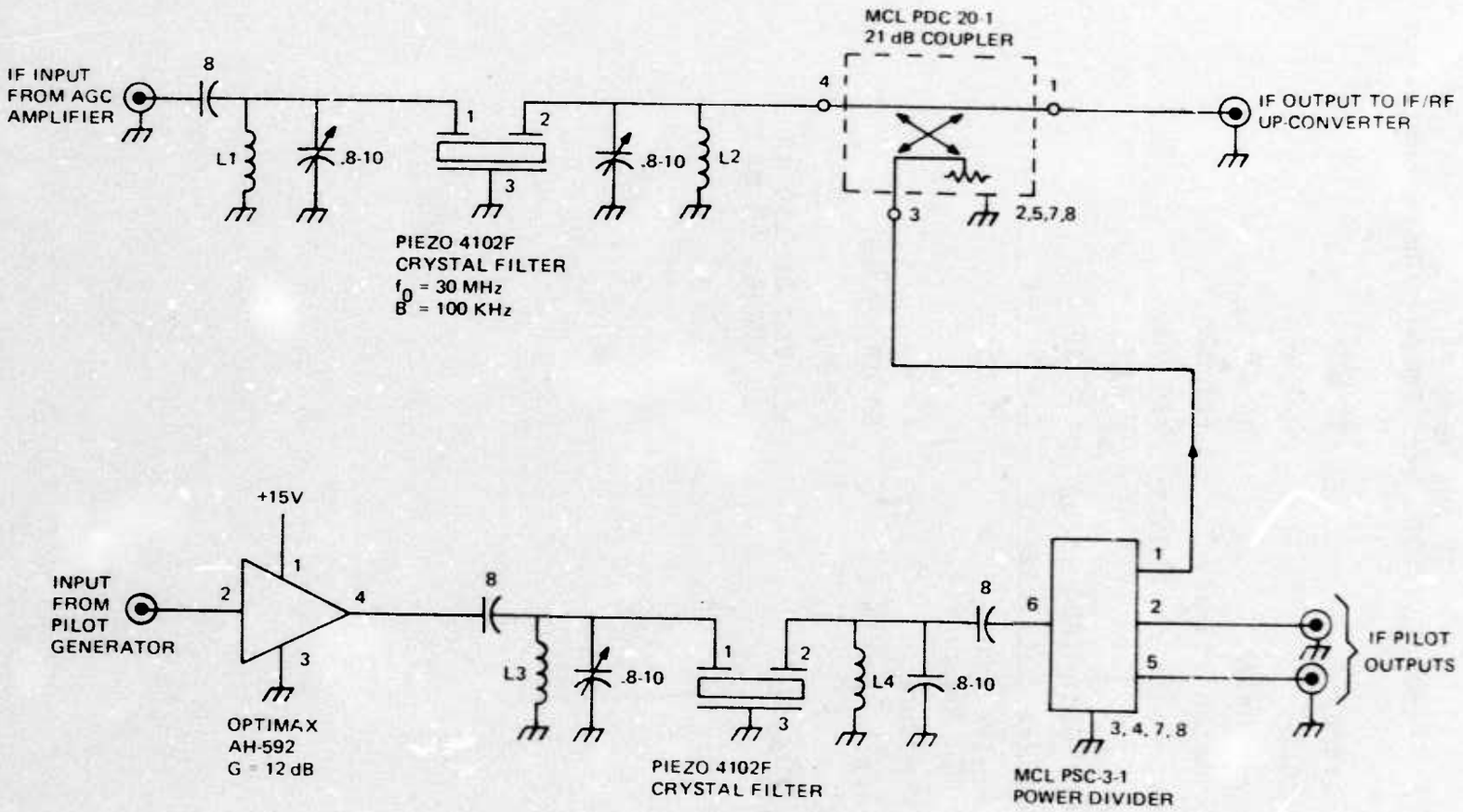

FIGURE 50

SFR IF BANDPASS FILTER AND PILOT DISTRIBUTION SYSTEM M'

j. Signal Up-Converter, LO Distribution and Reference Down-Converter, Box M

A schematic diagram of Box M is given in Figure 51. The 30 MHz IF input is up-converted by mixing it with the 261.8 MHz local oscillator to the 291.8 MHz RF. It is then bandpass filtered in a two-section L-C filter and amplified by 12 dB. The 12 dB amplifier is followed by a 30 MHz notch filter to reject the IF, and a delay line notch filter with a null at 231.8 MHz and a peak near 291.8 MHz to reject the lower sideband.

The LO input is a 261.8 MHz sinusoid at a 0 dBm level. It is distributed through a network of hybrid splitters, filters, pads, and amplifiers which are used to prevent signal flow through the LO distribution network. For example, there are LO outputs to the pilot up-converter and to the signal down-converter. If the pilot signal flows through this path, it reaches the receiver IF input through a path which is not shared by the transmitted signal. Thus, when the IF ICS adapts to cancel the pilot, it will not be cancelling the transmitted signal in the same manner.

The LO is used in two mixers in Box M -- one to up-convert the transmitted signal, and the other to down-convert the RF ICS Reference for use as the IF ICS Reference. The LO is outputted from Box M for use in two other places -- in Box C for up-converting the pilot and in Box B for down-converting the signal.

k. Transmitter Power Amplifier

The transmitter power amplifier is manufactured by Microwave Power Devices, Inc., Model #LWA055-2. Its performance features are summarized in Table 5.

ℓ. 455 kHz Waveform Generator, Box N

A schematic diagram of Box N is given in Figure 52. The 455 kHz squarewave is generated in a CD4047AE oscillator. Four outputs are taken directly from the CD4047AE to drive the synchronous detectors in the RF ICS and IF ICS weight control units. These outputs supply low current levels. Two higher current outputs are provided through Class C buffers at +7 dBm each to drive the error signal choppers in theRF ICS and IF ICS.

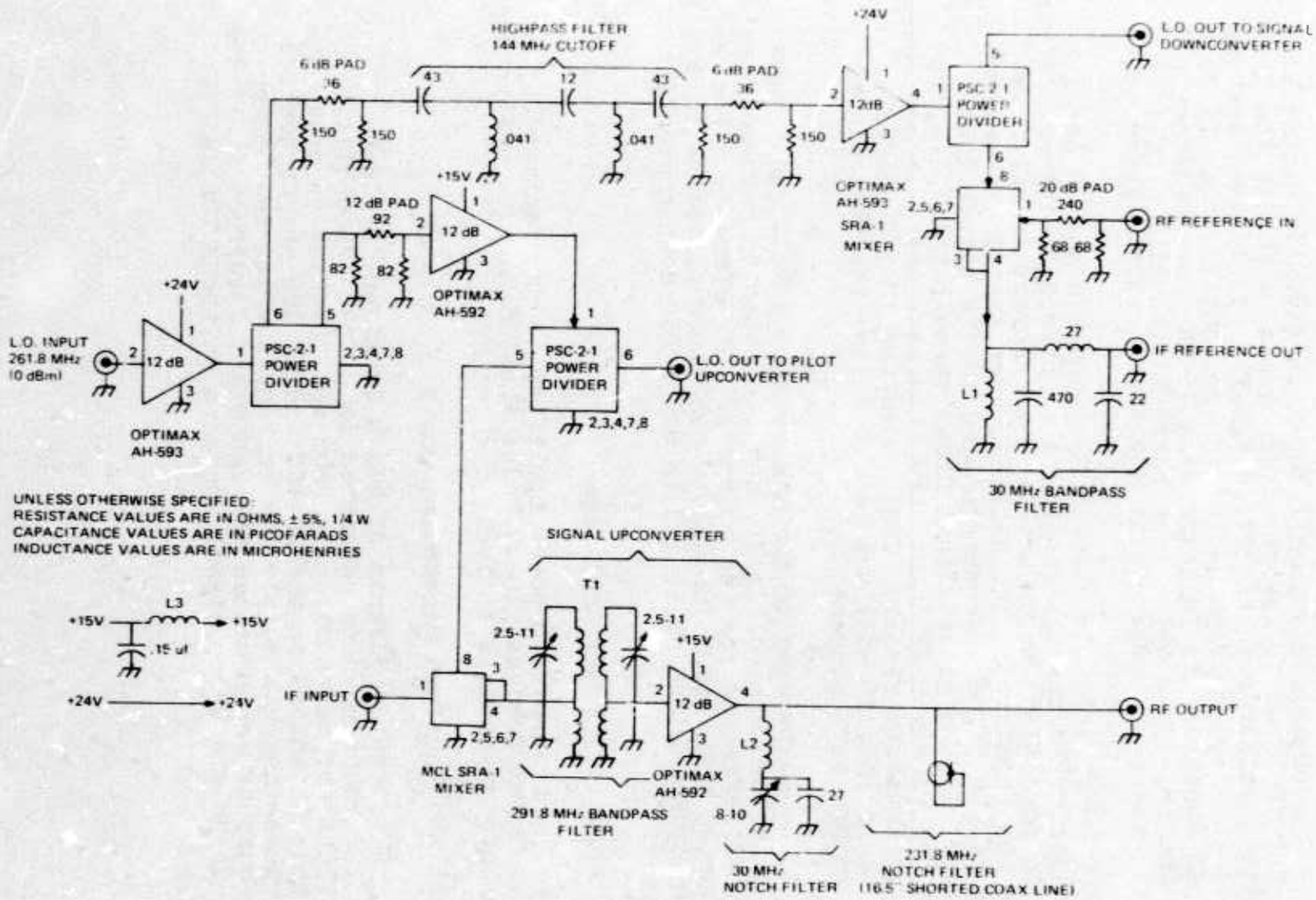

FIGURE 51

SFR SIGNAL UP CONVERTER, LOCAL OSCILLATOR
DISTRIBUTION AND REFERENCE DOWN CONVERTER [M]

Table 5

SFR Transmitter Power Amplifier
(MPD #LAA055-2) Performance Characteristics

Frequency Range	5-500 MHz
Power Output	+33 dBm, 1 dB compression +35 dBm, saturated
Third-Order Intercept	+43 dBm
Harmonic Levels	-20 dB, max
Gain	38 dB, min
Gain Flatness	±1.0 dB
Noise Figure	8 dB
Input Power	+24 VDC, 1.65 amps

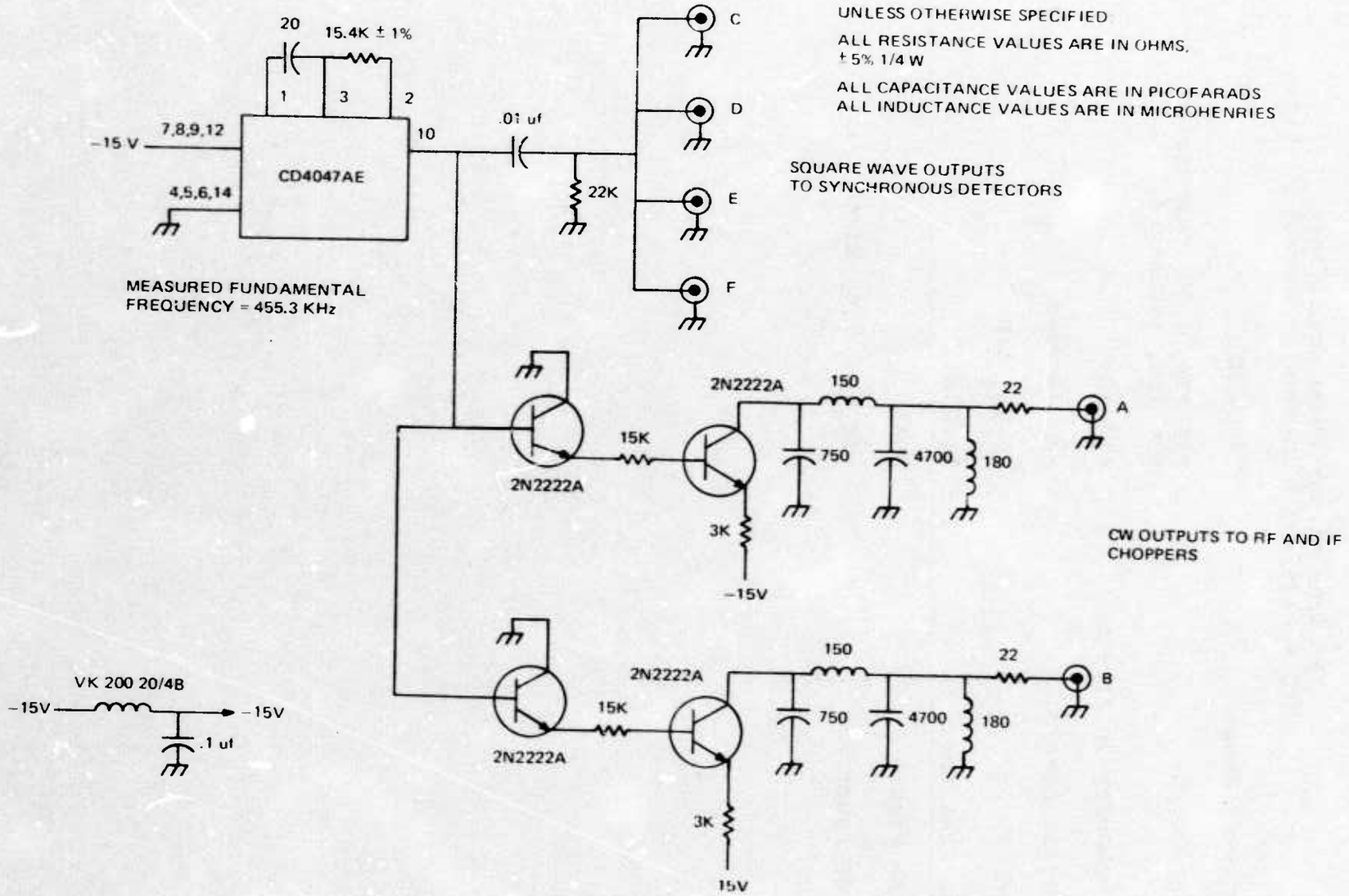

FIGURE 52

SFR 455 KHZ WAVEFORM GENERATOR N

SECTION VII

EXPERIMENTAL RESULTS WITH THE SFR BREADBOARD

Tests were conducted on the SFR breadboard which were aimed at establishing the following principles of operation:

1) Pilot direction of an ICS is valid and can be used in an SFR.
2) An IF ICS can further improve the cancellation of an RF ICS and thus improve the forward gain of an SFR.
3) A multichannel notch-filter ICS can be used to improve broadband cancellation performance and SFR forward gain.
4) The ICS is applicable to an SFR to increase forward gain.
5) The SFR is linear and can be used as a multichannel relay.

These operating principles have been experimentally established. The SFR experiments also have demonstrated the performance limitations in the present breadboard and point out the need for further improvements.

1. PILOT DIRECTION AND CASCADED ICS'S

The RF ICS by itself provides 40-45 dB of cancellation, both on the pilot and on the coupled transmitted signal. The IF ICS (single channel) provides an additional 43 dB of cancellation beyond that on a CW pilot. The shape of the resulting IF ICS cancellation notch, however, is very narrow, producing great variations in the transmitted signal cancellation as a function of its location in the 100 kHz transmission band. The same frequency-dependent cancellation performance is noted on an FM pilot (100 kHz wide), where the band-center cancellation is deep, but the band-edge cancellation is only 5 dB down from the RF ICS cancellation. If a transmitted signal is added to the pilot, its cancellation spectrum follows that of the pilot.

The cancellation performance described above is illustrated in the photographs of Figure 53. The photographs show the FM pilot at the output of the IF ICS. The upper photo is with the RF and IF cancellation disabled. The center photo is with only the RF ICS operating. The lower photo is with both RF and IF ICS's operating. It may be noted that the cancellation notch formed by the RF ICS is broad, but the IF ICS notch is narrow, accounting for the degraded cancellation at the band edges.

A narrow cancellation notch is caused by imperfect match of the phase and amplitude vs frequency characteristics between the circuitry along the main input and along the reference input. Correction of a phase mismatch was attempted by adjusting cable lengths both at the IF ICS inputs and at the RF ICS inputs, but

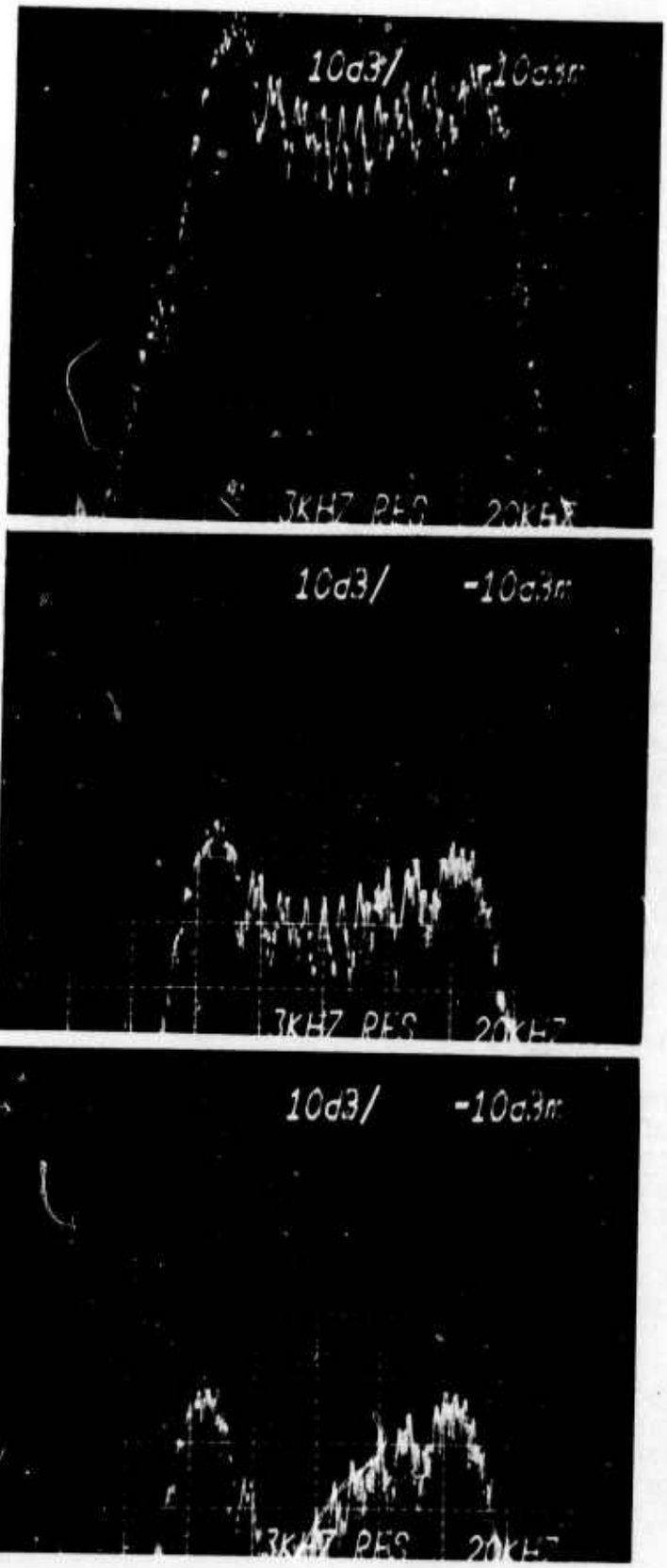

HORIZONTAL SCALE:
20 KHZ/DIV
30 MHZ CENTER LINE
VERTICAL SCALE:
10 DB/DIV
-10 DBM TOP LINE

UPPER PHOTO: RF AND IF ICS'S DISABLED

CENTER PHOTO: RF ICS ONLY ENABLED

LOWER PHOTO: RF AND IF ICS'S ENABLED

FIGURE 53

CANCELLATION CHARACTERISTICS OF RF AND IF ICS'S

no improvement was gained. It has been concluded that the mismatch problem must be in amplitude, but further diagnosis and correction has yet to be done.

2. MULTICHANNEL NOTCH FILTER ICS

The IF ICS was designed as a three-channel notch filter ICS. It has the capability of improving broadband cancellation performance over that of a single-channel ICS when non-flat amplitude or phase vs frequency characteristics limit the cancellation bandwidth as is the case here. The implementation of the notch filter ICS in the SFR breadboard, however, was found to be ineffective with a signal as narrowband as 100 kHz. That is, the three-channel ICS performance was the same as that of the single-channel ICS.

Tests were run on the three-channel IF ICS alone to demonstrate its operating principles. The tests were conducted using a 600 kHz bandwidth FM test signal at 30 MHz, which represents the SFR pilot. Boxes D, D', E and L (see Figure 33) of the ICS breadboard were used in the test setup shown in Figure 54. The performance results are shown in the photographs of Figure 55.

Each photograph in Figure 55 shows four traces, labelled 0, 1, 2 or 3. The label number represents the number of notch filter channels activated, with 0 referring to no cancellation at all. In Figure 55a, where there is little delay between the ICS inputs, the cancellation with one channel is good to begin with, so that the addition of the second and third channels causes only slight improvement. As the delay is increased in Figures 55b and 55c, the improvement offered by the second and third channels is far more significant. In fact, in Figure 55c, the single-channel ICS provides no cancellation at the band edges, but the three-channel ICS provides at least 40 dB of cancellation across the band.

The notch filters used in the IF ICS are of the L-C type, using ferrite toroid cores to obtain a high-Q inductor. Even so, the Q is not high enough to allow the last expression of Equation (68) to be satisfied when the signal bandwidth is 100 kHz. With a 600 kHz bandwidth, the notch filter operates as desired. Further improvement in the notch filter design to provide a narrow notch bandwidth without sacrificing notch depth will allow operation with a 100 kHz bandwidth, but such improvement requires an approach other than a series or shunt tank circuit. The analysis of Appendix A shows that in these two configurations the product of the notch depth times its bandwidth is a constant determined by the center frequency and the unloaded Q of the inductor.

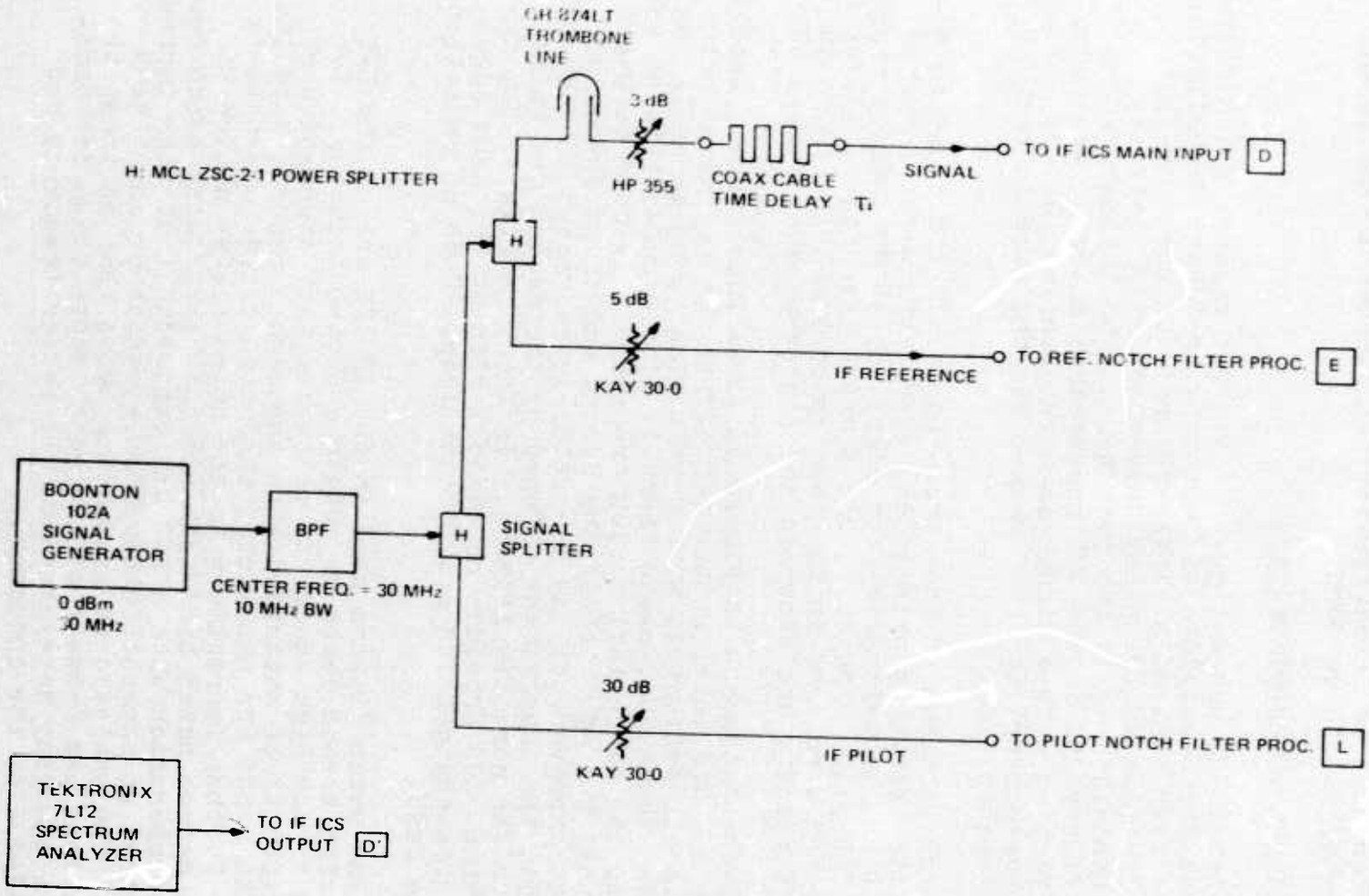

FIGURE 54

TEST SETUP USED FOR NOTCH FILTER ICS PERFORMANCE MEASUREMENTS

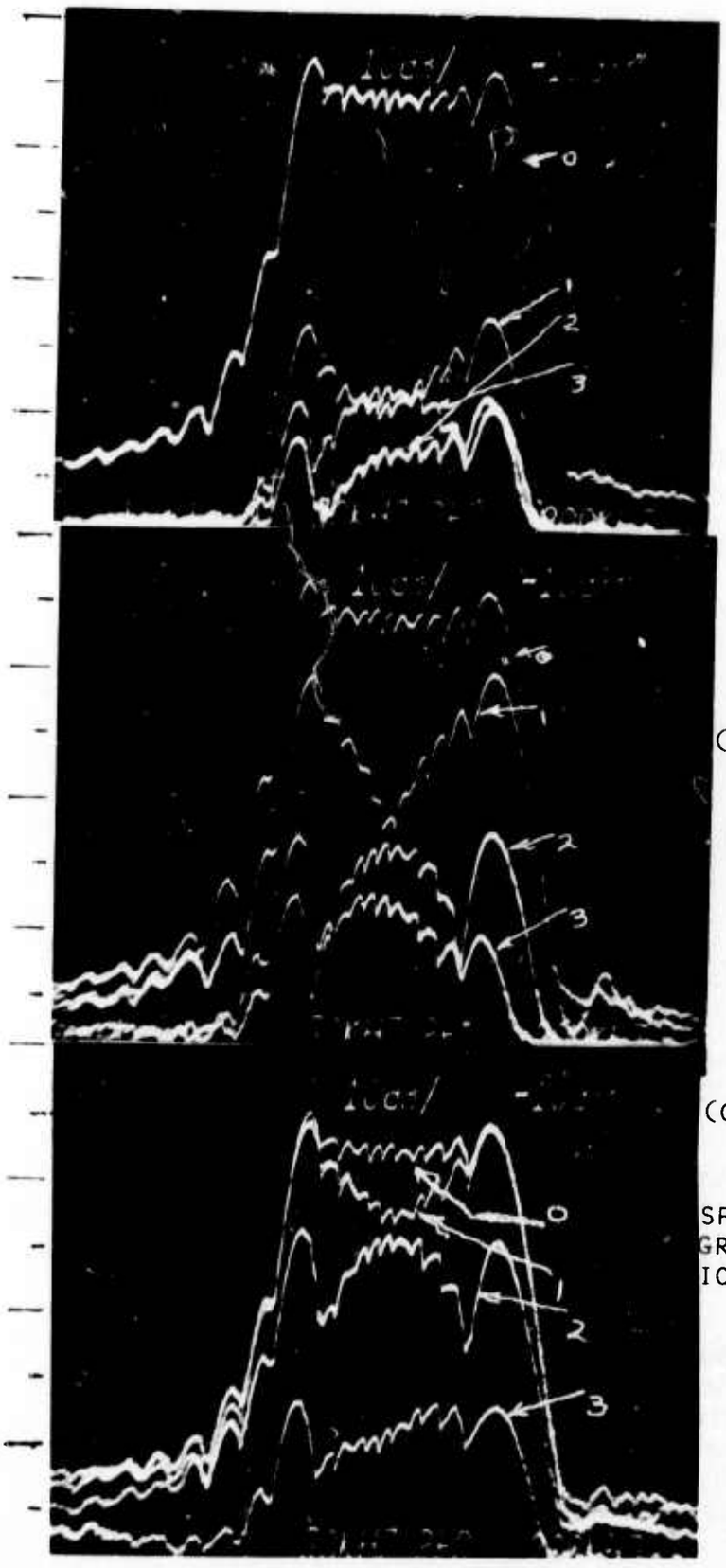

(A)

VERTICAL SCALE:
-10 DBM TOP LINE,
10 DB/DIV
HORIZONTAL SCALE:
30 MHZ CENTER LINE,
?00 KHZ/DIV

(B)

(C)

FIGURE 55

SPECTRUM ANALYZER PHOTO-
GRAPHS OF NOTCH FILTER
ICS PERFORMANCE

The multichannel notch filter ICS was also tested in cascade with the RF ICS, as required in the SFR design. In order to use a 600 kHz wide pilot, the 100 kHz wide crystal filters were bypassed. The test setup used is illustrated in Figure 56 with the SFR loop opened at port 5 and monitored there. Figure 57 gives a sequence of spectrum analyzer photographs taken at the IF ICS output showing the progressive reduction (improvement) of cancellation residue with the use of the RF ICS, the first channel of the IF ICS, the second channel of the IF ICS, and the third channel of the IF ICS.

It was noted that both the weight and correlator notch filter chains exhibited a spectral component at the LO frequency (261.8 MHz) which gets progressively stronger proceeding along the chain. This is due to a small amount of LO leaking through the downconverter, into the inputs of the notch filter chain and being amplified by the broadband amplifiers but not being notched by the filters. The result is that this LO component interferes with the operation of the IF ICS control loops by a progressively increasing amount. This effect is negligible in the first loop, noticeable in the second loop, and strong in the third loop. Lowpass filters were incorporated at the inputs to both notch filter chains in order to obtain the photos in Figure 57, but they did not eliminate the problem. Because of this problem, the multichannel notch filter IF ICS did not provide as much cancellation when cascaded with the RF ICS as it did when tested alone.

3. FORWARD GAIN MEASUREMENTS

a. Test Setup

Forward gain measurements were made on the SFR breadboard using the equipment arrangement shown in Figure 56. The IF crystal filters limited the pilot and signal bandwidths to 100 kHz. Because the multichannel IF notch filter ICS with a 100 kHz signal bandwidth does not enhance the single-channel performance, only a single channel was used.

The coupler and pads within the dashed region are used to permit the application of a simulated received signal to the repeater input. The repeater output is then examined directly at (2), after attenuation to a safe power level for the spectrum analyzer.

The repeater signal path is shown by the heavy line on Figure 56. The incoming wave, incident on the antenna coupler, enters port 2 and is coupled to port 1' with 6 dB coupling loss. It passes through variable attenuator #2 and enters the RF ICS weight assembly A , where an additional 3 dB loss occurs. The signal is amplified and down-converted to a 30 MHz intermediate

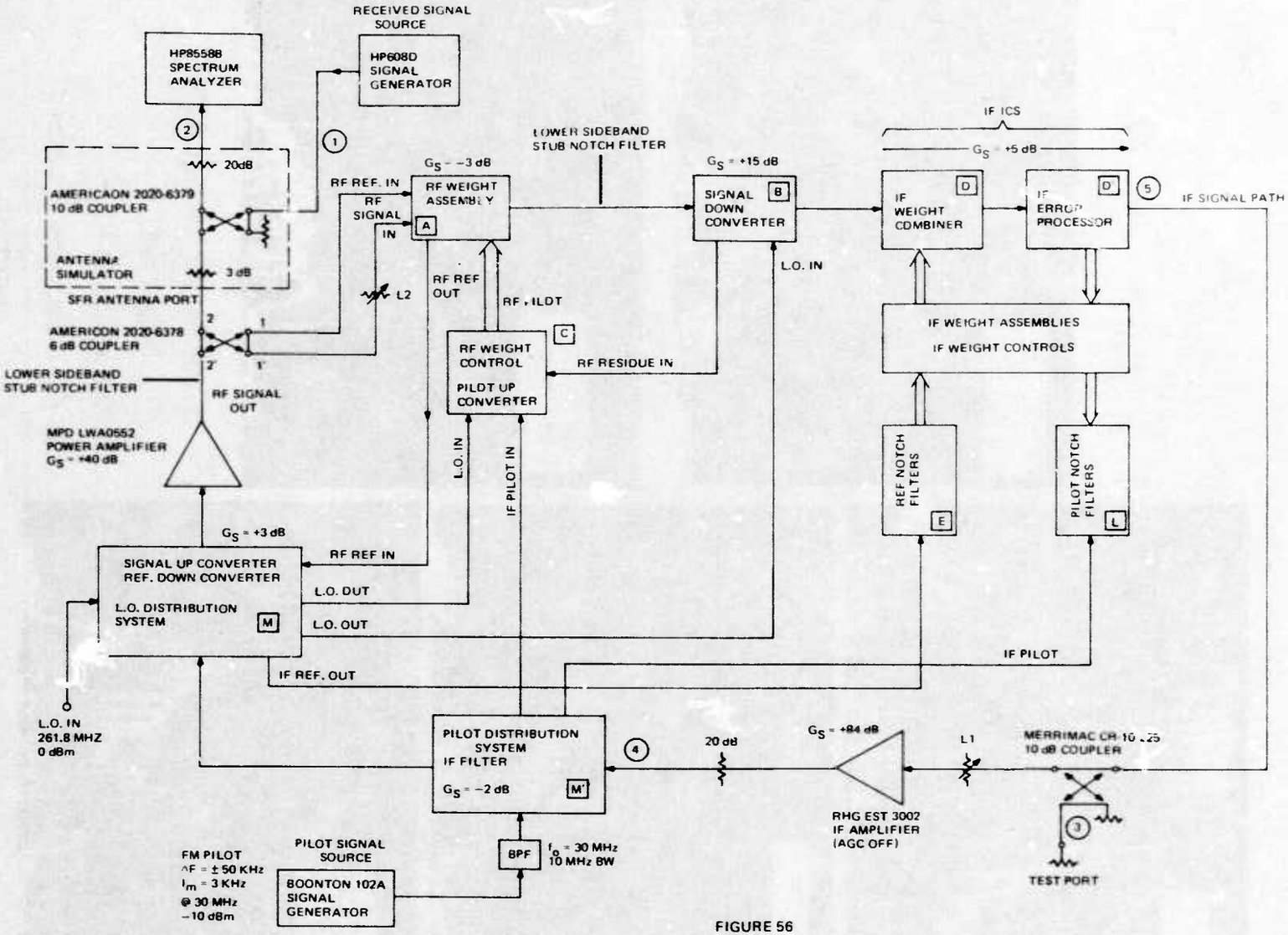

FIGURE 56

SFR FORWARD GAIN MEASUREMENT SETUP

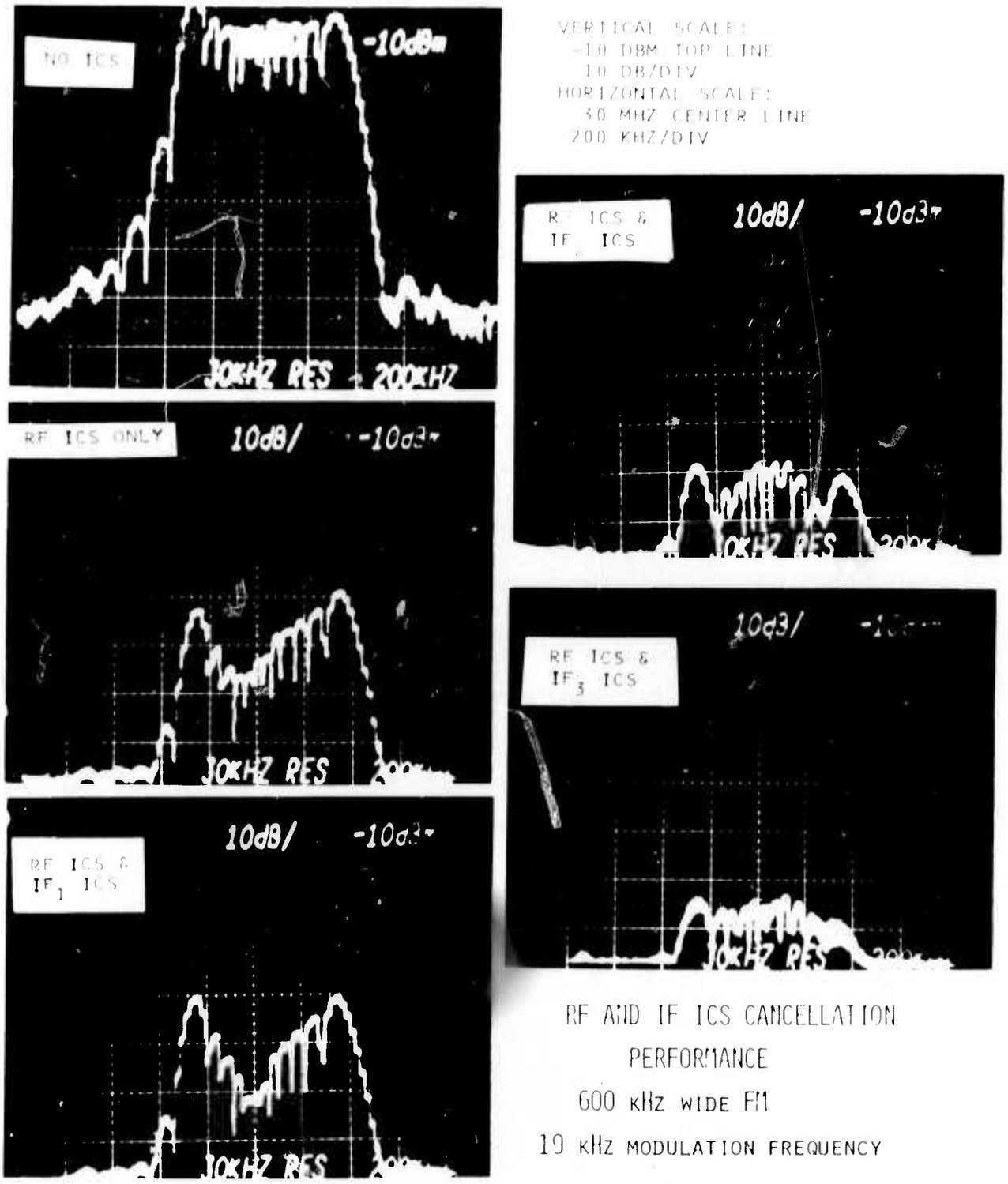

RF AND IF ICS CANCELLATION
PERFORMANCE
600 kHz WIDE FM
19 kHz MODULATION FREQUENCY

FIGURE 57

frequency in B, with 15 dB overall gain. The IF signal passes through the IF ICS weight, combiner, error processor and the IF amplifier, where variable attenuator #1 is used to adjust the forward gain of the repeater. The AGC action of the IF amplifier was disabled for this test. The repeater frequency response is established by the 100 kHz 3 dB bandwidth crystal filter at the output of the IF amplifier. The signal is then up-converted to the original carrier frequency, amplified by the MPD LWA 055-2 linear power amplifier, and leaves the repeater through the main line of the antenna coupler.

The repeater forward power gain is calculated from the gains of the individual blocks to be

$$G_F = -6-L_2-3+15+5-L_1+64-2+3+40 = 116 - (L_1+L_2) \text{ dB} \qquad (141)$$

where L_1 and L_2 are the attenuator insertion losses in dB. In the experiments that follow, L_2 = 5 dB was maintained so that the forward gain is given by

$$G_F = 111 - L_1 \quad \text{(dB)} \qquad (142)$$

The repeater forward gain is determined experimentally by application of a CW signal at port (1) and measurement of the resultant output power at (2). The loss on the input signal from (1) to the SFR antenna port is 13 dB. The loss on the output signal from the SFR antenna port to (2) is 23 dB. Thus, with G_I the insertion gain from (1) to (2), it follows that the SFR forward gain is

$$G_F = G_I + 36 \qquad (143)$$

where both G_I and G_F are in dB.

b. Forward Gain Measurements

The purpose of this test is to determine the maximum possible forward gain that can be used without repeater instability due to closed loop feedback via the antenna network. In this case, the output-to-input coupling is primarily due to the finite antenna coupler isolation between ports 1 and 1'. (The insertion loss between these ports was measured as 22 dB.)

It was found that, with no desired receivedsignal present and both RF and IF cancellers disabled, oscillation developed when L_1 = 97 dB. With the received signal absent and the RF and IF cancellers operating, L_1 could be decreased to 44 dB before the repeater oscillation started, so that the RF and IF cancellers provide at least 53 dB of isolation across the 100 kHz band. From Equation (142) the achievable forward gain is

$$G_F = 67 \text{ dB} \qquad (144)$$

A -18 dBm CW signal at 261.77 MHz was then connected at port (1) (-31 dBm at the SFR antenna input). It was found that L_1 could be decreased to 58 dB before oscillation started, for which the signal output power measured at point (2) = 0 dBm (+25 dBm at the antenna coupler output). The forward gain of the repeater is found from (143) to be

$$G_F = 54 \text{ dB} \qquad (145)$$

a 39 dB improvement over the maximum possible forward gain when the RF and IF cancellers are not used.

Spectrum analyzer photographs are shown in Figure 58 of a CW pilot and a low power output CW desired signal with the SFR on the verge of oscillation. The upper photo shows the spectrum at the SFR output (port 2), and Figure 58B shows the IF spectrum at port 3. The pilot at screen center has been greatly reduced by the RF and IF ICS's relative to the desired signal. The left edge of the 100 kHz wide passband in both photos shows a highly peaked response, indicating that oscillation is imminent. The onset of oscillation occurs at a band-edge frequency where the degradation of ICS cancellation from that of the band-center pilot is most severe.

It was also determined that as the signal input was reduced from -18 dBm, the achievable forward gain increased from 54 dB to 67 dB, with the output power at point (2) remaining at 0 dBm. Investigation of this effect revealed that when the output power at point (2) reached 0 dBm, its corresponding -15 dBm level at (4) was found to be coupled into the pilot path to the ICS correlators. A level of -15 dBm at point (4) was found to produce a level of -60 dBm at the correlator inputs. This level was sufficient to overcome the pilot control of the ICS's and anything higher causes them to abruptly cease cancelling. With increased isolation to prevent this effect, it is expected that a forward gain of 67 dB would have been measured for any output level up to the design goal of +30 dBm.

Another stray coupling problem was found which is a potential limitation to forward gain. It is caused by stray coupling of the pilot signal through the LO distribution network into the receiver IF. It appears at the output of Box B 80 dB lower than its level at the pilot input of Box M (see Figure 34). Filtering has been added in Box M to provide isolation, but an additional 30 dB of isolation is required to achieve full forward gain. The coupling of the pilot into the receiver IF would cause the IF ICS to lose cancellation on the transmitter signal in its attempt to cancel the pilot, since the transmitter and pilot signals then would not follow identical paths from the SFR's transmitter to the IF ICS input.

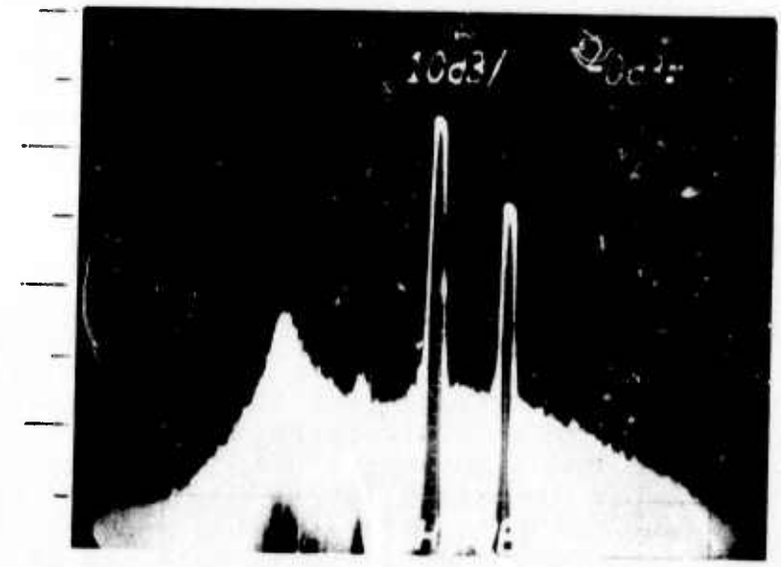

100 KHZ
PASSBAND

SFR RF
OUTPUT

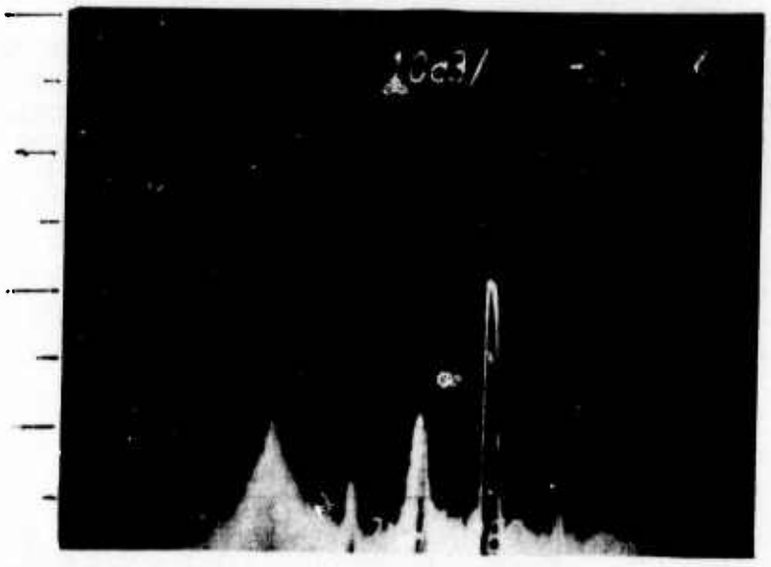

IF ICS
OUTPUT

MARGINAL
OSCILLATION
RESPONSE

CW
PILOT

DESIRED
SIGNAL

FIGURE 58

SFR SPECTRA AT ONSET OF OSCILLATION
(RF & IF_1 ICS CONFIGURATION)

4. REPEATER LINEARITY

The test setup used for forward gain measurement was also used to demonstrate the repeater linearity. A second tone was combined with the test used to measure forward gain, separated from it by 25 kHz and 6 dB below it. The same forward gain performance was found as for the single input case, and the two output tones were retransmitted with the same 6 dB ratio. In-band third order intermodulation products between the two tones were in excess of 30 dB below the lower level tone.

5. SUMMARY OF EXPERIMENTAL RESULTS

The experiments described above have demonstrated the operating principles on which the SFR design is predicated. They also have uncovered some problems in the breadboard implementation which need to be corrected for the SFR to operate as designed. These problem areas are: bandwidth limitations in the IF notch filter ICS which prevent its effective performance with the 100 kHz repeater bandwidth; stray coupling of the IF transmitted signal into the pilot distribution network which degrades the pilot-directed cancellation in both the RF and IF ICS's; and stray coupling of the pilot into the receiver through a path not shared by the transmitted signal, namely through the LO distribution network.

The experiments have shown, however, that the SFR operating principles are valid. Forward gain has been measured to be as large as 67 dB; and with modifications to the breadboard, forward gain in excess of 100 dB appears to be achievable.

SECTION VIII

RECOMMENDATIONS FOR FURTHER WORK

The experiments on the SFR breadboard have uncovered areas in which further work is needed. They are: isolation to prevent coupling of the transmitted signal into the pilot distribution network, isolation to prevent coupling of the pilot signal into the receiver IF via the LO distribution network, and narrowing the notch filter bandwidth in the IF ICS without sacrificing notch depth. Recommended approaches for solving these problems are outlined in the subsections below.

Following these circuit modifications, further laboratory tests should be run to establish the new performance levels. At that point it is recommended that field tests be conducted on the SFR with a real antenna in a real terrain environment.

1. ISOLATION IN THE PILOT DISTRIBUTION NETWORK

The pilot distribution network, contained in Box M' (see Figure 34), consists of a three-way splitter and a directional coupler which combines the pilot with the IF transmitter signal. It is the coupling of the IF transmitted signal into the ICS correlators through the isolated directions of the directional coupler and the three-way splitter that causes the problem. Additional isolation may be obtained by inserting an isolation amplifier between the three-way splitter and the directional coupler, and by shielding this isolation amplifier, three-way splitter, and pilot crystal filter from the IF transmitter signal. Filtering would not be an effective means of isolation because the spectra of the transmitter signal and the pilot overlap.

2. ISOLATION IN THE LO DISTRIBUTION NETWORK

Much has already been done in the LO distribution network with filters and isolation amplifiers (Figure 51) to prevent the pilot from finding its way through the network and across mixers into the receiver IF. The principle coupling paths are now by radiation around the isolation amplifiers and filters. The LO distribution network should be laid out anew to incorporate RFI shielding that will allow the isolation amplifiers and filters to be fully effective. In addition, higher-isolation mixers should be substituted in the breadboard for the ones presently in use.

3. NOTCH FILTER IMPROVEMENT

The design of the notch filters presently in use in the IF ICS represents a compromise between narrow bandwidth and notch depth. As shown in Appendix A, for the commonly used L-C

series resonant or shunt resonant notches, this tradeoff is constrained by the unloaded Q of the notch components. The highest Q components available were used in these circuits. The improvement needed is a reduction in notch bandwidth by a factor of six without degrading the notch depth. In either of these two configurations, unloaded Q's of 1000 would be required.

Crystal notches have been considered, but their bandwidth is too narrow. In addition, a single-pole crystal notch usually has spurious responses near the notch center which would distort the spectrum.

There are means of using the L-C components in circuit configurations that remove the dependence of notch depth on component Q. One such approach is a Q-multiplier circuit which in effect presents a negative resistance to cancel out most of the component loss resistance. Once the negative resistance is set, the notch depth then becomes dependent only on the variations in component Q (with environment, age, etc.). However, if the variations cause the component Q to become too large, the circuit will oscillate.

Another approach that trades the dependence on component Q to dependence on Q variations is illustrated in Figure 59. The notch is implemented by forming the difference between the input signal (slightly attenuated) and a narrow bandpass version of the input signal. The attenuator is adjusted to equal the center frequency attenuation of the resonator, so that the center frequency transmission of the circuit is zero, equivalent to an infinite notch depth. Variations in the component Q in the bandpass resonator will then degrade the notch depth, but the circuit will not become unstable. This approach is the one recommended for improvement of the SFR breadboard.

The differential amplifiers used in the notch filter chains should be tuned at 30 MHz so that low level LO component at 261.8 MHz and other spurious signals are rejected instead of amplified. This bandwidth is not critical, as long as it is much greater than the notch bandwidth.

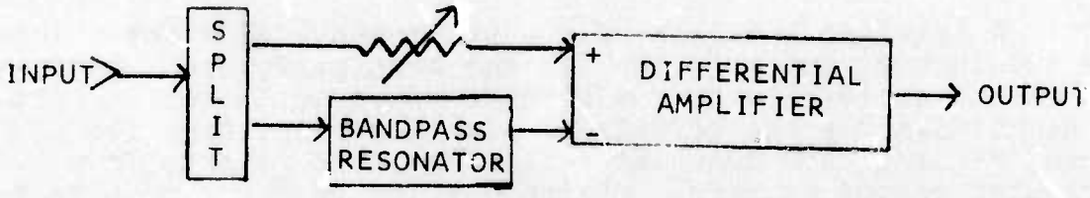

FIGURE 59

NOTCH FILTER IMPLEMENTATION WITH NOTCH DEPTH INDEPENDENT OF COMPONENT Q

SECTION IX

SUMMARY AND CONCLUSIONS

The concept of a pilot-directed multichannel notch filter interference cancellation system (ICS) has been developed to provide transmitter-to-receiver isolation in a same-frequency repeater (SFR). Laboratory experiments have been described which verify the operating concept.

A detailed analysis of the performance of a one-channel and a two-channel notch filter ICS has been performed. Limitations on the achievable transmitter-to-receiver isolation have been quantified for the effects of signal returns from the antenna, returns from specular reflectors, and returns from distributed ground clutter. Extrapolation of these results to a three-channel notch filter ICS indicates that with a 100 kHz bandwidth at a center frequency of 300 MHz, close to 120 dB of isolation is theoretically achievable. The returns from distributed ground clutter appear to be an irreducible limitation for a ground-based SFR.

A breadboard has been designed with a 100 kHz bandwidth at 291 MHz, for which forward gain up to 120 dB can be tested. It incorporates a pilot-directed single-channel ICS at RF and a pilot-directed three-channel notch filter ICS at IF. The minimum signal level is -90 dBm, with a dynamic range of 60 dB. The signal-to-noise ratio in the SFR for the minimum signal is +17 dB in a 100 kHz bandwidth. The SFR output power is 1 watt PEP.

Methods for implementing a highly linear complex weight circuit for use in the ICS have been investigated. A complex weight circuit has been developed which will keep in-band distortion products generated in the weight at least 20 dB below the minimum level signal to be relayed.

Experiments with the SFR breadboard have demonstrated the following principles of operation on which the design concept is based:

1) Pilot direction of an ICS is valid.
2) An IF ICS can further improve the cancellation of an RF ICS.
3) A multichannel notch filter ICS can be used to improve broadband cancellation performance.
4) The ICS is applicable to an SFR to get forward gain.
5) The SFR is linear and can be used as a multichannel relay.

The SFR experiments also have demonstrated the performance limitations in the present breadboard, pointing out areas where improvements are required and critical design points for future SFR designs.

The experimental results indicate that special care must be taken to prevent strong signals in the SFR transmitter circuits from leaking into the SFR receiver's circuits. Specifically, the pilot reference to the ICS correlators must be clear of transmitted signal components or ICS performance will suffer. In addition, the pilot added in the transmitter must be prevented from coupling into the receiver by any path not shared by the transmitted signal, or operation of the ICS's by pilot direction will not optimize transmitted signal cancellation.

The multichannel notch filter ICS has been shown to be a powerful tool for obtaining broadband cancellation performance, but the design of the notch filters is closely dictated by the bandwidth of the signal (or pilot) to be cancelled. The design used in the breadboard worked well with a 600 kHz bandwidth, but provided no improvement for the 100 kHz bandwidth in the SFR breadboard.

Without stray coupling problems, the SFR breadboard was shown to attain forward gains up to 67 dB. Had the notch filter ICS worked with 100 kHz bandwidth as it did with 600 kHz bandwidth, a minimum of 35 dB more isolation would have been achieved, allowing a forward gain in excess of 102 dB.

The modifications to the breadboard in the areas of notch filter design and elimination of stray coupling paths that are needed to attain this level of forward gain have been outlined. Further performance refinements may then be possible to push the forward gain capability to 120 dB. The SFR breadboard should then be field tested, where natural reflecting terrain will provide a far more realistic performance test than can be accomplished in the laboratory.

APPENDIX A

L-C NOTCH FILTER ANALYSIS

1. INTRODUCTION

In this appendix two commonly used notch filter configurations are analyzed to determine the trade-off between the depth of the notch and its bandwidth. The two configurations, a resonant circuit in series with the load and a resonant circuit shunting the load, are shown in Figure 60. The analysis is conducted with a general source resistance and load resistance, so that the results can be used whether impedances are matched or not.

2. RESONANT CIRCUIT IN SERIES WITH LOAD

From the circuit in Figure 60A, it may be seen that the loaded Q of the tank circuit is given by

$$Q_L = \frac{R||(R_S+R_L)}{\omega_0 L} = \frac{R(R_S+R_L)}{\omega_0 L(R+R_S+R_L)} \tag{146}$$

while the unloaded Q is given by

$$Q_U = R/\omega_0 L \tag{147}$$

Thus, we have

$$Q_L/Q_U = (R_S+R_L)/(R+R_S+R_L) \tag{148}$$

The voltage attenuation factor in the center of the notch, normalized to the out-of-band attenuation factor, is given by

$$\alpha = \frac{R_L/(R+R_S+R_L)}{R_L/(R_S+R_L)} = \frac{R_S+R_L}{R+R_S+R_L} \tag{149}$$

Thus, for (148) and (149) we have

$$\alpha = Q_L/Q_U \tag{150}$$

3. RESONANT CIRCUIT SHUNTING THE LOAD

From the circuit in Figure 60B, it may be seen that the loaded Q of the tank circuit is given by

$$Q_L = \frac{\omega_0 L}{r+R_S||R_L} = \frac{\omega_0 L(R_S+R_L)}{r(R_S+R_L)+R_S R_L} \tag{151}$$

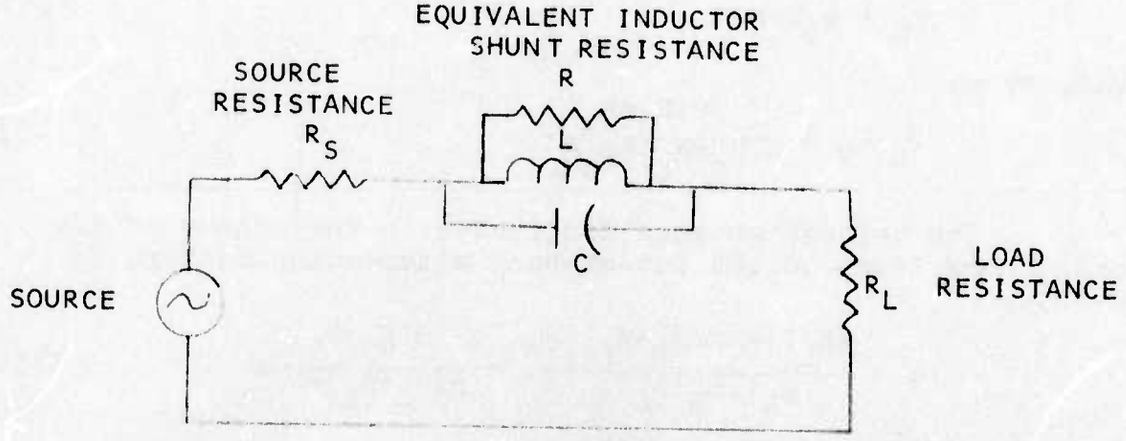

FIGURE 60A

RESONANT NOTCH IN SERIES WITH LOAD

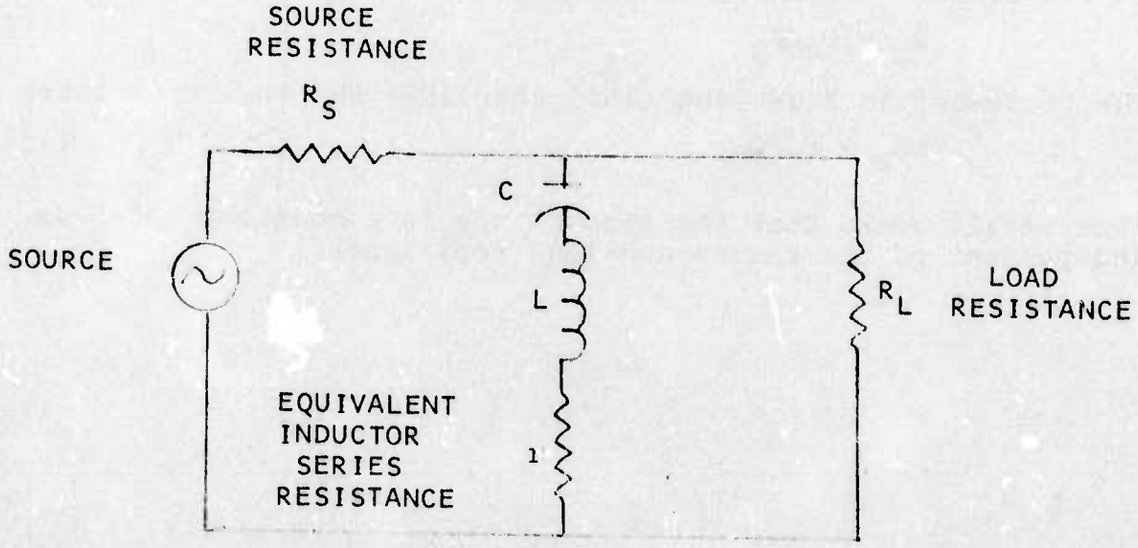

FIGURE 60B

RESONANT NOTCH SHUNTING THE LOAD

while its unloaded Q is given by

$$Q_U = \omega_0 L/r \tag{152}$$

Thus, we have

$$Q_L/Q_U = \frac{r(R_S+R_L)}{r(R_S+R_L)+R_S R_L} \tag{153}$$

The voltage attenuation factor in the center of the notch, normalized to the out-of-band attenuation factor, is given by

$$\alpha = \frac{(R_L||r)/(R_S+R_L||r)}{R_L/(R_S+R_L)} = \frac{r(R_S+R_L)}{r(R_S+R_L)+R_S R_L} \tag{154}$$

Thus, for (153) and (154) we have

$$\alpha = Q_L/Q_U \tag{155}$$

4. CONCLUSIONS

Both the series and shunt resonant notch filter configurations have the same trade-off between notch bandwidth and notch depth. If B_N is the 3 dB bandwidth of the notch and f_0 is its center frequency, we can write

$$Q_L = f_0/B_N \tag{156}$$

The trade-off in Equations (150) and (155) may then be written as

$$\alpha B_N = f_0/Q_U \tag{157}$$

This result shows that the product αB_N is a constant which is independent of the source and load resistance.

ACRONYMS AND PRINCIPAL SYMBOLS

a = magnitude of the signal returned from a particular reflector relative to the transmitted signal strength

B = repeater bandwidth

B_{ant} = two-sided 3 dB bandwidth of the SFR antenna

B_N = two-sided 3 dB notch filter bandwidth

BPF = bandpass filter

C_i = coefficient of the i-th term in the power series expansion of $H_C(f)$

c = free space propagation velocity = 3×10^8 meters/second

D.U.T. = device under test

F_D = $I_{AC/DC}$ = PIN diode distortion factor

F_{RCVR} = numerical value of the receiver noise figure

F_1 = numerical value of the noise figure of the first gain stage in the receiver with the preceding losses included.

F_1' = numerical value of the noise figure of the first gain stage in the receiver without including the preceding losses

F_2 = numerical value of the noise figure of the second gain stage in the receiver

F_3 = numerical value of the noise figure of the third gain stage in the receiver.

f_0 = RF carrier frequency

G = numerical value of the SFR antenna gain in the direction of a particular reflector

G_i = gain constant of the i-th feedback control loop in the ICS

g_1 = numerical value of the gain of the first gain stage in the receiver

GLOSSARY [continued]

G_2 = numerical value of the gain of the second gain stage in the receiver

$H_C(\omega), H_C(f)$ = equivalent lowpass transfer function of transmitter-to-receiver coupling channel

$H_N(\omega), H_N(f)$ = equivalent lowpass transmitter-to-receiver transfer function presented by the N-channel ICS

$H_{ON}(f)$ = $H_C(f)+H_N(f)$ = equivalent lowpass composite transmitter-to-receiver transfer function resulting from the combined effects of the coupling channel and the N-channel ICS

h_{iN} = coefficient of the i-th term of the power series expansion of $H_{ON}(f)$

I_{AC} = RF current in PIN diode

I_{DC} = DC bias current in PIN diode

ICS = interference cancellation system

K_1 = constant relating PIN diode resistance R_0 to its bias current, σ_{DC}

L = inductance in the resonant circuit antenna model

L_{RF} = numerical value of RF losses preceding first gain stage in SFR receiver

MX-200 = model number of General Atronics two-channel VHF ICS

N = number of channels in an ICS

$N_i(\omega), N_i(f)$ = filter transfer function in the i-th ICS channel

N_0 = -174 dBm/Hz = thermal noise spectral density

P_0 = output power of SFR transmitter

R = transmitter output resistance

R_D = RF resistance of PIN diode

$(R/T)_N$ = transmitter-to-receiver isolation provided by an N-channel ICS

r = one-way propagation distance to a particular reflector

S_{min} = minimum received signal power for SFR activation

GLOSSARY [continued]

$S_R(\omega)$ = Fourier transform of the ICS output waveform to the SFR receiver

$S_T(\omega)$ = Fourier transform of the SFR transmitter output

SFR = same-frequency repeater

SNR_{min} = signal-to-noise ratio in SFR receiver for minimum level received signal

W_i = value of complex weight in the i-th ICS channel

X_C = capacitive reactance of antenna input impedance

X_L = inductive reactance of antenna input impedance

XTAL BPF = crystal bandpass filter

Z_{in} = antenna input impedance

α = numerical value of the center frequency depth of a notch filter

γ = B/B_N

Δ = $(\tan^{-1}\gamma)/\gamma$

λ = carrier wavelength

$\rho(\omega)$ = antenna reflection coefficient

σ = radar cross-section of a particular reflector

σ_0 = area reflectivity of ground clutter

τ = propagation delay to a particular reflector

τ_{min} = propagation delay corresponding to the nearest reflector

ϕ = phase shift of the signal returned from a particular reflector

ψ = azimuthal angle about the SFR antenna

ω_0 = $2\pi f_0$ = carrier frequency in radians/second

REFERENCES

[1] Abrams, B.S., *et al*, "Interference Cancellation," General Atronics Rpt 2324-2626-15, prepared for Rome Air Development Center under Contract F30602-72-C-0459, August 1973.(B001 101)

[2] Rosenberg, J.R., E.J. Thomas, "Performance of an Adaptive Echo Canceller Operating in a Noisy, Linear, Time-Invariant Environment, *Bell System Technical Journal*, vol. 50, no. 3, March 1971, pp. 785-913.

[3] Sandhi, M.M., "An Adaptive Echo Canceller," *Bell System Technical Journal*, vol. 46, no. 3, March 1967, pp. 497-511.

[4] Becker, F.K., H.R. Rudin, "Application of Automatic Transversal Filters to the Problem of Echo Suppression," *Bell System Technical Journal*, vo. 45, no. 12, December 1966, pp. 1847-1850.

[5] Sandhi, M.M., A.J. Presti, "A Self-Adaptive Echo Canceller," *Bell System Technical Journal*, vol. 45, no. 12, December 1966, pp. 1851-1854.

[6] Widrow, B., *et al*, "Adaptive Antenna Systems," *Proc* IEEE, vol. 55, no. 12, December 1967, pp. 2143-2159.

[7] Bryn, F., "Optimum Signal Processing of Three-Dimensional Arrays Operating on Gaussian Signals and Noise," *Journal of Acoustical Society of America*, vol. 34, March 1962, pp. 289-297.

[8] DeRusso, P.M., R.J. Roy, C.M. Close, *State Variables for Engineers*, John Wiley and Sons, New York, 1967.

[9] Papoulis, A., *Probability, Random Variables, and Stochastic Processes*, McGraw-Hill Book Co., New York, 1965.

[10] Brennan, L.E., *et al*, "Control-Loop Noise in Adaptive Array Antennas," IEEE *Trans on Aerospace and Electronic Systems*, vol. AES-7, no. 2, March 1971, pp. 254-262.

[11] Widrow, B., *et al*, "Adaptive Antenna Systems," *Proc* IEEE, vol. 55, no. 2, December 1967, pp. 2143-2159.

[12] Skolnik, M.I., *Introduction to Radar Systems*, McGraw-Hill Book Co., New York, 1962.

[13] Barton, D.K. and H.R. Ward, *Handbook of Radar Measurement*, Prentice-Hall Book Co., 1968.

REFERENCES [continued]

[14] Mumford, W.W., E.H. Scheibe, *Noise Performance Factors in Communications System*, Horizon House-Microwave, Inc., Dedham, Mass., 1968.